• U C •

FCTUC FACULDADE DE CIÊNCIAS
E TECNOLOGIA
UNIVERSIDADE DE COIMBRA

DEPARTAMENTO DE
ENGENHARIA MECÂNICA

Metal Oxide Nanoparticle Formation through Detonation – Modeling Evaluation

Submitted in Partial Fulfilment of the Requirements for the Degree of Master in Mechanical Engineering in the speciality of Energy and Environment

Author

Luís Diogo dos Santos Bastos

Advisor

Professor Doutor José Leandro Andrade Campos

Jury

President	**Professor Doutor José Carlos Miranda Góis** **Professor Auxiliar da Universidade de Coimbra**
Vowel	**Professor Doutor Ricardo António Lopes Mendes** **Professor Auxiliar da Universidade de Coimbra**
Advisor	**Professor Doutor José Leandro Simões de Andrade Campos** **Professor Associado da Universidade de Coimbra**

Coimbra, July, 2015

“Learn from yesterday, live for today, hope for tomorrow. The important thing is not to stop questioning”

Albert Einstein

ACKNOWLEDGEMENTS

I would like to thank my advisor, Dr. José Leandro Simões de Andrade Campos for its help and guidance throughout this work. I would also like to thank to all my friends and family that helped me in this journey that is life, experiencing and learning every day. I want to thank to Coimbra for all the experiences and challenges that put me through and helped me to grow up.

"Sentes que o tempo acabou
Primavera de flores adormecida,
Qualquer coisa que não volta que voou,
Que foi um rio, um ar, na tua vida.

E levas em ti guardado
O choro de uma balada
Recordações de um passado
O bater da velha cabra.

Capa negra de saudade
No momento da partida
Segredos desta cidade
Levo comigo p'ra vida

Sabes que o desenho do adeus
É fogo que nos queima devagar,
E no lento cerrar dos olhos teus
Fica a esperança de um dia aqui voltar

E levas em ti guardado
O choro de uma balada

Recordações de um passado
O bater da velha cabra.

Capa negra de saudade
No momento da partida
Segredos desta cidade
Levo comigo p'ra vida."

Balada da despedida do 5º ano jurídico de 88/89

Abstract

The production of ceramics nanoparticles by detonation of metalized emulsions is an important alternative to the traditional metallurgic methods. The small size of the obtained particles (high pressure reaction), the reliability of reaction process (detonation), high temperature post-detonation particles formation with extremely fast cooling (due to the speed of adiabatic expansion of the gases), and the control of product condensed phase composition are the main advantages.

This innovative emulsion detonation synthesis method (EDSM), can be included in either solid or gas-phase synthesis manufacturing process depending on the chosen conditions, and emerges as the most promising technique for the industrialization of the nanoparticles production.

In this work, this production method is studied for metal oxide formation. These materials are chosen given its excellent properties, due to the combination of covalent and ionic links with strong chemical bonds, such as: high hardness and mechanical resistance at high temperature, high melting temperatures which allows good thermal and electric insulating applications and the exhibition of high chemical stability in hostile environment. These properties make these ceramic materials appropriate for several industrial applications.

Metal oxide production from detonation can be predicted using Thermochemical Codes, in this case with THOR Code. For the modelling of this particles formation, the temperature of detonation is the most important parameter to know, as well as the products concentration, being these variables the focus of the modeling problem. Given this problem, the implementation of a thermal equation of state and energetic equation of state is essential in order to better define solid products. Therefore, it's necessary to derive this equations for each phase of solid condensed species.

In this work a Cowan & Fickett Thermal Equations of State and a Mie-Grüneisen approach with thermal contribution given by Debye model Energetic Equation of State are used to describe these solids. These equations are different and characterize more accurately the behavior of metal oxide particles (solid condensed phase) formation in Thor than the

ones previously used (which represented metal oxide particles as a high density gas (Gordon McBride Polynomials)).

The parameters used in this models are known only for common and well-studied products, so the objective of this work was finding these parameters for Alumina, Zirconia, Titania and Magnesia, and simulate each one of this material formation.

Before the metal oxide condensed specie formation analysis, a benchmark was made with Carbon condensed species formation, given its common and abundant presence in reactive mixtures formed in shock compressed energetic materials. The results comparison proved the validity of the models and methods used in the derivation of the parameters and the possibility of extrapolate them for other simulations.

Multiple papers were studied and reviewed in order to derive this parameters for each material at a given phase. These equations were applied in Thor Database, which allowed the simulation of their formation and comparison with the previous method, proving the better accuracy in obtaining the Temperature and Pressure of Detonation, as well as the product concentration.

Keywords Prediction detonation products composition and properties, Carbon, Alumina, Magnesia, Titania, Zirconia, Powder Production, Thermodynamic Equilibria, Detonation calculations.

Resumo

A produção de nanopartículas cerâmicas por detonação de emulsões metalizadas é uma alternativa importante aos métodos metalúrgicos tradicionais. O tamanho reduzido das partículas obtidas (reação a alta pressão), a fiabilidade do processo da reação (detonação), a formação de partículas em altas temperaturas na pós-detonação com arrefecimento rápido (devido à elevada velocidade de expansão adiabática dos gases) e o controlo da composição da fase condensada são as principais vantagens deste método.

Este processo de fabricação inovador, Emulsion Detonation Synthesis Method (EDSM), pode ser definido como um processo de síntese em fase sólida ou gasosa, de acordo com as condições escolhidas, e destaca-se como uma técnica promissora na industrialização da produção de nanopartículas.

Neste trabalho é analisada a produção de nanopartículas de Óxidos Metálicos por detonação. Estes materiais são escolhidos devido às suas excelentes propriedades, devido à coexistência de ligações iónicas e covalentes com fortes ligações, tais como: elevada dureza e resistência mecânica a temperaturas elevadas, altas temperaturas de fusão que permitem a sua introdução em aplicações de isolamento térmico e elétrico e ainda a elevada estabilidade química em ambiente adverso. Estas propriedades fazem destes materiais cerâmicos apropriados para diversas aplicações industriais.

A produção de óxidos metálicos por detonação pode ser modelada através de programas termoquímicos, neste caso através do programa termoquímico THOR. Para a modelação da formação destas partículas, a temperatura de detonação é a variável mais importante de obter, tal como a concentração dos produtos, sendo considerados o principal objetivo de modelação. Por esta razão, a implementação de equações de estado (térmicas e energéticas) é essêncial, de modo a melhor definir os produtos sólidos. Assim, é necessário derivar estas equações para cada fase de material condensado nos produtos da detonação.

Neste trabalho, são utilizadas as Equações Cowan & Fickett para a definição do estado térmico e uma abordagem Mie-Grüneisen com a contribuição térmica dada pelo modelo de Debye para a equação de estado energética, de modo a descrever os sólidos definidos. Estas equações caracterizam mais fielmente o comportamento da formação de

partículas de óxidos metálicos (fase sólida condensada) no THOR do que as equações usadas previamente (que representavam as partículas como um gás de elevada densidade (Gordon McBride Polynomials)).

Os parâmetros usados nestes modelos são conhecidos apenas para produtos extensamente estudados. Por este motivo, este trabalho centra-se na determinação destes parâmetros para a Alumina, Zircónica, Titania e Magnésia, simulando posteriormente a formação de cada um destes materiais através das equações definidas.

Antes da análise da formação de óxidos metálicos na detonação foi realizado um estudo de referência através da formação de espécies condensadas de Carbono, dado o seu extenso estudo e a sua presença nos produtos de misturas reativas de materiais energéticos. A comparação destes resultados provou a validade dos modelos e métodos utilizados na derivação dos parâmetros, bem como a possibilidade de extrapolação para outras simulações.

Foram analisados vários artigos com o objetivo de derivar os parâmetros referidos para cada material numa dada fase. Estas equações foram implementadas na base de dados do THOR, o que permitiu a simulação da sua formação e a comparação com os métodos anteriormente usados, provando uma melhor precisão na obtenção das temperaturas e pressões de detonação, bem como na previsão de concentração dos produtos.

Palavras-chave: Carbono, Alumina, Magnésia, Titania, Zircónica, Produção de Nanopartículas, Equilíbrio Termodinâmico, Modelação e Previsão da Detonação.

Contents

LIST OF FIGURES

LIST OF TABLES

SIMBOLOGY AND ACRONYMS

Simbology

T – Temperature

P – Pressure

G – Gibbs free energy

$G0_i$ – Minimum value of Global Gibbs free energy for i component

μ_i – Gibbs Free Energy of i component

E – Internal Energy

e_i - Internal Energy of i component

H – Enthalpy

x_i – Molar Fraction of i component

X_i – Mole Number of i component

ρ – Density

Cp – Specific Heat Capacity at Constant Pressure

Cv – Specific Heat Capacity at Constant Pressure

D – Detonation Velocity

M – Molar Mass

R – Perfect Gas constant

V - Volume

V_0 - Volume at T_0

B_0 - Bulk modulus at T_0 (reference temperature)

B'_0 - Bulk modulus pressure derivative

V_{0T} - Volume at T chosen

B_{0T} - Bulk modulus at T chosen

α - Thermal expansion coefficient

n - Number of modes

θ_D - Debye Temperature

k - Boltzmann's Constant

ω - Frequency

Acronyms

AN – Ammonium Nitrate

Al_2O_3 – Alumina

ZrO_2 – Zirconia

TiO_2 – Titanium

MgO- Magnesium

THOR – Thermochemical Code

1. INTRODUCTION

1.1. Nanomaterials

A new subject area, designated nanotechnology, has recently emerged and is associated to structures and behavior of materials inferior to 100 nm. This nanometric-sized particles or structures present a set of electrical, optical, magnetic, and mechanical properties that are different from that same material of larger size. The most common behaviors of this particles are: high plasticity, super hardness, lower melting point, transparency, increased magnetic effect, high surface area by mass unit with consequential improvement of catalytic activity, high semiconductor luminescence, low thermal conductivity, changes of color, and act upon the laws of quantum mechanics.

There are enormous fields of applications in the nanotechnology (Haick 2015; Silva & Antunes 2013), namely as nanocoatings, magnetic nanofluids, nanocatalysts, biological nanosensors, nanopigments for several industries, nanoadditives for fuels, photocatalytic effect in air and water purification, ultra-light nanocomposites, nanoparticles for drug controlled release in the human body, nanomarkers and nanometric films.

1.2. Nanomaterial Production Methods

Recently, a great development in investigation of new material production methods has been observed. These investigations motivated toward the industrialization of these methods, have to comply two fundamental requirements:

a) production at an industrial scale (Mg/day);
b) reproducibility of nanomaterial properties,

These are essential conditions to support the large scale incorporation of the nanomaterial thus produced, either creating new products or improving the functionalities of those already existing in multiple cross applications. It should be noted that these new developments also allow to decrease costs of raw materials and reagents, as well as facilitate the disposal of final waste products.

Nanomaterial synthesis methods are framed within three major categories and are presented in the next subchapters (Abou El-Nour et al. 2010; Haick 2015; Overney 2010; Neves et al. 2014).

1.2.1. Liquid-Phase Methods

In this type of synthesis there are methods that are already established or yet in industrialization imminence (Neves et al. 2014), such as:

a) sol-gel,
b) precipitation
c) microemulsion reaction method
d) hydrothermal and electrochemical synthesis.

These methods share a common principle: a starting material in solution or gel form, where precursors are either dissolved to a molecular scale or dispersed in the desired stoichiometric proportion. In a following stage, these precursors are decomposed in controlled manner, with the formation of a precipitate, usually an hydroxide, which requires several subsequent treatment stages, such as calcination, for its conversion into an oxide with the desired crystalline structure. This is followed by a final breakdown by grinding process.

1.2.2. Solid-Phase Methods

In this methods, nanoparticles are usually prepared from a first slow reaction in the solid state among different precursors, namely carbonates and oxides. It is also designated as a mechanical synthesis, where the reaction activation energy is supplied by a mill, being followed by an intensive grinding process until particles inferior to 200 nm are obtained.

1.2.3. Gaseous-Phase Methods

This category comprises processes for both the production of individual nanoparticles and for direct application in surface coating, namely:

a) combustion synthesis,
b) spray pyrolysis,
c) evaporation/oxidation of metals, thermal plasma, CVD (Chemical Vapor Deposition), PVD (Physical Vapor Deposition) and laser-ablation.

There are, generally, three production stages:

a) Precursor conversion into vapor, with the formation of an aerosol;
b) Condensation as nanoparticles (with heat release), subsequently to the precursor's oxidation reaction;
c) Control and preservation of nanomaterial dispersion state.

These methods are mainly "bottom-to-top" approaches, so the higher the oversaturation state becomes, the smaller the first thermodynamically-stable particles in condensed form will be (stage b)). This oversaturation state is favored by very high pressures or low temperatures. On the other hand, in order to avoid undesirable coagulation/coalescence phenomena, which lead to a large growth of the particles (stage c)), it is necessary to produce extremely dispersed aerosols, which translates into extraordinarily reduced production rates (g/h). The other two alternatives, such as immediate cooling, after nanoparticle condensation or the use of high-speed gas flows and turbulence, have so far demonstrated to be of difficult industrial implementation.

The main weak point of these methods are the very low production capacity and the difficulty in obtaining complex (ternary) structures and composites.

For this reason, a new production method, called Emulsion Detonation Synthesis Method, has been investigated (Campos et al. 2014; Campos et al. 2008; Matias et al. 2010; Neves et al. 2014; Silva & Antunes 2013), and is going to be presented in the next section.

This innovative emulsion detonation synthesis method (EDSM), can be included in either solid or gas-phase synthesis manufacturing process depending on the chosen conditions, and emerges as the most promising technique for the industrialization of the nanoparticles production.

1.2.4. Emulsion Detonation Synthesis Method

The emulsion detonation is a singular method in nanomaterial synthesis, usually in gaseous phase, containing some highly interesting characteristics which allow overcoming some of the limitations inherent to gaseous-phase synthesis:

a) Extremely high pressures, that might go up to 10 GPa (100,000 bar), turning the first structure of stable condensed matter into very small dimension;

b) Detonation process, which is a very reliable reaction process and allows the control of product condensed phase composition;
c) Extremely fast cooling, due to the speed of adiabatic expansion of the gases resulting from the reaction;
d) Gas flow with high-speed expansion and turbulence

These reasons led to an interest towards the use of the emulsion detonation concept as nanomaterial synthesis method, usually in gaseous phase. However some weak points must be referred, as the use of some explosives and/or detonator (classe-1 matter), represent a high risk in discontinuous production operations. Recently a patent was released (Silva & Silva 2013) and this problem was solved through:

a) Sensitization of the emulsion (transformation into class-1 matter) only at the later stage of reactor feeding;
b) Detonation ignition without detonators or any class-1 matter;
c) Simultaneous and continuous combination of emulsification and detonation operations of the emulsion.

As a result, the process provides a nanomaterial production yield superior to 100 kg/h, with high reproducibility in an automatic process and increased safety, as it avoids the use or accumulation of any explosive substances along the whole synthesis process. Nanomaterial collection is carried out in secco, thus avoiding all problems associated to liquid effluent toxicity.

Another advantage of this method of production is the formulation flexibility of the emulsion, which allows a large set of precursors in its composition, from metals and metal alloys to different metal salts, which constitute the precursors that will transform into all range of crystalline structures, such as oxides with binary, ternary, or higher crystalline structures, non-oxides with crystalline structures of the nitride type, composites and solid solutions. It allows to consider a multiplicity of nanotechnology applications where this diverse set of structures is required, which reinforces its importance.

1.3. Thermochemical Modeling

The process described above for the manufacture of nanometric materials starts with the selection of the mixture reagents (emulsion, precursors and surfactants) according to the desired ceramic compound. Thereafter, the adjustment of the final composition is done through the detonation temperature (with C-J condition) and post detonation cooling process (adiabatic expansion), being the most relevant parameters in formation of final particles. For this reason the detonation temperature influence is studied. It has to be lower than the melting point of the desired ceramic material in order to reduce the coalescence time, maintaining the primary particles in the nanometric state, and also, to attain with great accuracy the required point of the phase equilibrium diagram corresponding to the formation of the ceramic compound.

Considering the experimental difficulties of measuring the detonation temperature at point (C-J) and the products concentration, they are determined with use of computational programs (BKW, Tiger, THOR), from the composition and initial density of the emulsion. When this stage is completed, the final composition of the emulsion is established. Therefore the thermochemical modeling of detonation is an important step in the production method, being the core interest of this work.

For this modeling to be accurate it's essential to better represent condensed solid species. Therefore, this will be the main focus of this thesis, with an implementation of new equations, Thermal Equations of State (Cowan Fickett EoS) and Energetic Equations of State (Mie-Grüneisen approach) , for each material studied phase. The accuracy of these equations has the highest relevance, given the sensibility of detonation temperature with the modeling of detonation product composition.

The materials that will be studied are Carbon (for benchmark) and Alumina, Zirconia, Titania and Magnesia (Metal Oxides). These materials are selected because of their mechanical and thermal properties, such as a high hardness and mechanical resistance at high temperature, due to the combination of covalent and ionic links, and high melting temperatures which allows good thermal and electric insulating applications. They also exhibit high chemical stability in hostile environmental, due to their strong chemical bonds, making these ceramic materials appropriate for several industrial applications, specially for Abrasives, Thermal Barrier Coating (TBC), Structural Ceramics and Bioceramics and Glues.

This work will start with the presentation of each material, it's phases and phase diagrams for an overall analysis. Followed by the description of THOR code and the equations possible to use and implement for solid phase representation. Moreover are derived each of these parameters equation for each phase and used to simulate product formation in Thor code. In these simulations a first analysis is made with carbon formation due to the extensive studies already made, for verifying the veracity of the implemented method. After these modeling, the formation of the metal oxides is studied and the results with the presented method is compared with previous ones, used for similar simulations, correlated with experimental results (Campos et al. 2008; Matias et al. 2010; Campos et al. 2014).

1.4. Cases Studied - Materials

1.4.1. Carbon (C)

Carbon is an excellent structural material and is prevalent in nature. In high-temperature, high-pressure energetic mixtures containing carbon, solid or liquid carbon can be formed in an oxygen-deficient environment. The two solid phases, graphite and diamond, have been extensively studied by other authors (Erskine & Nellis 1992; Van Thiel & Ree 1989; Cowan & Fickett 1956; Eggert et al. 2010; Bundy et al. 1996), and will be considered in this work in order to benchmark the results obtained by the methods that will be presented. The phase diagram for carbon is presented in Figure 1

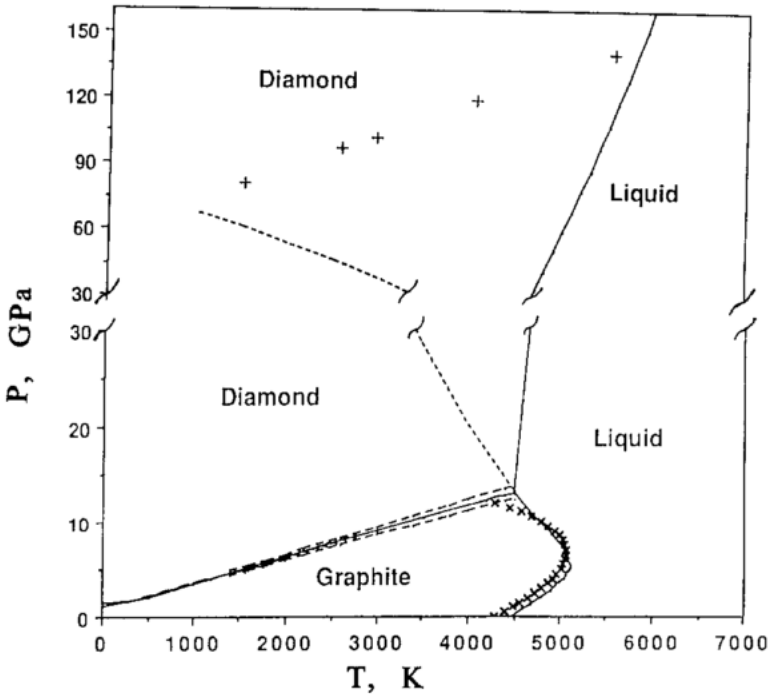

Figure 1 – Carbon Phase Diagram (Van Thiel & Ree 1989)

1.4.2. Alumina (Al_2O_3)

Several papers were analyzed, both with experimental and theoretical data, for Alumina. At atmospheric pressure and temperature, alumina exists in α-phase, Corundum, a much studied material in earth science. At an increasing pressure, some Al_2O_3 compounds transform into Rh_2O_3(II)-type structure with space group Pbcn (Ono et al. 2006), that takes place at approximately 100GPa. Some Theoretical studies have also predicted that Al_2O_3 can transform into perovskite structure with space group Pbnm at pressures above 200 GPa (Hama & Suito 2002) (Figure 3). However, Oganov & Ono, 2005, synthesized $CaIrO_3$-type (post-perovskite structure) Alumina with space group Cmcm in high-pressure experiments. Oganov & Ono, 2005; Caracas & Cohen, 2005; Tsuchiya et al., 2005, also showed that post-perovskite structure is stable at high pressures when compared to perovskite structure, by first-principle calculations (Figure 2).

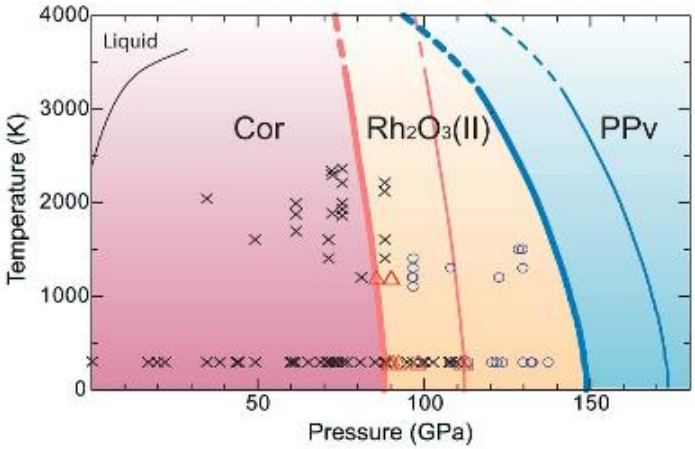

Figure 2 - Alumina Phase-Diagram without Perovskite Structure (Tsuchiya et al. 2005)

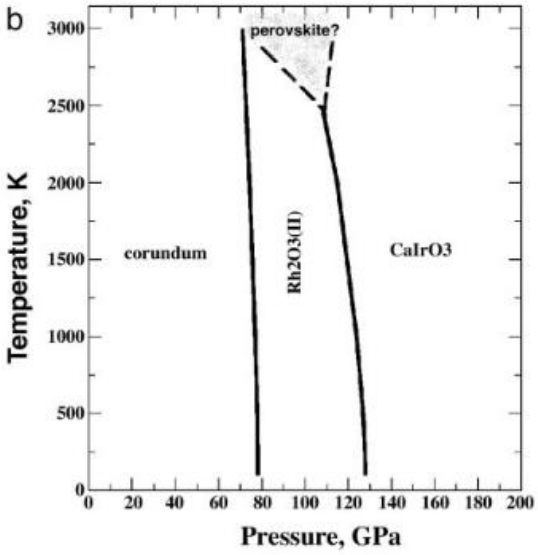

Figure 3 - Alumina Phase-Diagram with the possibility of Perovskite Structure (Oganov & Ono 2005)

1.4.3. Zirconia (ZrO_2)

ZrO_2 has at least ten different solid structures at high pressures or temperatures, but there are only five polymorphic forms confirmed up to now (which will be studied here) (Dewhurst & Lowther 1998). The monoclinic (baddeleyite P21/c, below 1500 K), tetragonal (P42/nmc, between 1500 and 2650 K), and cubic (fluorite Fm3m, above 2650 K) polymorphs are derived at ambient pressure, while the two high-pressure orthorhombic structure, Pbca and Pnma polymorphs (isostructural to brookite TiO2 and to cotunnite PbCl2, respectively) are obtained at 3–10 GPa and 12.5–20 GPa, respectively (Fadda et al. 2009). Therefore, there will be a solid EoS and ES for each phase of each material. Some

phase-diagrams are presented in the following figures (Figure 4, Figure 5 and Figure 6), illustrating the information above, along with the large uncertainty that exists in defining the phases.

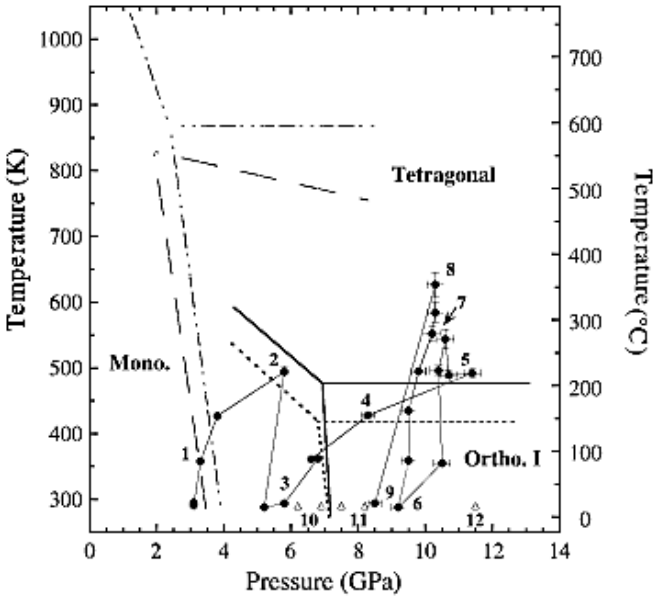

Figure 4 - Zirconia Phase-Diagram (Bouvier et al. 2002)

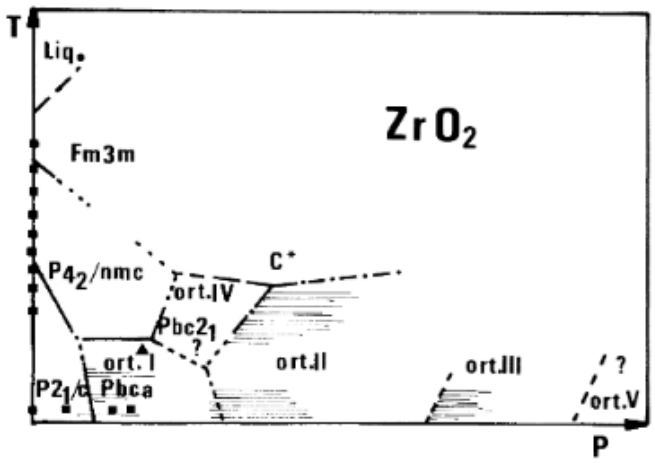

Figure 5 - Zirconia Phase-Diagram (Leger et al. 1993)

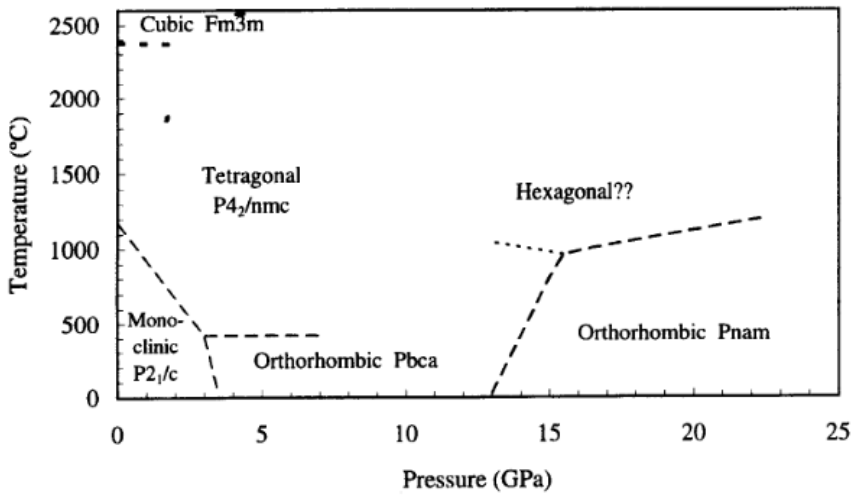

Figure 6 - Zirconia Phase-Diagram (Kisi & Howard 1998)

1.4.4. Titania (TiO_2)

Titanium Dioxide exists in nature as the minerals rutile, anatase and brookite (Arlt et al. 2000). Under high pressure, TiO_2 transforms into (in order of increasing pressure) α-PbO2 type (columbite or TiO_2 II, space group Pbcn), baddeleyite (MI, $P2_1/C$), Orthorombic I (OI, Pbca), and cotunnite (OII, Pnma) phases (Nishio-Hamane et al. 2010). Since several metal dioxides are known to transform into cubic fluorite phase at high pressure, the existence of a fluorite phase has been postulated for TiO_2 (Haines & Léger 1993), and Mattesini et al., 2004, reported the existence of fluorite-like cubic phase together with cotunnite phase at 48 GPa after heating at 1900-2100K. However, theoretical calculations predict (Figure 7) that cotunnite phase is more stable than the fluorite phase above 40 GPa (Muscat et al. 2002) and cotunnite phase formation was reported at 64 GPa after heating at 1800K (Dubrovinsky et al. 2001) and also at 56-48GPa and 1800K (Al-Khatatbeh et al. 2009). Phase-diagrams for this material are presented in Figure 8, Figure 9 and Figure 10 .

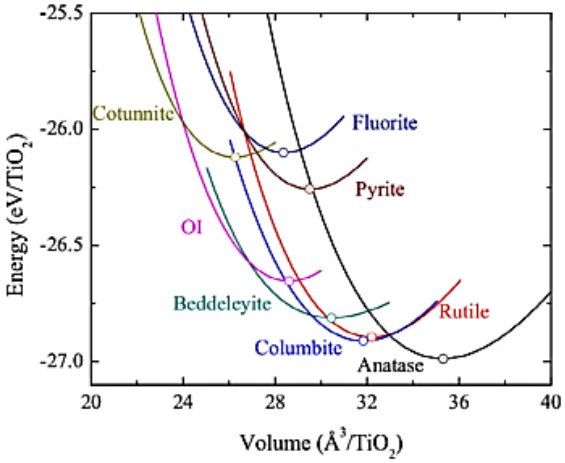

Figure 7 - Calculated total energy for eight TiO2 polymorphs with respect to volume at T=0K (Mei et al. 2014)

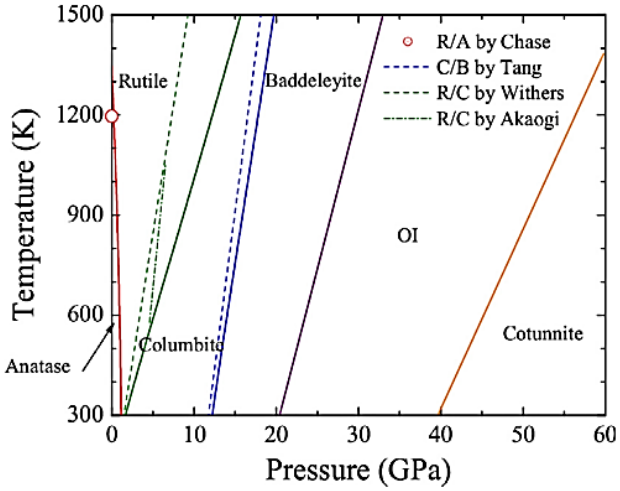

Figure 8 - Titania Phase-Diagram (Mei et al. 2014)

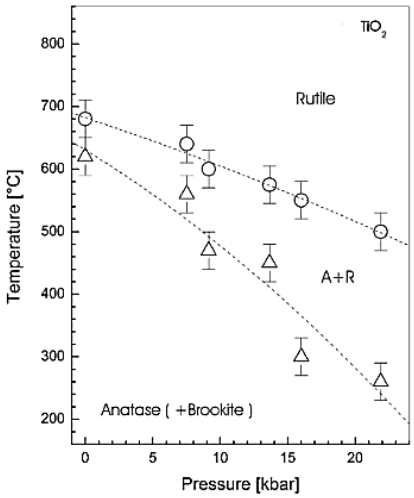

Figure 9 - Titania Phase-Diagram (Stir et al. 2006)

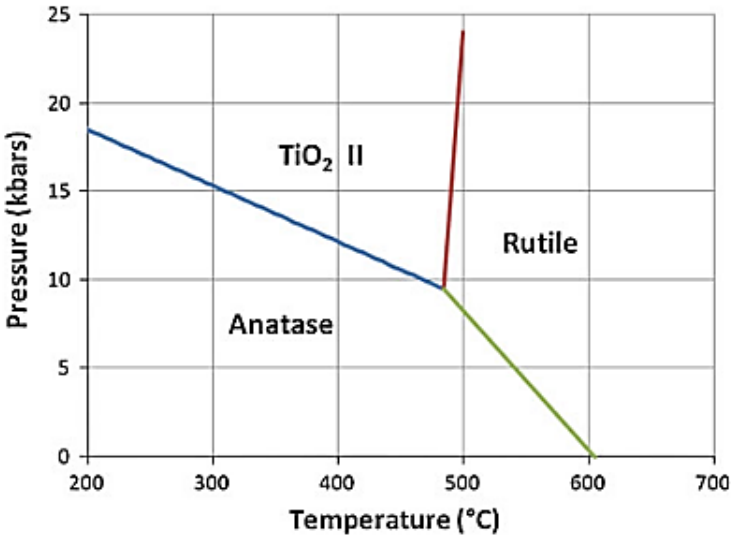

Figure 10 - Titania Phase-Diagram (Hanaor & Sorrell 2011)

1.4.5. Magnesia (MgO)

Magnesia is a well-studied material for high pressure-high temperature conditions. It is a simple structured material, NaCl (B1 or Periclase) structure, and upon compression, it undergoes a SPT into CsCl (B2) structure, at 410.6-1050 GPa (Vahora et al. 2013). This could be observed in Figure 11.

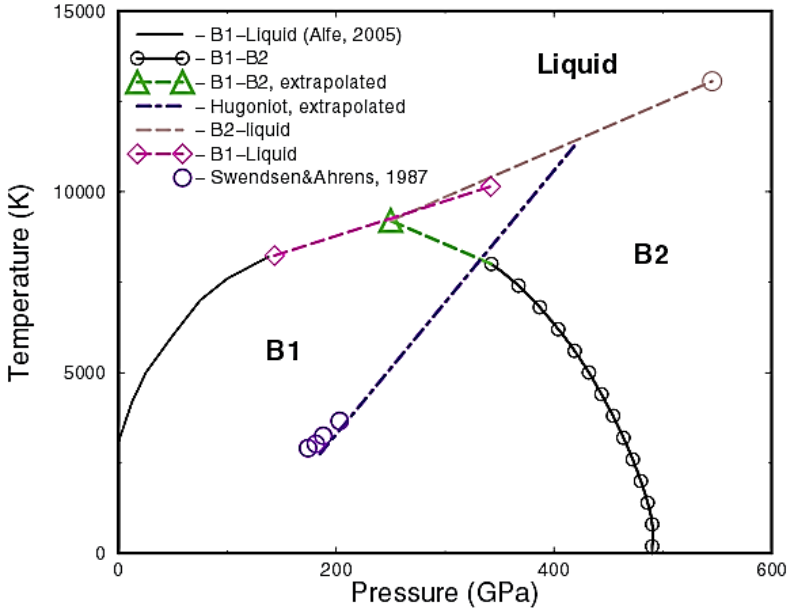

Figure 11 - Magnesia Phase-Diagram (Belonoshko et al. 2010)

2. THOR

2.1. Thermochemical Prediction Method

The thermochemical computer code, THOR, was developed to predict combustion and detonation behavior based in products thermodynamic properties, including solids species (Campos et al. 2007).

This code is formed by four interactive calculating clusters (Figure 12):

a) the conservation equations (mass, atomic species, momentum and energy), being the thermodynamic equilibrium for

$$G = G_{min}\,(P, T, x_i) \quad \textbf{(1)}$$

With

$$G = \sum x_i \mu_i \quad \textbf{(2)}$$

The Gibbs free energy of each component is defined by μ_i

$$\mu_i = G_{0i}(T) + RT\ lnP + R\ T\ \ln(x_i) \quad \textbf{(3)}$$

b) the thermal equation of state (EoS)

c) the energetic equation of state (ES), related to the internal energy

$$E = \Sigma x_i e_i(T) + \Delta e,\ e_i(T) \quad \textbf{(4)}$$

d) the combustion condition regime, isobaric or isochoric adiabatic combustion, or a Chapman-Jouguet detonation.

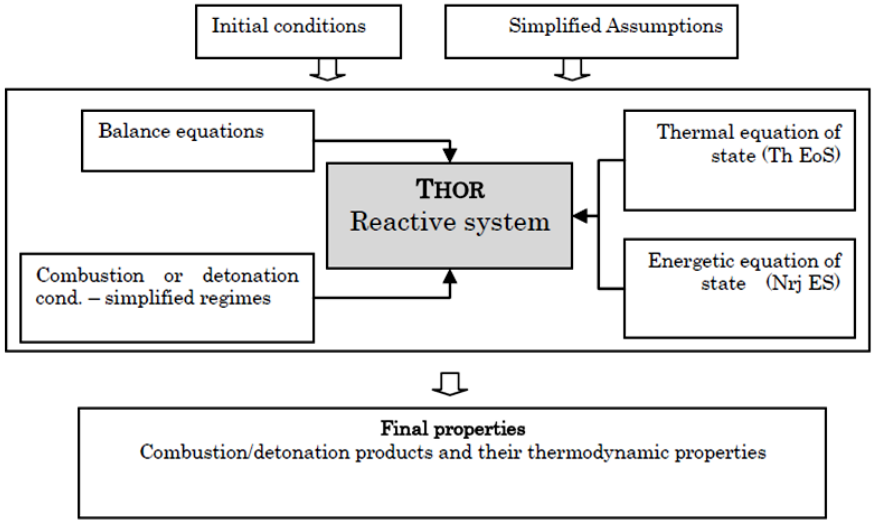

Figure 12 - THOR Calculation Structure

The choice of an accurate model to be used in high pressure, high temperature simulations is essential to ensure better prediction of energetic substances performances. Therefore, is important to know the equations and methods used.

In this work, this program is used to implement the equations that are going to be derived in section 6 and compare with results from previous authors (Matias et al. 2010; Campos et al. 2014), validating it's formulation.

2.2. Thermal Equations of State (EoS)

Several P-V-T equations of state are available in THOR, namely perfect gases, Boltzmann, Percus–Yevick, BKW, Charnahan–Starling, H_9,H_{12} , H_L and JCZ3 equations. In this modeling, for gaseous phase, it's used H_L equation of state (EoS), $PV/RT=\sigma(V,T,X_i)$, being $\sigma=1+x+0.625x^2+0.287x^3-0.093x^4+0.014x^5$ with $x(V,T,X_i)=\Omega/VT^{3/\alpha}$ and $\Omega=\Sigma(X_i\omega_i)$ (Campos et al. 2014), which is supported by a Boltzmann EoS, however is based on physical intermolecular potential parameters of gas products instead of correlations from final experimental results. It was validated in earlier works with several energetic systems (Durães et al. 1996).

In THOR, the equations of state are used to calculate the gaseous products phase volume for a given temperature and pressure, which is added with volumes of each of the

condensed phases that are in equilibrium with the gaseous phase at the same temperature and pressure.

2.3. Energetic Equations of State (ES)

The evaluation of the products energetic state consists in the computation of the enthalpy, entropy and internal energy for a given temperature and pressure, considering the individual contribution of the products weighted by their molar fractions.

For this purpose, Thermochemical data (NIST-JANAF thermochemical Tables (Chase 1998)) and Gordon and McBride polynomial expressions (Gordon & McBride 1994) are used to represent gaseous products. Generating the numerical expressions for the main thermodynamic properties (Campos et al. 2014):

$$\frac{Cp^{\circ}}{R} = \frac{a_1}{T^2} + \frac{a_2}{T} + a_3 + a_4 T + a_5 T^2 + a_6 T^3 + a_7 T^4 \quad \textbf{(5)}$$

$$\frac{H^{\circ}}{RT} = -\frac{a_1}{T^2} + \frac{a_2}{T}\ln T + a_3 + a_4\frac{T}{2} + a_5\frac{T^2}{3} + a_6\frac{T^3}{4} + a_7\frac{T^4}{5} + \frac{b_1}{T} \quad \textbf{(6)}$$

$$\frac{S^{\circ}}{R} = -\frac{a_1}{2T^2} - \frac{a_2}{T} + a_3\ln T + a_4 T + a_5\frac{T^2}{2} + a_6\frac{T^3}{3} + a_7\frac{T^4}{4} + b_2 \quad \textbf{(7)}$$

And the internal energy will be $E = H - P.V$, with E representing $e_i(T)$ from the equation (4).

This method is widely used for gaseous phase products modeling. It's also one of the simplest ways to calculate the contribution of the condensed products to thermodynamic functions in THOR, assuming Gordon–McBride's polynomials and their corresponding coefficients, modeling the condensed phase as a high density gas (Matias et al. 2010; Campos et al. 2008; Campos et al. 2014).

For each product, the Gordon and McBride coefficients are calculated in ranges of temperature. These temperature intervals are defined according to the prevailing phases of the products under study, as it is established in NIST-JANAF thermochemical tables.

This procedure allows a straightforward calculation of the energetic state of condensed species for two reasons: (i) as it is also used in the NASA-CEA Code (Gordon & McBride 1994), the resulting Thermo Build database (NASA Glenn Reasearch Center 2010) already contains ready-to-use information on the Gordon and McBride coefficients of a wide

range of products; (ii) it does not weaken the algorithms convergence due to the generalization of the polynomial formulas for gases and for condensed phases.

3. DETONATION PREDICTION

3.1. Detonation Regime – Classical Phenomenological Basis

The first theory of detonations was proposed by Chapman in 1899 (England), Jouguet in 1905 (France), and by Mikhelson in 1890 (Russia). In this theory, it's assumed that the detonation wave causes each element of explosive to transform instantaneously from its initial unreacted state into gaseous detonation products, with the chemical reactions taking place instantaneously inside the shock. It assumes that the entire flow is one-dimensional and the front as a non-thickness discontinuity plane, where conservation laws for shock waves (mass, momentum and energy) are applied. These assumptions takes to a steady state condition, meaning that the front and the plane of the end of the reaction propagate at the same velocity D (Detonation Velocity) in a plane semi-infinite geometry, which is called the Chapman-Jouguet condition (Davis & Fauquignon 1995).

As presented above, the behavior of the detonation products is represented by the Chapman Jouguet detonation condition

$$\text{Mass, Momentum, Energy balance and Hugoniot equation } \left(\frac{dP}{dV}\right]_S = \frac{P-P_0}{V-V_0}\right) \quad \textbf{(8)}$$

For the detonation regime based on the assumption that the detonation velocity D is obtained adding sound velocity a with particular velocity U_P ($D = a + U_P$).

This theory combines the shock and reaction, respectively in fresh and products mixtures, developing the basic physical model of detonation, with the simple approach (Campos et al. 2008): a)shock front compresses and heats the fresh material; b)the exothermic reactions are completed instantly; c)the heat produced by the reaction feeds the pressure shock front and drives it forward; d)gaseous products behind the shock wave are expanding and a rarefaction wave is then generated; e)in the shock front, the chemical reactions and the leading edge of the rarefaction are in equilibrium – they are moving with the same velocity called detonation velocity; f)the shock front can be assumed as mono-dimensional - pressure step value and detonation velocity constants, as a function of time.

Zeldovich(1940), von Neumann (1942) and Doering (1943) independently made additions to C-J theory to account for finite chemical reaction zone. ZND theory assumes that the detonation wave shocks the unreacted explosive to a high-temperature state, initiating chemical reactions, which transform the explosive into gaseous detonation products over a finite reaction zone.

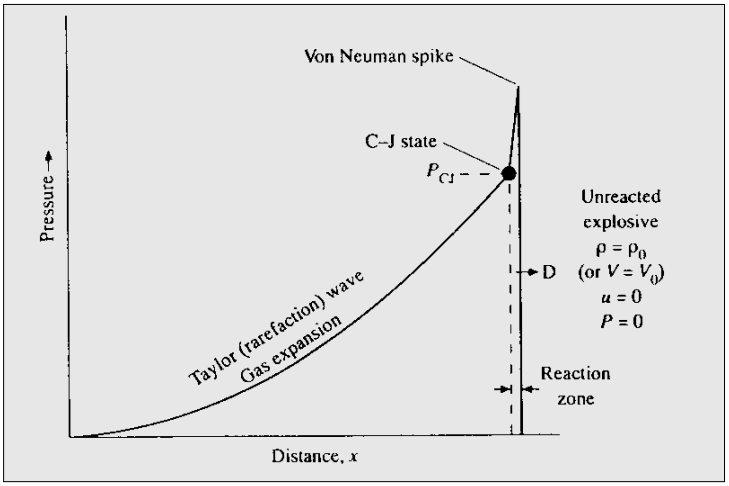

Figure 13 - ZND basic Physical model of Detonation (Campos et al. 2008)

The reactive Euler equations are solved in the shock wave frame, to calculate the thermodynamic properties and chemical species concentrations through the reaction zone. Inside condensed heterogeneous explosives this schema is more complex, with shock interactions and rarefaction waves. For the presented work it can assumed the preceding configuration like the basic scheme. Those conditions can be coupled with the basic knowledge of behavior properties of solids, under high shock conditions, predicting its plastic, micro-droplet and vapor transition, under high stress levels (Campos et al. 2008).

The presented assumptions and simplifications are the phenomenological basis of adding metal material to an existing explosive detonation zone, in order to get a condensed metal oxide

3.2. Thermal Equations of State (EoS) for Condensed Solid Species

The previous presented equations (Section 2.2) are not applicable to condensed solid species, which lead to a review in this work about solid equations of state that can be used to represent condensed phase P-V-T relations. A definition of these equations can lead

to more accurate results, as the formation of solid products in detonation reaction can have a significant effect on the detonation characteristics and associated isentropic expansions, because of the form of the EoS (Braithwaite & Allan 2006). For this purpose, equations such as, Cowan and Fickett EoS (Cowan & Fickett 1956), Murnaghan EoS (Murnaghan 1937), Murnaghan-Birch EoS (Birch 1952) and Vinet EoS (Vinet et al. 1987) are presented next.

These equations are extrapolated from data that can be obtained from different calculations or experimental procedures, namely: Diamond Anvil Cell (DAC) in conjunction with X-Ray Diffraction Measurements; Neutron Powder Diffraction; Shock Hugoniot measurements; Theoretical Ab Initio Calculations. Which provides points or equations with the P-V or P-V-T relations that are represented in tables and figures in section 4.

A wide variety of equations of state have been proposed for condensed species. The most used Equations of State are represented next.

3.2.1. Isothermal Equations of State

3.2.1.1. Murnaghan EoS (M)

$$V = V_0(1 + \frac{B'_0\, P}{B_0})^{\frac{-1}{B'_0}} \quad (9)$$

Murnaghan (1937) has derived this simple equation where V, B_0, B'_0 are the volume, bulk modulus and bulk modulus pressure derivative, respectively. The 0 subscript defines the parameters for P=0, at a given T.

3.2.1.2. Birch-Murnaghan EoS (MB)

$$P(V) = \frac{3}{2}\, B_0 \left(\left(\frac{V_0}{V}\right)^{\frac{7}{3}} - \left(\frac{V_0}{V}\right)^{\frac{5}{8}} \right) \left(1 + \frac{3}{4}(B'_0 - 4) \left(\left(\frac{V_0}{V}\right)^{\frac{2}{3}} - 1 \right) \right) \quad (10)$$

The represented equation of state is the third-order Birch-Murnaghan Equation (Birch 1952), at a given T.

3.2.1.3. Vinet EoS (V)

The equations above, due to power series expansions involved, lose their accuracy for very high pressures.

$$P(V) = 3B_0 \left(\frac{V}{V_0}\right)^{-\frac{2}{3}} \left(1 - \left(\frac{V}{V_0}\right)^{\frac{1}{3}}\right) e^{\left(\frac{3}{2}(B'_0 - 1)\left(1 - \left(\frac{V}{V_0}\right)^{\frac{1}{3}}\right)\right)} \quad (11)$$

The presented expression (Vinet et al. 1987) addresses this issue by expressing the bulk modulus and its derivatives in terms of the interatomic distances and a scaling parameter. This equation is also for a given T.

3.2.2. Temperature Dependent Equations of State

There are several approaches to include the temperature dependence of the unit cell volume, being the P-V-T equations.

3.2.2.1. Cowan Fickett EoS (CF)

$$P = p_1(\eta) + a(\eta)\mathrm{T} + b(\eta)T^2 \quad (12)$$

With

$$\eta = \frac{\rho}{\rho_0} \quad (13)$$

This equation was first presented in Cowan & Fickett, 1956, where $p1(\eta), a(\eta), b(\eta)$ are polynomial function, ρ is the density, and the 0 subscript defines the parameters for P=0, at a given T (in this case for T_0). This is an empirical equation and will be explored more deeply in section 4.1.

3.2.2.2. The Thermal Pressure Approach

The Thermal Pressure Approach (Poirier 2000) , is represented by a Cold Compression term (Isothermal EoS) and a Thermal Pressure term (P_{th}). This last term could be represented by the definition or by a Mie-Grüneisen EoS (MG).

$$\mathrm{P(V,T)} = \mathrm{P(V,T_0)} + \mathrm{P_{th}(V,T)} \quad (14)$$

By the definition (Poirier 2000)

$$\mathrm{P_{th}} = \int_0^{\mathrm{T}} \left(\frac{\partial \mathrm{P}}{\partial \mathrm{T}}\right)_{\mathrm{V}} \mathrm{dT} = \int_0^{\mathrm{T}} \alpha\, \mathrm{B_{0T}}\, \mathrm{dT} \quad (15)$$

Where α is the thermal expansion coefficient and B_{0T} is the bulk modulus, the two parameters are dependent of temperature.

By Mie-Grüneisen EoS (MG) (Poirier 2000)

$$P_{th} = \frac{\gamma}{V} E_{th}(V, T) \quad (16)$$

Where γ is the Grüneisen Parameter and E_{th} is the Thermal Energy.

3.2.2.3. High Temperature EoS

The High Temperature EoS approach (Lowitzer et al. 2006) is obtained by replacing V_0 and B_0 in the Birch-Murnaghan EoS or in Vinet EoS by V_{0T} and B_{0T} (volume and bulk modulus for P=0 in T chosen).

$$V_{0T} = V_0 e^{\int_{T0}^{T1} \alpha \, dT} \quad (17)$$

And

$$B_{0T} = B_0 + \left(\frac{\partial B_{0T}}{\partial T}\right)_P (T - T_0) \quad (18)$$

Where B_0 is the bulk modulus for T_0.

3.3. Energetic Equations of State (ES) for Condensed Solid Species

Through the implementation of the simplified model presented before for condensed species, the program obtains a different pressure and temperature from reality because it models the condensed phase as a gas, without phase change.

A different and more accurate approach can be taken in thermochemical calculations, as the behavior of condensed phases at high temperature and pressure can be described for the internal energy and entropy from its definition (Cowperthwaite 1965):

$$dE = TdS - PdV = \left(\frac{\partial E}{\partial T}\right)_V dT + \left(\frac{\partial E}{\partial V}\right)_T dV = C_V dT + l dV \quad (19)$$

$$\left(\frac{\partial E}{\partial T}\right)_V = C_V \quad (20)$$

$$\left(\frac{\partial E}{\partial V}\right)_T = -P + T\left(\frac{\partial P}{\partial T}\right)_V \quad (21)$$

Expressing the internal energy mathematically by

$$E(T,V) = E(T) + E(V) \quad (22)$$

Which for a given temperature:

$$E - E^0 = \int_{Vo}^{V} \left[T \left(\frac{\partial P}{\partial T} \right)_V - P \right] dV \quad (23)$$

That could lead to simplified equations that represents internal energy at each temperature, depending on B_0 and B'_0. The most important ones are:

From Fu & Ho (1983), the Murnaghan ES

$$E(V) = E_0 + \frac{B_0\, V}{B'_0} \left(\frac{\left(\frac{V_0}{V}\right)^{B'_0}}{B'_0 - 1} + 1 \right) - \frac{V_0\, B_0}{B'_0 - 1} \quad (24)$$

And from Al-Khatatbeh et al. (2009), Birch-Murnaghan ES

$$E(V) = \frac{9}{2} B_0 V_0 \left(\frac{1}{2} \left(\left(\frac{V_0}{V} \right)^{\frac{2}{3}} - 1 \right)^2 \right) \left(1 + (B'_0 - 4) \left(\frac{1}{2} \left(\left(\frac{V_0}{V} \right)^{\frac{2}{3}} - 1 \right) \right) \right) + E_0 \quad (25)$$

Equation 22 can also be described by other semi-empirical models and equations, as the one that will be implemented in this work, given its high accuracy and simple representation, a Mie-Grüneisen approach with thermal contribution given by the Debye model.

$$E(V,T) = E_c + E_{th} \quad (26)$$

Where E_c is the internal energy relative to 0K, that can be defined by CW2 equation or HZ model (Heuzé et al. 2001; Heuzé 2001) and E_{th} is the internal energy relative to thermal energy, that can be represented by Debye Model (Anderson 1995).

$$E_{th} = \frac{9nRT}{\left(\frac{\theta_D}{T}\right)^3} \int_0^{\frac{\theta_D}{T}} \frac{z^3}{e^z - 1} dz \quad (27)$$

With $z = \frac{\hbar\, \omega}{k\, T}$, where n are the number of modes, θ_D is the Debye Temperature, k is the Boltzmann's Constant, ω represents the frequency, $\hbar = \frac{h}{2\,\pi}$ with h the Planck's Constant .

The formulation represented above can lead to the Debye function

$$D\left(\frac{\theta_D}{T}\right) = 3\left(\frac{T}{\theta_D}\right)^2 \int_0^{\frac{\theta_D}{T}} \frac{z^3}{e^z - 1} dz \quad (28)$$

For Entropy calculation the same method could be applied, as above, for a better accuracy. The Entropy S can be defined as (Blanco 1986):

$$dS = \left(\frac{\partial S}{\partial V}\right)_T dV + \left(\frac{\partial S}{\partial T}\right)_V dT \quad (29)$$

As

$$\left(\frac{\partial S}{\partial V}\right)_T = \left(\frac{\partial P}{\partial T}\right)_V \quad (30)$$

$$dS = \left(\frac{\partial P}{\partial T}\right)_V dV + \left(\frac{\partial S}{\partial T}\right)_V dT \quad (31)$$

That could also be represented for a given temperature:

$$S = \int_{Vo}^{V} \left(\frac{\partial P}{\partial T}\right)_V dV \quad (32)$$

Given this equations, the Entropy can also be described by other semi-empirical models and equations, as the one that will be here implemented given its high accuracy and simple representation, the CW2 model (Heuzé 2001).

The implementation of this approach, both for the calculation of internal energy and entropy, requires the introduction of new parameters which will be presented and defined in the next subchapter. The parameters derived will have a further introduction in THOR Database, which as the model already implemented to represent condensed carbon phases (Graphite and Diamond). This representation proves the validity of the approach and shows the effect on temperature and pressure with condensed species formation (Campos et al. 2008), however a review on this equations parameters for carbon species will also be made in order to prove the validity of the parameters extrapolation method.

The parameters used in this model are known only for common and well-studied products, for that reason the objective of this work is to find this parameters for the Metal Oxides presented. In the next subchapter these parameters are presented and defined.

3.3.1. Energetic Model Parameters for Solids

Calculation of condensed species product formation can be modeled through the use of the energetic equation of state presented before. This implementation needs the values

of density (ρ), bulk sound velocity (C_0) and S_0 (slope in U_S-U_P relation), Grüneisen parameter (γ), Debye temperature (θ_D) , entropy ($S_{formation}$) and enthalpy ($H_{formation}$) of formation, that could be inscribed in THOR Database. Consequently, any existing condensed specie implies the previous knowledge of these parameters, specially the Grüneisen parameter which translates the relation between thermomechanical and energetic behavior under high pressure condition.

3.3.1.1. Bulk Sound velocity C_0 and S_0

These two parameters can be defined by the equation between shock velocity (U_S) and particle velocity (U_P) (Marsh 1980):

$$U_S = C_0 + S_0\, U_P + Q\, U_P{}^2 \quad (33)$$

However for most solids this relation turn to be linear, being:

$$U_S = C_0 + S_0\, U_P \quad (34)$$

Where C_0 represents the bulk sound velocity at zero pressure and S_0 is the slope in the relation of shock velocity to shock particle velocity. These parameters are obtained from Shock Hugoniot experimental data, through the method of least squares, and it represents the dynamic behavior of the material.

The sound velocity can also be represented by the longitudinal sound velocity V_l, a static measure of the material. However for the equations presented above the C_0 is preferably used.

3.3.1.2. Debye Temperature

To impose a finite limit on the number of modes in the solid, Debye used a maximum allowed phonon frequency, called the Debye frequency ω_D (Anderson 1995). The Debye temperature is a constant associated with this frequency:

$$\theta_D = \frac{\hbar\, \omega_D}{k} \quad (35)$$

3.3.1.3. Grüneisen Parameter

The Grüneisen Parameter is important for the description of condensed species. It is defined as

$$\gamma = V \left(\frac{\partial P}{\partial E}\right)_V \quad (36)$$

γ is a measure of the change in pressure produced by a change in system total energy under the condition of constant volume (Harris 1972). This means that when condensed species are formed, the pressure of the Reactive System will drop and energy will be released from that change of state, being γ the relation between them.

By a macroscopic thermomechanical consideration (Harris 1972)

$$\gamma = V \left(\frac{\partial P}{\partial E}\right)_V = V \frac{\left(\frac{\partial P}{\partial T}\right)_V}{\left(\frac{\partial E}{\partial T}\right)_V} \quad (37)$$

And

$$\alpha = \frac{1}{V}\left(\frac{\partial V}{\partial T}\right)_P \quad (38)$$

$$B_0 = -V\left(\frac{\partial P}{\partial V}\right)_T \quad (39)$$

$$C_V = \left(\frac{\partial E}{\partial T}\right)_V \quad (40)$$

Therefore

$$\gamma = \frac{V}{C_V}\left(\frac{\partial P}{\partial T}\right)_V \quad (41)$$

And most Grüneisen parameters are calculated by

$$\gamma = \frac{V\ \alpha\ B_0}{C_V} \quad (42)$$

Another way to define Grüneisen is through vibration modes (Poirier 2000), being

$$\gamma_i = -\frac{\partial \ln w_i}{\partial \ln V} \quad (43)$$

With this two definitions it's possible to derive the next three equations, as shown in Figure 14.

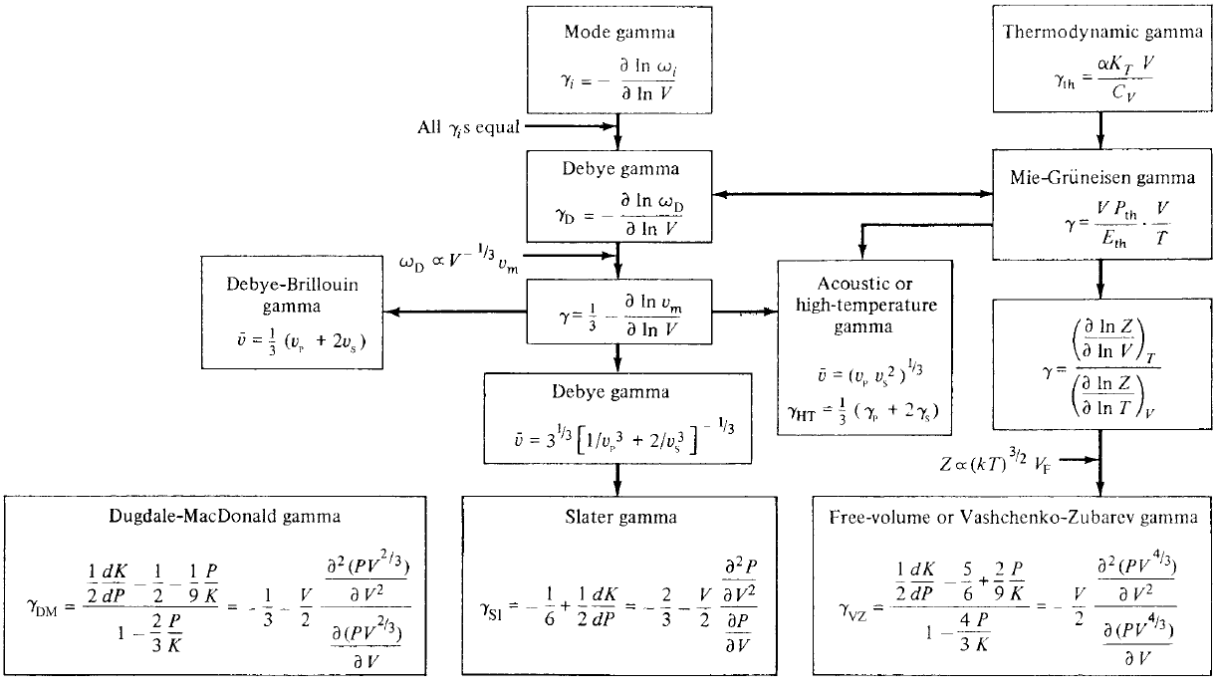

Figure 14 - Relations among the various definitions of the Grüneisen parameter (Poirier 2000)

This equations represent a simplified γ, they are:

Slater γ_S (Poirier 2000)

$$\gamma_S = -\frac{1}{6} - \frac{1}{2}\frac{\partial \ln B}{\partial \ln V} \tag{44}$$

$$\gamma_S = -\frac{2}{3} - \frac{V}{2}\frac{\left(\frac{\partial^2 P}{\partial V^2}\right)_T}{\left(\frac{\partial P}{\partial V}\right)_T} \tag{45}$$

Which explicitly depends on the assumption that Poisson's ratio is independent of volume or pressure. All the vibrational modes are equal.

Dugdale and MacDonald γ_{DM} (Dugdale & MacDonald 1953)

$$\gamma_{DM} = -1 - \frac{V}{2}\left(\frac{\frac{\partial^2 P}{\partial V^2} - \frac{10}{9}\frac{P}{V^2}}{\frac{\partial P}{\partial V} + \frac{2}{3}\frac{P}{V}}\right) \tag{46}$$

Dugdale and MacDonald proposed this expression in order to correct the alleged error by slater, in neglecting the effect of finite strain under applied pressure (Poirier 2000). DM used a simplification of lattice undergoing one-dimensional harmonic oscillations.

Vachenko and Zubarev γ_{VZ} (Poirier 2000)

$$\gamma_{VZ} = -\frac{V}{2}\left(\frac{\frac{\partial^2(P\,V^{\frac{4}{3}})}{\partial V^2}}{\frac{\partial(P\,V^{\frac{4}{3}})}{\partial V}}\right) \quad \textbf{(47)}$$

This equation was an improvement of DM, considering three-dimensional oscillations of a lattice with interatomic interactions described by an anharmonic central potential.

Giving the importance of these parameter, in section 5 , it will be derived for each material through different methods and analyzed the sensibility of THOR with this parameter, section 7.1.

4. CASES STUDIED – THERMAL EQUATION OF STATE

In this section were studied and reviewed multiple papers in order to derive an Equation of State for each material at a given phase.

The following graphics include points (which were directly obtained from papers) and lines (which represent the Equations of State presented above, with parameters also obtained from papers).

4.1. Cowan and Fickett EoS Adaptation

In this work, Cowan and Fickett EoS is used to describe solids, thanks to its empirical form, which can be modulated to represent with great accuracy the data from the papers analyzed, and its easy to derive formulation in calculation methods.

The detonation products of explosives can include solid products such as graphite. Due to the very high detonation pressures of condensed-phase explosives, the compressibility of solid carbon becomes significant and the volume occupied by the solid carbon in the detonation products should be corrected. To describe the state of the solid carbon (graphite) in detonation products, an equation of state was developed by Cowan and Fickett (Cowan & Fickett 1956):

$$P = p_1(\eta) + a(\eta)\mathrm{T} + b(\eta)T^2 \quad \textbf{(48)}$$

$$\eta = \frac{\rho}{\rho_0} \quad \textbf{(49)}$$

Where $p1(\eta), a(\eta), b(\eta)$ are polynomial functions in Cowan and Fickett EOS. Which Cowan & Fickett, 1956, with P in Mbar and *T* in volts (i.e., in units of 11 605.6°K), derived for graphite as:

$$p1(\eta) = -2.467 + 6.769\eta - 6.956\eta^2 + 3.040\eta^3 - 0.3869\eta^4 \quad (50)$$

$$a(\eta) = -0.2267 + 0.2712\eta \quad (51)$$

$$b(\eta) = 0.08316 - 0.07804\eta^{-1} + 0.03068\eta^{-2} \quad (52)$$

In this work, this equation is adjusted, revising its polynomials in order to better fit the experimental and theoretical data from other studies and well represent solid phases for condensed phase detonation product species, with P in GPa and *T* in K.

As described earlier the solids in study are: Carbon (for revision and comparison), Alumina, Zirconia, Titania and Magnesia.

For these materials the polynomial functions $p1(\eta), a(\eta), b(\eta)$are written in the form:

$$p1(\eta) = a + b\eta + c\eta^2 \quad (53)$$

$$a(\eta) = \tau + \beta\eta + \mu\eta^2 \quad (54)$$

$$b(\eta) = \varphi + \delta\eta + \varkappa\eta^2 \quad (55)$$

The constant parameters: a, b, c, τ, β, μ, ϕ, δ, χ are derived in this chapter, in order to best describe the P-V-T relation of each material and phase presented in section 1.4

4.2. Carbon

4.2.1. Graphite

Table 1 synthetizes the papers data, both experimental and theoretical, the method and equation used to describe it. The letters in brackets indicate the type of EoS used.

Table 1 – Graphite Papers Data

	Technique	Paper	B0 [GPa]	B'0	T [K]	Pmax [GPa]	Tmax [K]
Exp	X-Ray Diffraction	(Lynch & Drickamer 1966)			298		
	Shock Hugoniot	(Doran 1963)					
	Shock Hugoniot	(Coleburn 1964)					
	Shock Hugoniot	(Marsh 1980)					
	Shock Hugoniot	(Gust 1980)					
	X-Ray Diffraction	(Hanfland et al. 1989) (M)	33.8	8.9	298	14	
	Shock Hugoniot	(Cowan & Fickett 1956)					
	Neutron Diffraction	(Lowitzer et al. 2006)					
	Neutron Diffraction	(Lowitzer et al. 2006) (V+HT)	38	9	298	6	1250
Theo	Thermal Pressure Approach	(Van Thiel & Ree 1989) (BM+MG)	51.1	5	0		
	Monte Carlo Simulation	(Colonna et al. 2011) (BM+HT)	36.27	9.73	0	20	2500
	Isotherm Calculation	(Coleburn 1964)			298		

Figure 15 represents these data at T=298K.

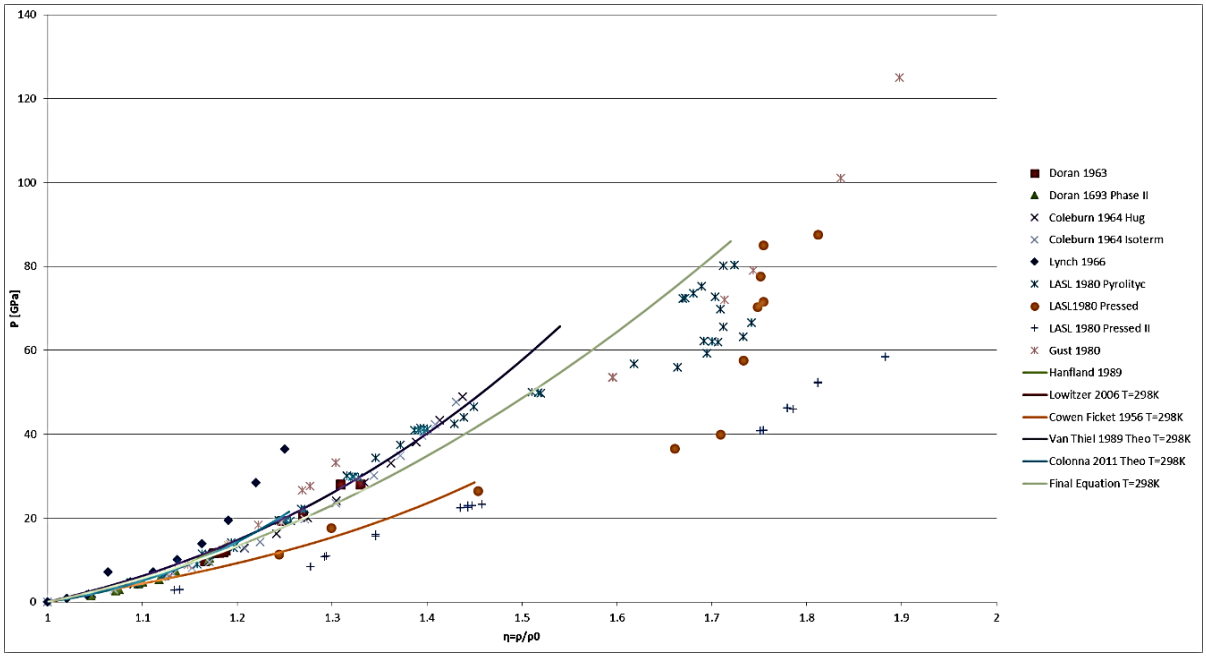

Figure 15 - Graphite EoS

The graphic represented above has a high scattered data, according to the different types of graphite used in each study. It also shows that the shock Hugoniot data of pressed graphite has a lower pressure for the same η than the data of Pyrolytic graphite. The equation derived by Cowan & Fickett, 1956, shows great agreement to the pressed graphite, which allows to determine that this was the material used in the experiments.

Analyzing data exclusively for Pyrolytic graphite, with most interest given its highest ρ_0, almost all data are in good correlation up until η=1.4, except Lynch & Drickamer, 1966.

For P-V-T relation is also necessary P-V data at other Temperatures. These relations are represented in the following graphics (Figure 16, Figure 17, Figure 18). For other temperatures, ρ_0 is equal to ρ_0 at T_0.

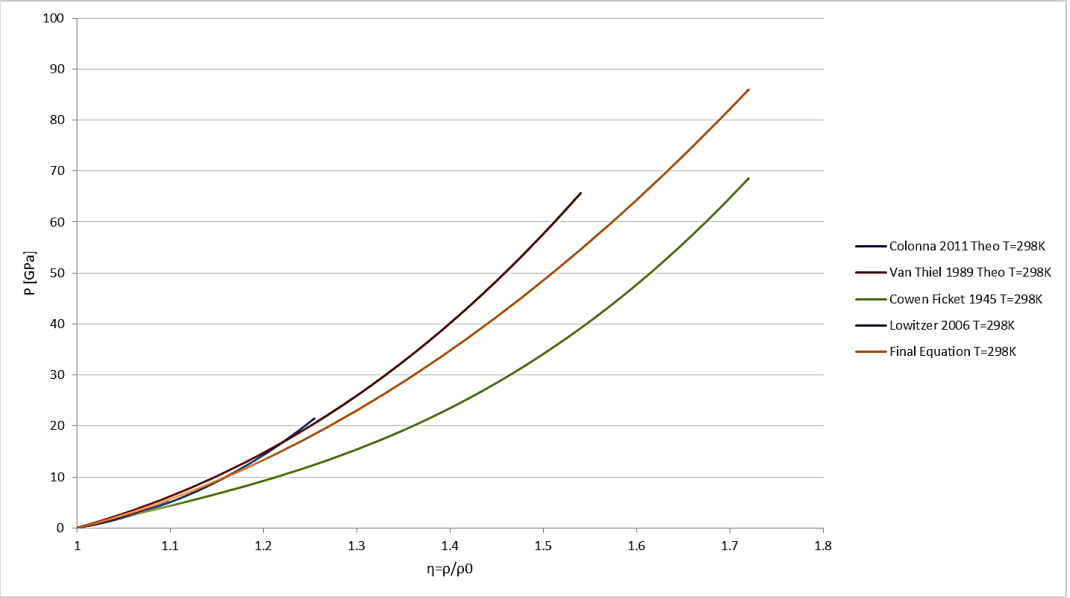

Figure 16 - Graphite EoS T=298K

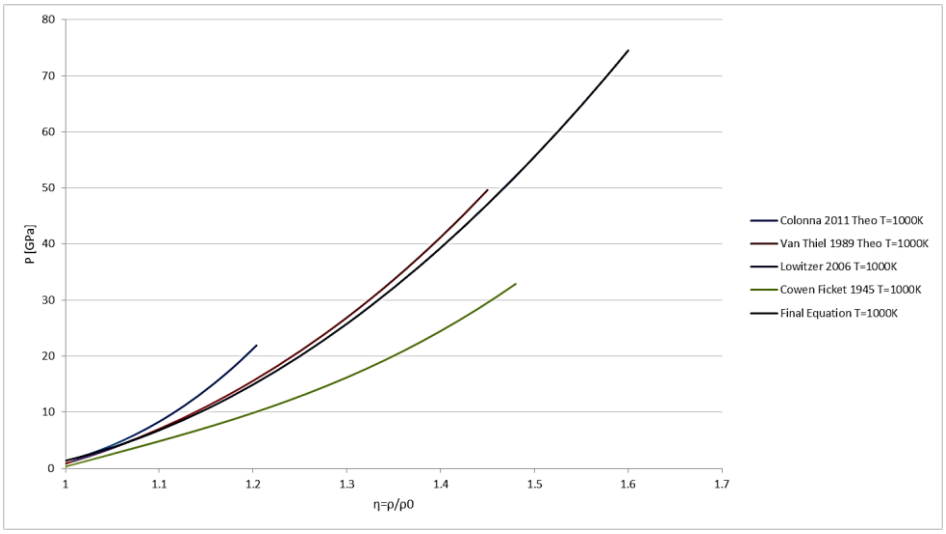

Figure 17 - Graphite EoS T=1000K

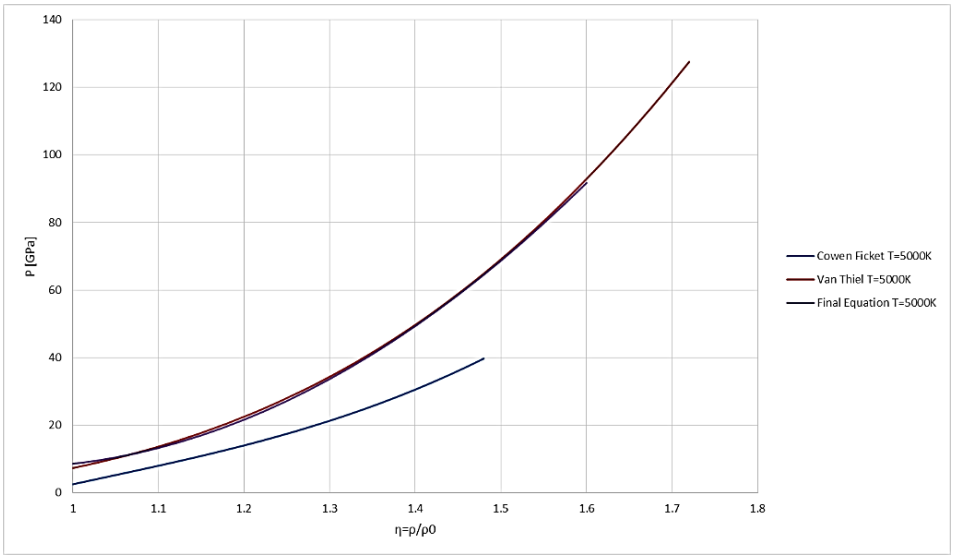

Figure 18 - Graphite EoS T=5000K

The solid EoS developed, as presented before, is a Cowen and Fickett EoS with the form:

$$P = p_1(\eta) + a(\eta)\mathrm{T} + b(\eta)T^2 \quad \textbf{(56)}$$

With

$$p1(\eta) = \mathrm{a} + \mathrm{b}\eta + \mathrm{c}\eta^2 \quad \textbf{(57}$$

$$a(\eta) = \alpha + \beta\eta + \mu\eta^2 \quad \textbf{(58)}$$

$$b(\eta) = \varphi + \delta\eta + \varkappa\eta^2 \quad (59)$$

With solver method in excel (that uses a non-linear GRG method) are obtained the coefficients a', b´ and c', for a second degree equation of P-η relation (suitable analytic representation):

$$P = a' + b'\eta + c'\eta^2 \quad (60)$$

This equation is derived for each temperature, giving table 2 as a result.

Table 2 - Extrapolated Coefficients for Graphite

T	a'	b'	c'
298	40.89765	-129.528	88.6306
750	114.7545	-265.998	152.6117
1000	114.7545	-265.998	152.6117
1500	118.2744	-271.149	155.0138
2000	133.2299	-295.006	164.9505
3000	148.4139	-318.264	174.8854
5000	168.3319	-347.853	188.0845

At T=298K the coefficients were extrapolated from all data for pyrolytic graphite, except Lynch & Drickamer, 1966. At higher temperatures, the coefficients were deduced from Van Thiel & Ree, 1989, which is in good agreement with Lowitzer et al., 2006, experimental data.

With these values defined is possible to make the final relation, the relation with temperrature, resulting in the Final Equation of State given by:

$$P = (34.9346 - 120.209\eta + 84.69398\eta^2) + (0.069307 - 0.12537\eta + 0.058024\eta^2)T + (-8.7 * 10^{-6} + 1.64 * 10^{-5}\eta - 7.7 * 10^{-6}\eta^2)T^2 \quad (61)$$

With ρ_0=2.21 g/cm^3 (for T_0=298K)

The equation derived is represented in all the graphics above as Final Equation and shows good correspondence with other data for pyrolytic graphite. At T=298K and low pressure, represents with excelent acccuracy the data from other studies. This equation is valid up until T=5000K, showing excelent agreement with the values from Lowitzer et al., 2006, at high temperature.

4.2.2. Diamond

Table 3 synthetizes the papers data, both Experimental and Theoretical, and the method and equation used to describe it.

Table 3 - Diamond Data

	Technique	Paper	B0 [GPa]	B'0	T [K]	Pmax [GPa]	Tmax [K]
Exp	Shock Hugoniot	(Ahrens & Kondo 1983)					
	Ultrasonic	(Ahrens & Kondo 1983) derived from McSkimin 1972 (M)	442.3	4.03	298		
	x-Ray Diffraction	(Fujihisa et al. 1996) (BM)	440	4	298	35	
	x-Ray Diffraction	(Gillet et al. 1999) Diamond C12			298		
	x-Ray Diffraction	(Gillet et al. 1999) Diamond C12 II			298		
	x-Ray Diffraction	(Gillet et al. 1999) Diamond C13 I e II			298		
	Shock Hugoniot	(Hicks et al. 2008)					
	Shock Hugoniot	(Marsh 1980)					
	DAC	(Occelli et al. 2003) (V)	446	3	298	140	
	x-Ray Diffraction	(Dewaele et al. 2008)				80	900
	x-Ray Diffraction	(Dewaele et al. 2008) (V+MG)	444.5	4.18	298	80	900
Theo	Ab-Initio Calculations Pseudopotential	(Fahy & Louie 1987) Cubic Diamond (M)	444	3.24	0		
	Ab-Initio Calculations Pseudopotential	(Fahy & Louie 1987) Hexagonal Diamond (M)	440	3.5	0		
	Ab-Initio Calculations DFT LDA	(Kunc et al. 2003) (V)	465	3.63	0	140	
	Ab-Initio Calculations DFT GGA	(Kunc et al. 2003) (V)	433	3.67	0	140	
	Thermal Pressure Approach	(Van Thiel & Ree 1989) (BM+MG)	439.7	3.65	0		

The data presented above is represented in Figure 19 at T=298K, except for Fahy & Louie, 1987, and Kunc et al., 2003, that are represented at T=0K.

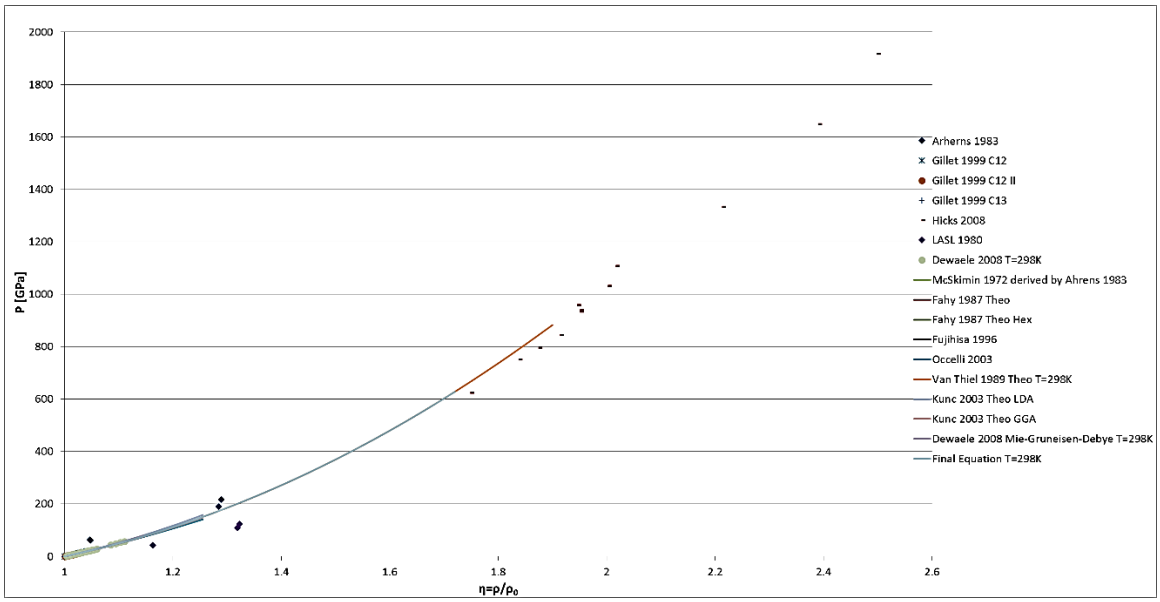

Figure 19 - Diamond EoS

From the graphic above is easy to perceive the excellent correlation between data, except for Ahrens & Kondo, 1983, and Marsh, 1980. Even at very high pressures, the equation of Van Thiel & Ree, 1989, shows an excellent agreement with experimental data from Hicks et al., 2008.

For P-V-T relation is also required P-V data at other Temperatures (Dewaele et al. 2008; Van Thiel & Ree 1989). In the following graphic, as an example, one of this relations is represented, for T=900K, and show excellent agreement between the data. For other temperatures, ρ_0 is equal to ρ_0 at T_0.

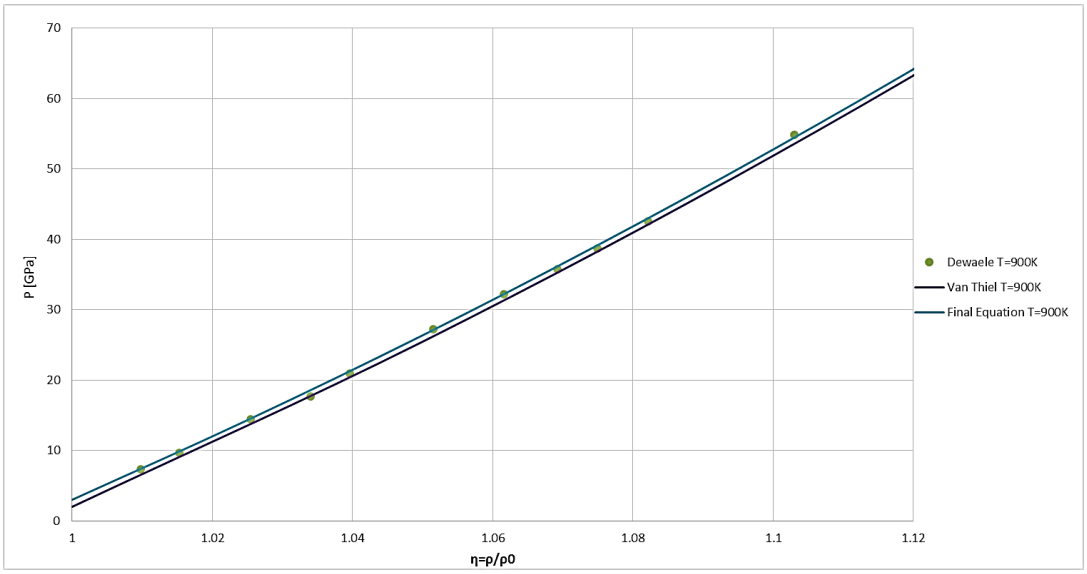

Figure 20 - Diamond EoS T=900K

As for graphite the same extrapolation method was used. At T=298K the coefficients were extrapolated from McSkimin & Andreatch, 1972; Gillet et al,. 1999; Dewaele et al., 2008; Fahy & Louie ,1987; Fujihisa et al., 1996; Van Thiel & Ree, 1989. At higher temperatures, the coefficients were deduced from Van Thiel & Ree, 1989, and Dewaele et al., 2008, experimental points.

The Final Equation of State is given by:

$$P = (166.3728 - 772.409\eta + 604.6547\eta^2) + (0.004931 - 0.00011\eta + 3.52 * 10^{-5}\eta^2)T + (2.61 * 10^{-8} + 1.09 * 10^{-8}\eta - 3.5 * 10^{-9}\eta^2)T^2 \quad (62)$$

With ρ_0=3.51 g/cm^3 (for T_0=298K)

The equation derived is represented in the graphic above and show good agreement with other data, up until T=10000K.

4.3. Alumina

For this material several phases were studied, as: Corundum (most important phase for pressures and temperatures of this production process) and Rh_2O_3(II)-Type, Perovskite and $CaIrO_3$-Type (represented in annex A).

4.3.1. Corundum

Table 4 synthetizes this data, the method and equation used to describe it. Most of experimental P-V relations were obtained from Shock Hugoniot. In this case, are also presented another parameters S_0 and C_0, which represent the relations of shock velocity vs particle velocity in Hugoniot ($U_S=S_0.U_P+C_0$).

Table 4 – Corundum Data

	Technique	Paper	EoS					Hugoniot	
			B0 [GPa]	B'0	T [K]	Pmax [GPa]	Tmax [K]	S_0	C_0
Exp	Shock Hugoniot	(Kleiser et al. 2011)						1.299	7.455
	Shock Hugoniot	(Marsh 1980)							
	Shock Hugoniot	(Mashimo et al. 1988)							
	DAC	(Sato & Akimoto 1979)			298				
	X-Ray Diffraction	(Lynch & Drickamer 1966a)			298				
	Ultrasonic Interferometry	(Schreiber & Anderson 1966)			298				
	Shock Hugoniot	(Ahrens et al. 1968)							
	Shock Hugoniot	(Gust & Royce 1971)							
	Shock Hugoniot	(Gust & Royce 1971) (M)	251	4.2					
	Shock Hugoniot	(Mashimo et al. 2000)							
	Shock Hugoniot	(Munson & Lawrence 1979)						1.28	8.14
	Linear Compression	(Bridgman 1949)							
	Shock Hugoniot	(Reinhart & Chhabildas 2003)							
	Shock Hugoniot	(Anderson 1995) (MB)	252	3.99					
	X-Ray Diffraction	(Dubrovinsky et al. 1998) (MB+HT)	258	4.88	300	68	1500		

	X-Ray Diffraction	(Dewaele & Torrent 2013)			298	165			
	X-Ray Diffraction	(Dewaele & Torrent 2013) (V)	254.1	4	298	165			
Theo	Ab-Initio Calculations DFT LDA	(Oganov & Ono 2005) (V)	252.6	4.237	0				
	Ab-Initio Calculations DFT LDA	(Caracas & Cohen 2005) (V)	248	4.13	0				
	LCGTO-FF	(Boettger 1997)(MB)	243.8	4.305	0	175			
	Ab-Initio Calculations DFT LDA	(Tsuchiya et al. 2005) (MB)	240.5	3.94	0	80			
	Ab-Initio Calculations DFT LDA	(Iuga et al. 2007)(MB)	241	4	0				
	Ab-Initio Calculations DFT LDA	(Thompson et al. 1996)(MB)	258.9	4.01	0				

Figure 21 represents these data at T=298K and also Theoretical calculations, at T=0K.

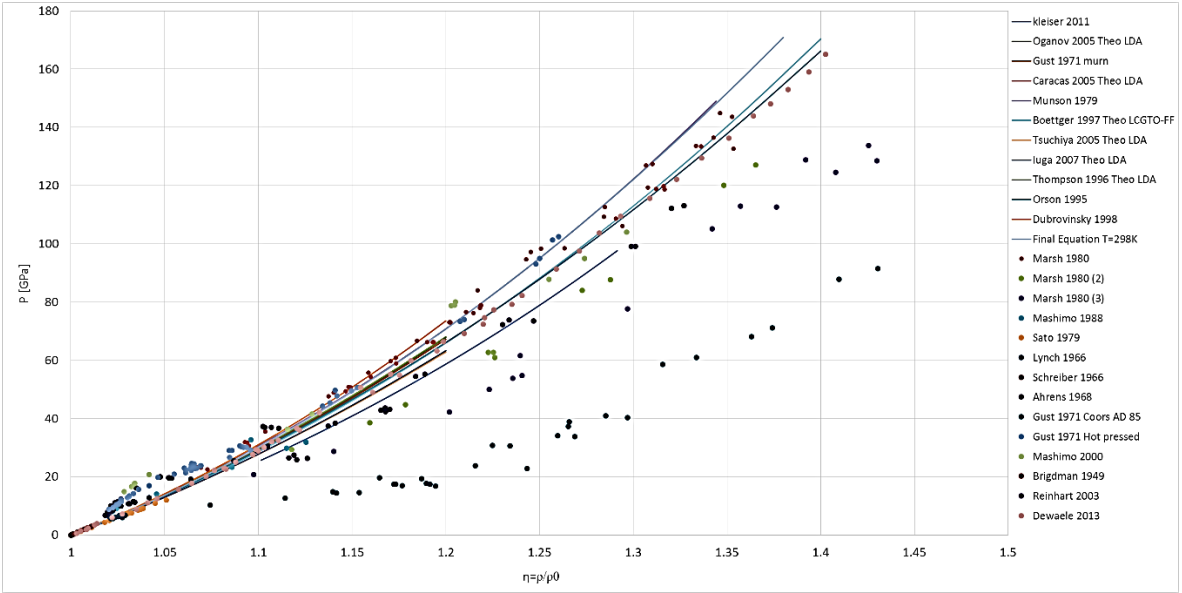

Figure 21- Corundum EoS

The graphic above has a high scattered data because it represents different types of Alumina. It shows that Gust & Royce, 1971, for Coors AD 85 material takes

great differences in Pressure-Volume relation, because its ρ_0 is lower than normal. Also Marsh, 1980, (2) and (3) have the same behavior.

For this reason an analysis in P-V relations without this data and theoretical calculations was made, perceiving a better correlation between the data and also the difference between the Hugoniot curve and Isotherm curve. For P-V-T relation is also necessary P-V data at other Temperatures, which can be obtained from Dubrovinsky et al., 1998, experimental data.

The solid EoS developed is obtained for T=298K with the data explicated before, with special focus on Dewaele & Torrent, 2013, and for higher T with Dubrovinsky et al., 1998. This data is represented by a High Temperature EoS, where $\eta=\rho/\rho_0$, however this ρ_0 depends on the temperature that each equation P-η is made. For this reason, it became necessary to make a change of variable in order to make the Cowan Fickett EoS, transforming each η into $\eta_{298K}= \rho/\rho_{0/298K}$. This means that, as before for other temperatures, ρ_0 is equal to ρ_0 at T_0.

Resulting:

$$P = (186.5879 - 639.35\eta + 449.0011\eta^2) + (0.351143 - 0.63477\eta + 0.296485\eta^2)T + (-5.2 * 10^{-5} + 9.41 * 10^{-5}\eta - 4.3 * 10^{-5}\eta^2)T^2 \quad (63)$$

With ρ_0=3.51 g/cm^3 (for T_0=298K)

The equation derived is represented in the graphic above and show good agreement with other data, up until T=5000K.

4.4. Zirconia

Through this work this material was studied for different phases. These phase were: Cubic Fluorite Structure (most important phase given its properties and possible stabilization at ambient temperature, see section 7.2.3), Monoclinic, Tetragonal, OrthoI and Ortho II (represented in annex A).

4.4.1. Cubic Fluorite Structure

In Table 5 and Figure 22 are represented the data from the papers studied, for this phase only theoretical results are found.

Table 5 - Cubic Fluorite Data

	Technique	Paper	B0 [GPa]	B'0	T [K]	Pmax [GPa]	Tmax [K]
Theo	Ab-Initio Calculations DFT LDA	(Dewhurst & Lowther 1998) (MB)	267	4.42	0		
	Ab-Initio Calculation DFT GGA	(Jaffe et al. 2005)(M)	251	4	0		
	Ab-Initio Calculation DFT GGA	(Terki et al. 2006)(M)	236.57	4.06	0		
	Ab-Initio Calculation DFT LDA	(Jaffe et al. 2005)(M)	278	4	0		
	Ab-Initio Calculation DFT GGA	(Zhao et al. 2011) (M)	215.8	4.43	0		
	Ab-Initio Calculation DFT LDA	(Zhao et al. 2011) (M)	226.1	4.21	0		
	Ab-Initio Calculation DFT LDA	(Lowther et al. 1999) (MB)	267	4.42	0		
	Ab-Initio Calculation DFT LDA	(Stapper et al. 1999) (M)	268	3.6	0		
	Ab-Initio Calculation DFT LDA	(Dash et al. 2004) (M)	269	4	0		

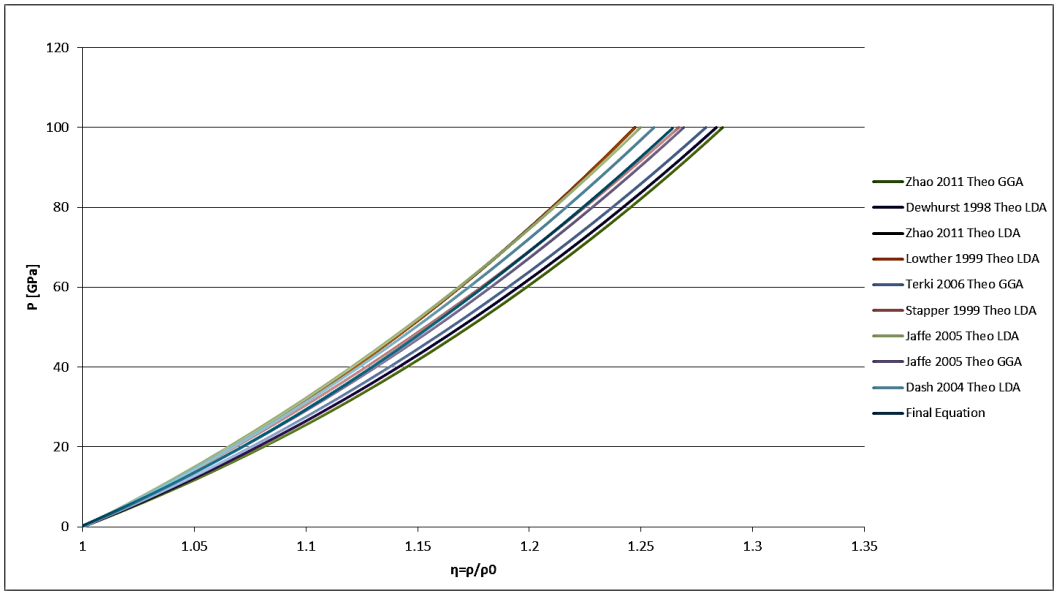

Figure 22 - Cubic Fluorite EoS

The solid EoS is only defined for one temperature (T=0K) as no data is available for other T. Making an average of the curves presented, the final equation is:

$$P = (279.6989 - 798.48\eta + 519.0639\eta^2) \quad (64)$$

With ρ_0=6.2 g/cm^3 (for T_0=298K and P=0 GPa) (Ingel & Lewis III 1986).

4.5. Titania

As presented in Figure 8, Titania can present different structures depending on the pressure and temperature. These phase are studied in this work: Rutile (most important to consider given its abundant presence), Anatase, Brookite, Columbite, Baddeleiyte, OrthoI, Ortho II and Cubic Fluorite Phase (represented in annex A).

4.5.1. Rutile

This phase of TiO_2 is the most abundant in nature and is well studied for T=298K. In the next table and Figure 23 are represented the equation of state from the studied papers.

Table 6- Rutile Data

	Technique	Paper	B0 [GPa]	B'0	T [K]	Pmax [GPa]	Tmax [K]
Exp	X-ray Diffraction	Hazen 1981			298		
	X-ray Diffraction	(Gerward & Staun Olsen 1997) (MB)	230	6.6	298	8	
	X-ray Diffraction	(Ming & Manghnani 1979)			298		
	X-ray Diffraction	(Olsen et al. 1999) (MB)	210	6.6	298	10	
	X-ray Diffraction	(Al-Khatatbeh et al. 2009) (MB)	235	4	298		
Theo	Ab-Initio DFT GGA	(Swamy & Muddle 2007) (MB)	215	5.35	0		
	Ab-Initio B3LYP	(Swamy & Muddle 2007) (MB)	224	5.64	0		
	Ab-Inition Calculation DFT LDA	(Mo & Ching 1995) (M)	209.34	6.11	0		

	Ab-Inition Calculation DFT LDA	(Al-Khatatbeh et al. 2009) (MB)	250	4	0		
	Ab-Inition Calculation DFT GGA	(Al-Khatatbeh et al. 2009) (MB)	216	4	0		
	PAW-GGA	(Wu et al. 2010) (MB)	206	5.2	0		
	Ab-Inition Calculation DFT LDA	(Iuga et al. 2007) (MB)	235	4	0		
	PBE	(Koči et al. 2008) (MB)	200	5.75	0		

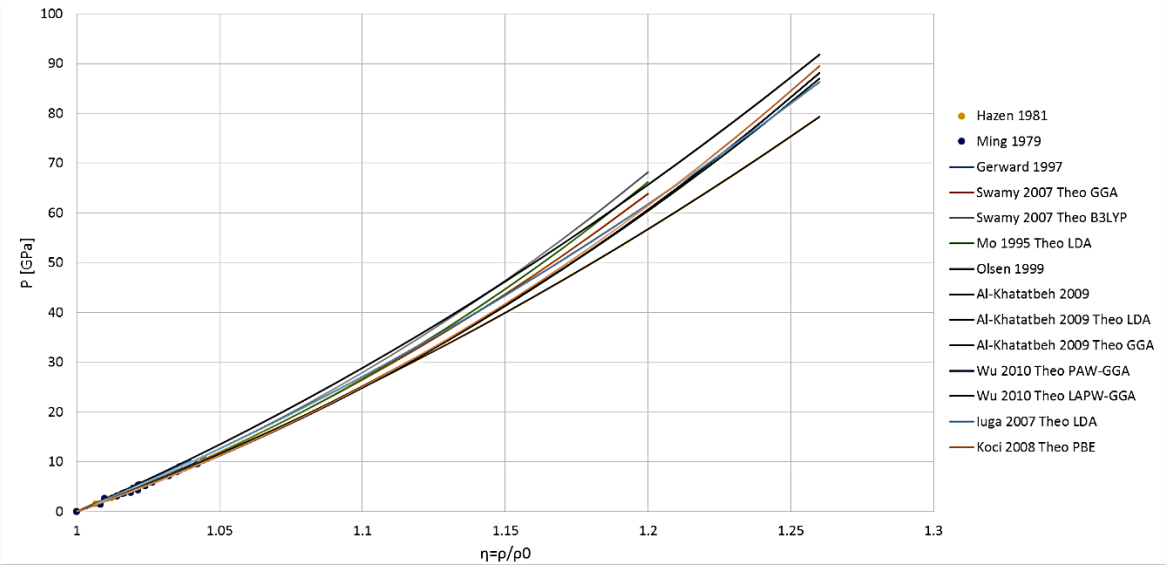

Figure 23 - Rutile EoS

It was denoted that for low pressure, data was very well defined, however at high pressure, data is unclear, hence only experimental data is considered.

With data for only T=298K, the derived equation of state will be independent on the temperature. The Solid EoS is:

$$P = (154.740 - 540.4612\eta + 385.815\eta^2) \quad \textbf{(65)}$$

With ρ_0=4.2485 g/cm^3 (for T_0=298K and P=0 GPa) (Gerward & Staun Olsen 1997)

4.6. Magnesia

For magnesia both B1 and B2 phase were studied, with the main focus in B1 (B2 represented in annex A)

4.6.1. B1

Table 7 synthetizes the papers data, both experimental and theoretical, and the method and equation used to describe it.

Table 7 - B1 Data

	Technique	Paper	B0 [GPa]	B'0	T [K]	Pmax [GPa]	Tmax [K]
Exp	Shock Huguniot	(Ahrens et al. 1968)					
	Shock Huguniot	(Marsh 1980)					
	Neutron Diffraction	(Lowitzer et al. 2006) (V+HT)	159.6	3	298	6	1250
	X-ray Diffraction	(Marquardt et al. 2011) nanoparticle RUN1 (MB)	185.8	4	298	46	
	X-ray Diffraction	(Marquardt et al. 2011) nanoparticle RUN2 (MB)	173.9	4	298	66	
	X-ray Diffraction	(Marquardt et al. 2011) nanoparticle RUN3 (MB)	145.8	4	298	45	
	X-ray Diffraction	(Marquardt et al. 2011) nanoparticle RUN4 (MB)	146.7	4	298	42	
	X-ray Diffraction	(Speziale et al. 2001)			300		
	X-ray Diffraction	(Fei 1999) Ne medium - NaCl			300		
	X-ray Diffraction	(Fei 1999) NaCl medium - Au			300		
	X-ray Diffraction	(Fei 1999) NaCl medium - NaCl			300		
	X-ray Diffraction	(Dewaele et al. 2000)					2500
	X-ray Diffraction	(Mao & Bell 1979)			298		
	X-ray Diffraction	(Zha et al. 2000) (BM)	162.5	3.99	300	55	
	X-ray Diffraction	(Jacobsen et al. 2008)			300		
	X-Ray Diffraction	(Fei 1999)NaCl medium - NaCl			1100		
	X-Ray Diffraction	(Fei 1999) NaCl medium - Au			1100		
	X-ray Diffraction	(Zhang 2000)					1073
Theo	PIB	(Isaak 1990) (MB)	183.1	3.95	300	150	3000
	High Temperature EoS	(Anderson & Zou 1990) (MB+HT)	166.2	4.07	0		

	Molecular Dynamics	(Matsui et al. 2000) (MB)	160.5	4.1	0	100	3000
	Ab-Initio Calculations DFT GGA	(Mukherjee et al. 2013) (MB)	157.2	3.97	300		
	Ab-Initio Calculations DFT GGA	(Vahora et al. 2013) (MB)	157.2	3.97	0		
	Ab-Initio Calculations DFT GGA	(Gueddim et al. 2009) (BM)	145.68	4.23	0		
	Ab-Initio Calculations DFT GGA	(Schleife et al. 2006) (BM)	148.6	4.3	0		
	Ab-Initio Calculations DFT GGA	(Jaffe et al. 2000) (M)	169.1	3.28	0		
	Thermal Pressure Approach	(Jin et al. 2010)				300	3000
	Thermal Pressure Approach	(Speziale et al. 2001) (MB+MG)	170	3.59	300		

In Figure 24 are represented all the data for T=298 or 300K and also at T=0K, for the theoretical results that are not represented at other temperatures.

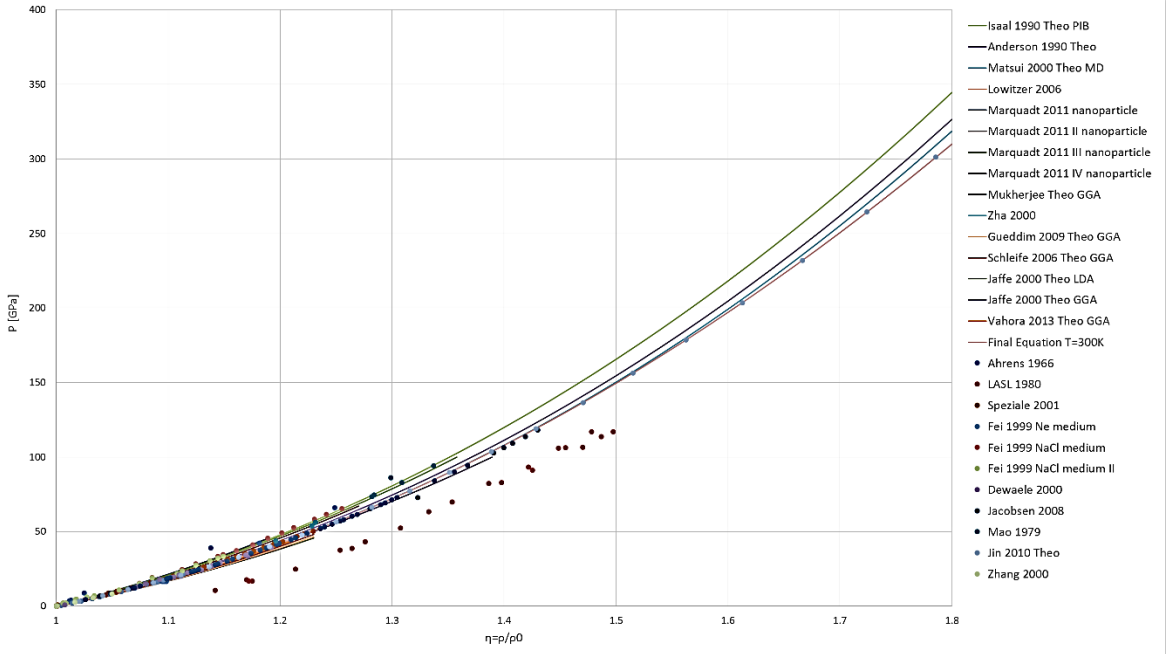

Figure 24 - B1 EoS

The graphic above denotes a good correlation between data, however Marsh, 1980, have a different correlation, because ρ_0 is lower than the normal value. With a better analysis only for experimental results, it demonstrates some scattered data, however it shows an excellent relation between Speziale et al., 2001, Jacobsen et al., 2008, and Dewaele et al., 2000, data used for the construction of the solid EoS at T=300K. This EoS is in very good agreement with Jin et al., 2010, Thermal Pressure Approach.

For P-V-T relation it is also necessary P-V data at other Temperatures, which can be obtained from Jin et al., 2010, Thermal Pressure Approach. This data is in excellent agreement with data for high temperatures (Matsui et al. 2000; Lowitzer et al. 2006; Fei 1999; Dewaele et al. 2000; Zhang 2000).

With this data the Solid EoS is derived:

$$P = (143.0449 - 439.967\eta + 295.3922\eta^2) + (0.005978 + 0.000107084\eta - 3.49204 * 10^{-5}\eta^2)\mathrm{T} + (2.10684 * 10^{-8} - 2.7654 * 10^{-8}\eta + 8.81202 * 10^{-9}\eta^2)T^2 \quad (66)$$

With ρ_0=3.585 g/cm3 (for T0=298K) (Zha et al. 2000)

5. CASES STUDIED - GRÜNEISEN PARAMETER

In thermochemical codes, Grüneisen parameter is a value that translates the relation between ΔP and ΔE. For this matter, is an important coefficient to account for. There are many ways of calculating the Grüneisen Parameter. The most common is:

$$\gamma = \frac{V\ \alpha\ B_0}{C_V} \tag{67}$$

This formula uses parameters that can be easily derived from experimental tests. However, by definition it leads to:

$$\gamma_{Cv} = \frac{V}{C_V}\left(\frac{\partial P}{\partial T}\right)_V \tag{68}$$

For the extrapolation of this parameter with the presented equation, are used P-V-T relations (derived in this work) and C_V functions of temperature (from other papers), and compared with Slater, Dugdale and MacDonald and Vachenko & Zubarev equations (also using the derived P-V-T relations). The obtained values will be compared with Grüneisen parameters derived by other authors.

5.1. Carbon

5.1.1. Graphite

For graphite, the first approach is made by the equation γ_{Cv}. This requires to take the P(V,T) derivative (easy to infer for a Cowan Fickett EoS) and to obtain C_v function (from other papers). The γ_{Cv} behavior with T is represented in Figure 25 as Gru C_v, with C_{V1} for the C_v function with temperature from Butland & Maddison, 1973. These values where found for η=1. In Figure 25 are also represented the Slater (Gru S), Dugdale and MacDonald (Gru DM) and Vachenko and Zubarev (Gru VZ) equations, for η=1.2 (from the various studies made the η gave the most accurate parameter for these equations, see magnesia case in section 5.5).

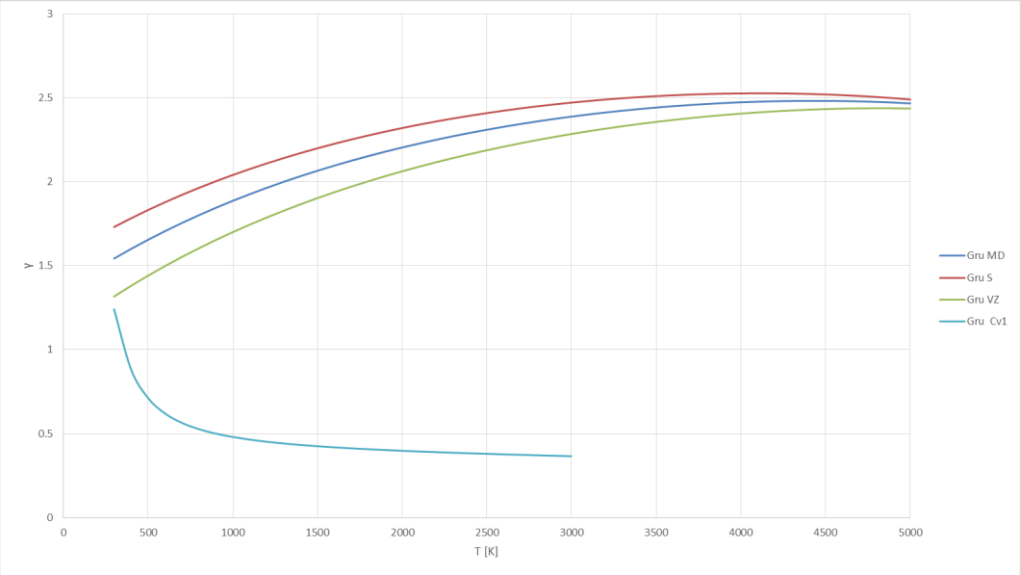

Figure 25 - Grüneisen Parameter - Graphite

There are also Grüneisen parameters derived by another authors. Lowitzer et al. 2006, calculates a γ=0.75 and γ=0.59 from different equations. Van Thiel & Ree 1989, in their equation uses γ_0=0.35. Nihira & Iwata 2003, obtained γ=0.62 at 293K. Butland & Maddison, 1973, estimated a γ=0.526. These values are in agreement with Gru C_{V1}, however they did not agree with the simplified equations from S, DM and VZ presented before.

5.1.2. Diamond

For Diamond the γ_{Cv} behavior with T is represented in Figure 26 as Gru C_v, with C_{V1} for the C_v function from Victor 1962, and C_{V2} for the C_v function from Reeber & Wang 1996. These values were found for η=1. In Figure 26 are also represented the Slater, Dugdale and MacDonald and Vachenko and Zubarev equations, for η=1.2.

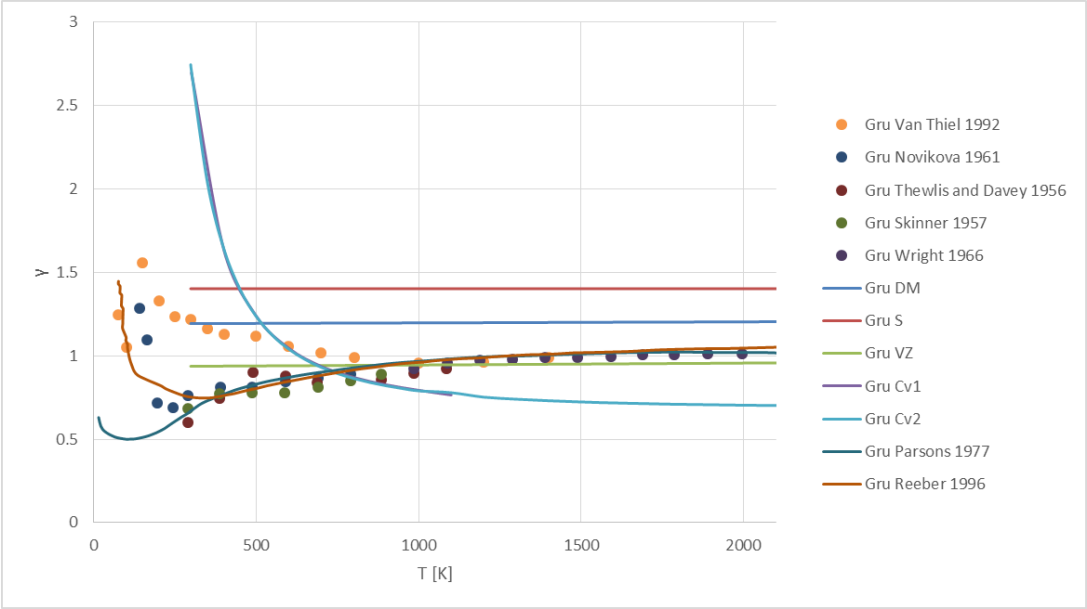

Figure 26 - Grüneisen Parameter - Diamond (0 to 2000K)

Dewaele et al. 2008, calculates a γ=0.85 from fitting experimental data to a Mie-Grüneisen-Debye Model. Van Thiel & Ree 1989, in their equation uses γ_0=1.15. Parsons 1977, obtained γ=1.19 from optical mode. Mitra et al. 1969, obtained γ=0.94 from optical mode using elastic constant data, while γ=1.2 using P-V data. Occelli et al. 2003, calculated a γ=0.97. Kunc et al., 2003, calculated γ=1.003 from LDA data, γ=0.995 from GGA data and γ=0.962 from Experimental Data at T=300K. The variation of Grüneisen coefficient with temperature is demonstrated in Van Thiel & Ree, 1992, and Reeber & Wang, 1996, (which also contains the results from Novikova, 1961, Thewlis and Davey, 1956, Skinner, 1957, and Wright, 1966) and are represented in the figure above. The values from Gru C_v1, Gru C_V2 and Gru VZ are in agreement with the values given, however Gru S and Gru DM have a higher value.

5.2. Alumina

Grüneisen for Corundum is represented in the following section, for the other phases is represented in Annex B.

5.2.1. Corundum

For Corundum the γ_{Cv} behavior with T is represented in Figure 27 as Gru C_v, with C_V1 for the C_v from Anderson 1995. These values were found for η=1. In Figure 27 are

also represented the Slater, Dugdale and MacDonald and Vachenko and Zubarev equations, for η=1.2.

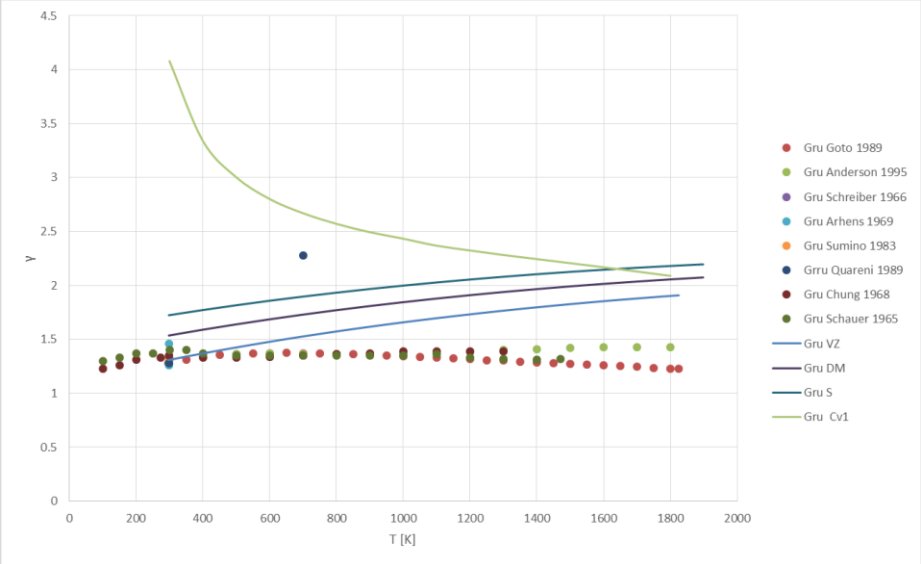

Figure 27 - Grüneisen Parameter - Corundum

In the graphic above are represented Grüneisen Parameters calculated and discussed in other papers (Goto et al. 1989; Anderson 1995; Schreiber & Anderson 1966; Ahrens et al. 1969; Sumino et al. 1983; Quareni & Mulargia 1989; Chung 1968; Schauer 1965). The results from this papers are in good agreement, however they are not with Gru Cv1 and with Gru VZ, DM and S for high temperatures.

5.3. Zirconia

For Zirconia is studied the Grüneisen for all the phases, being Cubic and Ortho I represented in the following section and the other phases in annex B.

5.3.1. Cubic Fluorite; Ortho I

For these phases, as we only have a P-V equation, only Slater, Dugdale and MacDonald and Vachenko and Zubarev equations can be used. For η=1.2 these equation are:

Table 8 - Grüneisen Parameter – Cubic Fluorite; OrthoI

Cubic Fluorite	Ortho I
$\boldsymbol{\gamma_S = 1.726}$	$\gamma_S = 1.846$
$\boldsymbol{\gamma_{DM} = 1.539}$	$\gamma_{DM} = 1.666$
$\boldsymbol{\gamma_{VZ} = 1.313}$	$\gamma_{VZ} = 1.450$

Yttria-stabilized Cubic Zirconia (way to obtain a cubic structure for low Temperatures) has been extensively studied at 300K (Cai et al. 1993; Kisi & Yuxiang 1999; Mashimo et al. 1995; Ingel & Lewis III 1986) and this data could make the extrapolation to Cubic Zirconia. For wt=10% (weight percentage of yttria), γ=1.9, for wt=15%, γ=2.0 and for wt=20%, γ=2.2 (Cai et al. 1993). For wt=9.4%, γ=1.4 (Kisi & Yuxiang 1999). Mashimo et al. 1995, for wt=9.6%, γ=2.15. From the data above an extrapolation for wt=0% was made and was given γ=1.4436, which is in close agreement with the values obtained in the table.

5.4. Titania

5.4.1. Rutile

For this phase, as we only have a P-V equation, only Slater, Dugdale and MacDonald and Vachenko and Zubarev equations can be used. For η=1.2 these values are represented in Figure 28.

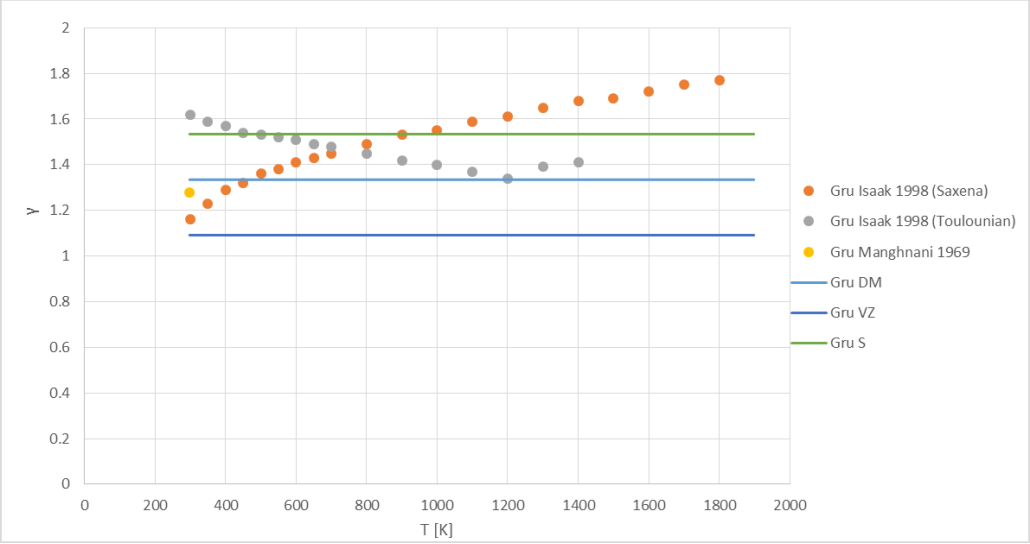

Figure 28 - Grüneisen Parameter - Rutile

In the graphic above are also represented Grüneisen Parameters calculated and discussed in other papers (Isaak et al. 1998; Manghnani 1969). From the relation $\rho\gamma=\rho_0\gamma_0$=6.17 g/cm^3, with ρ_0=4.25 g/cm^3, γ_0=1.6 (MCQueen et al. 1967). From the figure above a good correlation between results can be observed.

5.5. Magnesia

Grüneisen for B1 phase is presented in the following section, for B2 representation see annex B.

5.5.1. B1

For B1 the γ_{Cv} behavior with T is represented in Figure 29 as Gru C_v, C_V1 for the C_v from Anderson & Isaak 1992 and C_V2 for the C_v from Arthur 1950. This values were found for η=1. In Figure 29 are also represented the Slater, Dugdale and MacDonald and Vachenko and Zubarev equations, for η=1.2.

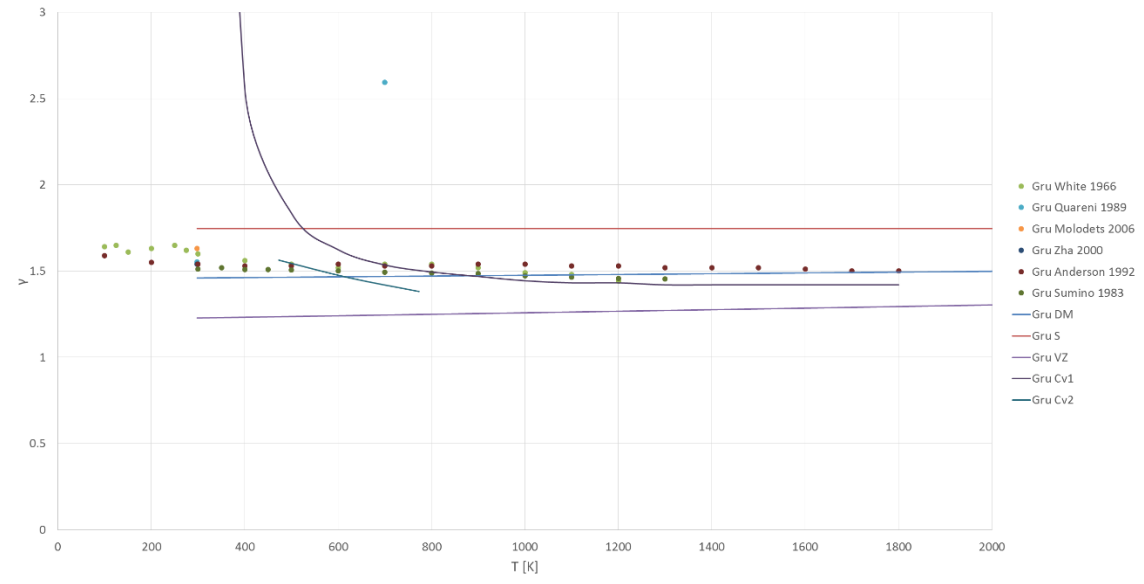

Figure 29 - Grüneisen Parameter - Magnesia B1

In the graphic above are also represented Grüneisen Parameters calculated and discussed in other papers (White & Anderson 1966; Quareni & Mulargia 1989; Molodets et al. 2006; Zha et al. 2000; Anderson & Isaak 1992; Sumino et al. 1983). Speziale et al., 2001, derived γ=1.524. This phase is in excellent agreement with all the calculations and prove the veracity of the different methods of calculation.

6. MODEL DATABASE PARAMETERS

In section 3.3.1 were discussed the parameters that have to be derived or studied in order to represent the ES of solid products. These parameters are represented next and the Grüneisen values were chosen from the evaluation made above. For implementation of the equation, only the first values of each column were used (for each phase)

Table 9 – Model Parameters

	ρ_0 [g/cm^3]	C_o [km/s]	S_0	γ	Θ_D [K]	$H_{formation}$ [kJ/mol]	$S_{formation}$ [J/mol.K]
Carbon							
Graphite	2.21 (Marsh 1980)	3.99 (Mashimo et al. 2007) 4.149 (Coleburn 1964)	1.33 (Mashimo et al. 2007) 1.690 (Coleburn 1964)	0.526	1280 (Van Thiel & Ree 1989) 1050 (Krumhansl & Brooks 1953)	0 (Fried & Howard 2000)	5.74 (Fried & Howard 2000) 5.6 (NIST,Mallard & Linstrom 2011)
Diamond	3.51 (Hicks et al. 2008)	11.22 (Mashimo et al. 2007) 7.81 (Marsh 1980)	1.12 (Mashimo et al. 2007) 1.43 (Marsh 1980)	0.97	1850 (Bradley et al. 2009) 1860 (Dewaele et al. 2008) 1411 (Van Thiel & Ree 1989)	0	2.448 0.0720 2.3782 (NIST,Mallard & Linstrom 2011) 2.70 (Fried & Howard 2000)
Alumina							
Corundum	3.92 (mean value)	8.91 (Mashimo et al. 2007) 8.7289 (extrapolated from (Marsh 1980)) 7.455 (Kleiser et al. 2011)	0.96 (Mashimo et al. 2007) 0.9714 (extrapolated from (Marsh 1980) 1.299 (Kleiser et al. 2011)	1.43	947 (Hama & Suito 2002) 1034.9 (T=300K) (Chung 1968) 1033.9 (T=296K) (Goto et al. 1989)	-1675.7 -1675.69 (NIST,Mallard & Linstrom 2011)	50.92 (NIST,Mallard & Linstrom 2011)
Rh_2O_3 (II) Type	2.755476 (Tsuchiya et al. 2005)	7.3655 (extrapolated from (Hama & Suito 2002)	1.2726 (extrapolated from (Hama & Suito 2002)	1.086	943 (Hama & Suito 2002)		
Perovskite	4.2595 (Caracas	6.6364 (extrapolated from	1.3071	1.201	895 (Hama & Suito 2002)		

	& Cohen 2007)	(Hama & Suito 2002)	(extrapolated from (Hama & Suito 2002)				
Post-Perovskite	4.219438 (Tsuchiya et al. 2005)	V_I=13.6 (Tsuchiya et al. 2005)		1.350			
Magnesia							
B1	3.585 (Zha et al. 2000)	6.15 (Ahrens 1966) 6.6 (Marsh 1980) 6.612 (Jin et al. 2010) 6.87 (Molodets et al. 2006) 6.84 (Mashimo et al. 2007)	1.85 (Ahrens 1966) 1.37 (Marsh 1980) 1.361 (Jin et al. 2010) 1.24 (Molodets et al. 2006) 1.24 (Mashimo et al. 2007)	1.524	800 (Dewaele et al. 2000) 931 (Ahrens 1966) 942 (Anderson 1995) 773 (Fei et al. 2004) 945 (Jin et al. 2010) 773 (Speziale et al. 2001)	-601.6 -601.24 (NIST,Mallard & Linstrom 2011)	26.95 26.85 (NIST,Mallard & Linstrom 2011) 27.024 (T=300K) (Anderson & Zou 1990)
B2	3.71 (Coppari et al. 2013)			1.560			
Zirconia							
Monoclinic	5.64 (Whitney 1962)	V_I=7.485 ((average of Voigt–Reuss–Hill approach) (Liu et al. 2011) V_I=7.261 (P=0GPa) (Wang et al. 2015)		1.040	585.67 (average of Voigt–Reuss–Hill approach) (Liu et al. 2011) 567 (Ren et al. 2011) 575 (Ren et al. 2011, derived from Nevitt et al. 1990) 572.8 (P=0GPa)(Wang et al. 2015)	-1097.46 (NIST,Mallard & Linstrom 2011)	50.34 (NIST,Mallard & Linstrom 2011)
Tetragonal	6.05 (Whitney 1962)			1.92	511 (wt=2.4% Y_2O_3) (Lawless & Gupta 1983) 723.6 K (T=0K and P=0) (Jin et al. 2012)		
Cubic Fluorite	6.2 (Ingel & Lewis III 1986)	5.7915 (extrapolate from (Mashimo et al. 1995) cubic Zirconia wt=8% Y_2O_3 Polycrystal) V_I=7.451 (wt=9.4% Y_2O_3) (Mashimo et al. 1995)	0.8015 (extrapolate from (Mashimo et al. 1995) cubic stabilized Zirconia wt=8% Y_2O_3 Polycrystal)	1.313	473 (Lawless & Gupta 1983) 528 (wt=10% Y_2O_3) (Jin et al. 2012, derived from Argyriou 1994) 963 (wt=9.4% Y_2O_3) (Kisi & Yuxiang 1999) 586.8 (wt=9.6% Y_2O_3) (Mashimo et al. 1995)	-1097.46 (approximation to Monoclinic values)	50.34 (approximation to Monoclinic values)

Ortho I	6.07 (Toraya et al. 1987)	V_I=7.942 (P=9.09GPa) (Wang et al. 2015)		1.450	627.4 (P=9.09GPa) (Wang et al. 2015)		
Ortho II	6.80 (Jayarama n et al. 1993)	V_I=7.755 (P=12.68GP a) (Wang et al. 2015) V_I=9.016 (Caravaca et al. 2009)		1.30	546.03 (P=0 GPa) (Ren et al. 2011) 632.0 (P=12.68GPa) (Wang et al. 2015) 695 (Caravaca et al. 2009)		
Titania							
Rutile	4.2485 (Gerward & Staun Olsen 1997)	7.551 (extrapolat ed from (Marsh 1980)) 5.355 (MCQueen et al. 1967) 6.91 (determine d from zero pressure bulk sound velocity) (MCQueen et al. 1967) V_I=10.300 (Caravaca et al. 2009)	0.3428 (extrapolated from (Marsh 1980)) 1.345 (MCQueen et al. 1967) 1.47 (determined from zero pressure bulk sound velocity) (MCQueen et al. 1967)	1.50	782.5 (Elastic) (Wu & Sladek 1982) 778 (Calorimetric) (Wu & Sladek 1982)	-944.0 -938.72 (NIST,Mall ard & Linstrom 2011)	50.62 (NIST,Mallar d & Linstrom 2011)
Anatase	3.8941 (Arlt et al. 2000)			1.206		-938.72 (NIST,Mall ard & Linstrom 2011)	
Alpha-PbO2	4.336 (Arlt et al. 2000)			1.472			
MI	4.728 (Arlt et al. 2000)			1.066			
Ortho I	4.8639 (Dubrovin skaia et al. 2001)			1.104			
OrthoII	5.275166 (Nishio-Hamane et al. 2010)	V_I=10.327 V_I=10.078 (Caravaca et al. 2009)c		1.094	897 899 904 (Caravaca et al. 2009)		
Cubic Fluorite				1.262	900 (P=0GPa) (Miloua et al. 2011)		

With this representation the parameters above are inscribed in THOR Database, in order to simulate some products formation in section 7.

7. THOR APLICATION - CASES STUDIED

7.1. Solid Carbon Formation

The formation of Carbon Alpha (diamond) and Carbon Beta (graphite) has been extensively studied and implemented in thermochemical codes. Therefore, it's used as a benchmark of the new equations to define solids and its parameters. In the following subchapter, comparisons with the results obtained from other codes and experimental data are made for testing the validity of this representation.

In the following sections, the values obtained for the isochoric and isobaric adiabatic combustion and detonation of Nitromethane are compared as well as the detonation of TNT and finally the relation with detonation of Ammonium Nitrate emulsion explosive previously studied in Campos et al., 2014.

7.1.1. Isochoric and Isobaric Adiabatic Combustion of Nitromethane

With this predictions, the implementation of condensed carbon species in products is compared with the simulation of formation of carbon gas product alone (C (gas) simulation) and also the sensibility of Grüneisen parameter in the modeling.

For the Isochoric Adiabatic Combustion of 1 mol/kg of Nitromethane, see Table 17 in annex C. For the Isobaric Adiabatic Combustion of 1 mol/kg of Nitromethane, see Table 18 in annex C.

In Isochoric combustion, considering the presence of condensed products, as the carbon changes of phase from gaseous to solid, the pressure will drop and the phase change will release energy that will be turned into a variation in temperature (adiabatic process). The results obtained from the parameters chosen in this work are very similar to the obtained with the parameters chosen in previous works (Campos et al. 2014; Campos et al. 2008), using the same equations, validating the parameters extrapolating method in this Thesis.

In Isobaric combustion case, the modeling with only C (gas) and the modeling with condensed phases results in similar values, because almost no condensed species are formed (C Alpha).

The sensibility test of THOR code with Grüneisen parameter was made through the variation of this parameter for C Beta and C Alpha as presented in Table 17 and Table 18. Mostly for the first modeling, for the variation with C Beta Grüneisen, it's denoted that when Grüneisen is greater or equal to $\boldsymbol{\Gamma} = \frac{\partial H}{\partial E}\Big)_{S}$ from the C (gas) modeling, the program will have a great divergence in calculation, proving the limit value for Grüneisen. Another calculation error in THOR is also denoted, when Grüneisen equals 1, which is an usual error created by the calculation methods used by the program. Moreover, this requires a critical analysis to all the simulations made.

7.1.2. Detonation of Nitromethane

In this modeling, as in previous sections, the results with or without condensed products and also the grüneisen sensibility test are analyzed

Table 19 in Annex C). Here becomes apparent the great difference between the results depending on the products chosen. When condensed phases are considered, the pressures drops and the temperature rises, as the formation of a large amount of Carbon (Beta) appears, which doesn't happen in C (gas) simulation. Table 19 also presents the sensibility test of THOR code with Grüneisen values for C Beta, where the results start deviating at values closer to $\boldsymbol{\Gamma} = \frac{\partial H}{\partial E}\Big)_{S}$, as verified in the first modeling.

The advantage of compare the results with Nitromethane detonation, is the large amount of data that exists from other studies. In the next tables (Table 10 and Table 11) these data are presented and compared with the results obtained by the simulation, 1 mol/kg NM detonation, which proves the validity of it.

Table 10 - Product Concentration Comparison

%mol/mol		THOR C(gas)	THOR This Work	(Ornellas 1968)	(Mader 1998)
N2	:	12.83572	16.38525	14.66865	16.68892
C(beta)	:	0	25.29093	3.536858	21.36182
CO2	:	20.52638	7.776784	9.717051	5.674232
H2O	:	26.80216	49.70594	32.83693	49.3992
NO	:	0.001032	0.399751	0	0
CH4	:	5.083043	0	3.090097	0
O2	:	0.000005	0.289355	0	0
H2	:	1.540473	0.049445	10.94564	0.400534

CO	:	16.63712	0.102544	20.47655	6.341789
NH3	:	16.57406	0	4.39315	0.133511
HCN	:	0	0	0.297841	0
C2H6	:	0	0	0.03723	0

A close agreement with Mader, 1998, results shows the veracity of the method used, for the concentration calculation.

Table 11 - Nitromethane Detonation Results Comparison

Paper		**Pcj [kbar]**	**ρ[g/cm3]**	**Tcj [K]**	**Dcj [m/s]**
THOR C(gas)		115.12	1.52439	3121.107	6325.89
THOR This Work		108.5	1.470588	3417.988	5918.43
(Hervouët et al. 2008)	Monte carlo simulation with carbon	118.4	1.515152	3430	6438
	Monte carlo simulation without carbon	121.3	1.497006	3274	6641
	Thermochemical Results	123.1	1.531394	3513	6493
	Experimental Results	-	-	-	6300
(Dobratz 1972)	Experimental	130	-	-	6320
	Experimental C-J Conditions	125	-	-	6280
(Sućeska 2004)	Experimental	120	-	3430	6280
	EXPLO5	120	-	3583	6400
(Mader 1963)	Experimental	141	-	3380	6290

The results obtained are in good agreement with other authors, mostly in the temperature values, which is the most important parameter to recognize with this simulation, as explained before.

7.1.3. Detonation of TNT

Another experimental and theoretical extensively studied reaction is the detonation of TNT. This can be modulated in THOR, with the detonation of 1 mol/kg of TNT, in order to compare the results obtained in another sources. Table 12 represents the formation of products of different authors and shows a great correlation whit the results obtained in THOR with condensed phase products.

Table 12 - Product Concentration Comparison

%mol/mol		**THOR C(g)**	**THOR This Work**	**(Mader 1998)**	**(Cengiz & Ulas 2009)**	**(Van Thiel & Ree 1987)**
N2	:	17.62107	13.33031	13.6376	13.63636	13
C(beta)	:	0	48.05916	46.82244	46.90909	47

CO2	:	2.907367	15.11456	15.09228	15.09091	18
H2O	:	0.000019	22.55645	22.72934	22.72727	20
NO	:	0	0.419456	0	0	0
CH4	:	14.66949	0	0	0	0
O2	:	0	0.469291	0	0	0
H2	:	0.000017	0.003445	0	0	0
CO	:	64.75787	0.037075	1.709246	1.636364	0
NH3	:	0.044163	0.010259	0.009092	0	1.8

The following table (Table 13) features the difference between the modeling with and without condensed species, proving that its introduction is essential for a good representation of the real reaction, comparing with experimental values.

Table 13 - TNT Detonation Results Comparison

Paper		**Pcj [kbar]**	**Tcj [K]**	**Dcj [m/s]**	$\Gamma = \frac{\partial H}{\partial E}\Big)_S$
THOR C(g)		254.16	2058.602	8693.75	3.92
Thor This Work		196.58	3360.299	6592.15	3.05
(Cowan & Fickett 1956)	Experimental ρ_0=1.64 g/cm^3	168		6719.28	3.44
(Cowan & Fickett 1956)	KW and CF EoS	196	2715	6894	2.88
(Brinkley & Wilson 1943)	Gaseous EoS	178	3170	7290	3.78
(Cook 1947)	Gaseous EoS	152	4170	7030	4.2
(Caldirola 1946)	Gaseous EoS	212	4030	6900	2.59
(Jones & Miller 1948)	Gaseous EoS	175	3300	7480	4.12
(Kihara & Hikita 1953)	Molecular Theory of Detonation	195	2270	6950	2.96
(Paterson 1948)		127	3900	6790	4.81
(Sućeska 2004)	Experimental ρ_0=1.64 g/cm^3	210		6950	
(Sućeska 2004)	Explo5 (BKW EoS)	202	3744	7.15	
(Turkel & Charlet 1995)	Cowan Fickett EoS	162		6.41	
(Turkel & Charlet 1995)	3 Phase Model EoS	179		6.813	
(Mader 1998)	-	190		6950	3.16
(Dobratz 1972)	Experimental ρ_0=1.63 g/cm^3	190		6930	
(Dobratz 1972)	JWL EoS	210		6930	3.738

7.1.4. Detonation of Ammonium Nitrate Emulsion Explosive

Another simulation was performed, presenting the initial steps in the production phase. This is prepared through a basic reactive media, a matrix of emulsion explosive,

obtained by an aqueous solution of ammonium nitrate emulsified with oil, wax and emulsifiers. The final density is controlled by the quantity of hollow glass or plastic microbaloons (Campos et al. 2014; Mendes et al. 2014). In this simulation, similar to the one in Matias et al., 2010, THOR code was used in order to establish the limits of fuel oil concentration, given its equivalence ratio. Assuming as initial reactant start composition [87.20 mass % of AN, 3.77 % of Fuel oil, 0.22 % of AIR (corresponding to the sensitizing air microballons) and 8.83 % of Water, corresponding to an equivalence ratio of 0.92] and the products of detonation [CO2, N2, O2, H2O, NO2, CO, H2, OH, H, CH2O2, C(alfa), C(beta), C(gas), NH3, NO, O, N components], the concentration of Fuel Oil was increased until an equivalence ration of 1.12, maintaining the mass concentration of the other reactants.

Table 14 - Ammonium Nitrate Emulsion Explosive Detonation Results for the parameters derived in this work

Equivalence Ratio	0.9194	0.9584	0.9999	1.0414	1.0746	1.0829	1.1244
P [kbar]	11.4	12.13	12.71	12.67	12.44	12.58	12.41
T [K]	2061.088	2197.851	2336.131	2257.864	2257.293	2249.632	2211.084

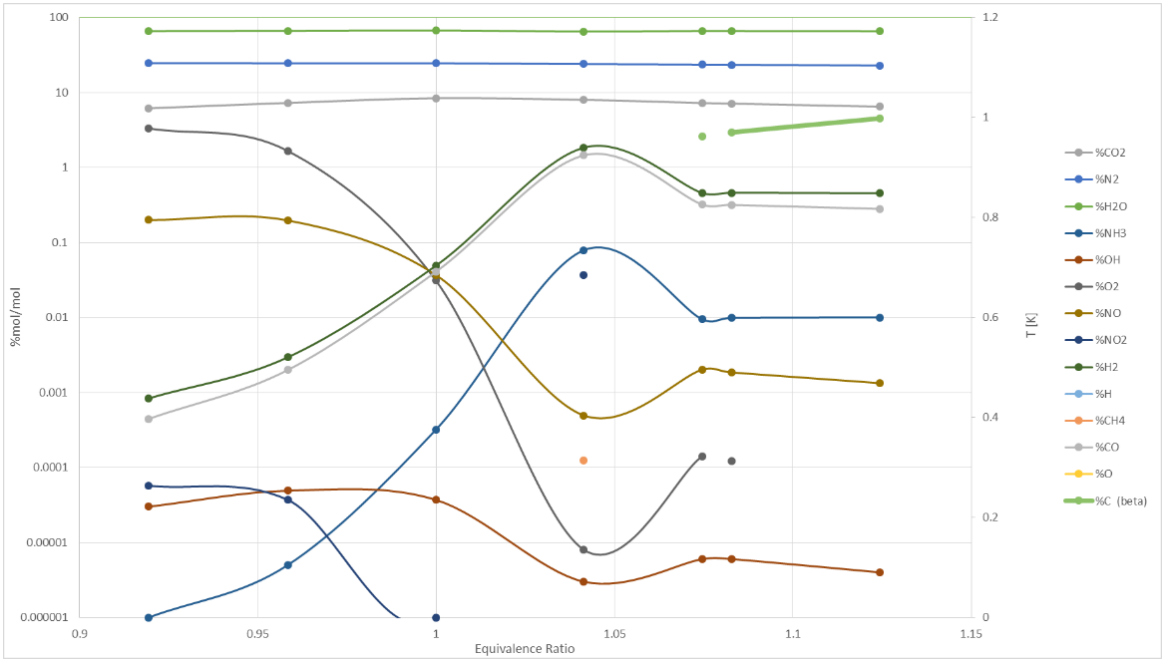

Figure 30 – Products Concentration of Ammonium Nitrate Emulsion Explosive Detonation

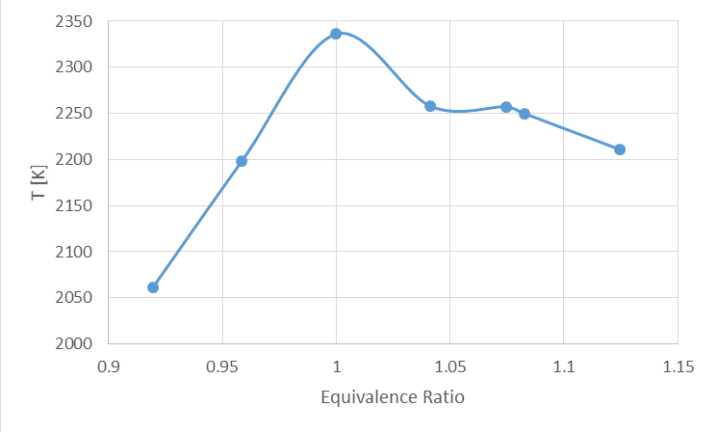

Figure 31 - Detonation Temperature of Ammonium Nitrate Emulsion Explosive Detonation

The temperature evolution (Figure 31), as a function of fuel concentration, show the maximum values close to the stoichiometry. However, the predicted detonation temperature presents quite lower values (~2000 K).

This modeling is in close agreement with previous studies (Campos et al. 2014), which used the same model for solid carbon with another parameters. With this simulation, the presented method is validated and can be extrapolated to the metal oxide modeling in the next section.

7.2. Case studies – metal/emulsion explosive - Predicted Products and Temperatures of Detonation

7.2.1. Alumina

The reaction of aluminum and emulsion explosive can be predicted using THOR code with previous presented parameters for corundum (or α-phase), phase formed at temperature and pressure of detonation (see phase diagram Figure 2). For a basic starting composition [of 83.34 mass % of AN, 4.33 % of Fuel Oil, 8.44 % of Water, 0.21 % of Air and 3.68 % of Aluminum] and the products of detonation [C(beta), H2O, N2, Al2O3(L), CO2, NO2, NO, O2, H2, OH, Al2O3 (corundum or Al2O3-A), Al2O3(g), H, N, O, C(gas), C(alpha), NH3, CO components] the mass concentration of Al was increased from 3.68 until ~18.64 %, maintaining the mass concentration of other reactants, using the same methodology as Campos et al., 2014.

For this simulation were analyzed two procedures. The first one uses Gordon McBride Polynomials to define Al_2O_3 condensed phase ES (referenced as Method Gordon McBride), representing this phase as a high density gas, with the polynomials used in previous works (Campos et al. 2014; Campos et al. 2008; Matias et al. 2010). The second attempt was made through the equation and parameters derived in this work (referenced as Method MG+Debye), with the parameters given in the Table 9 for corundum. Graphic in Figure 32 shows the results for the first model and graphic in Figure 33 shows the results of the second model.

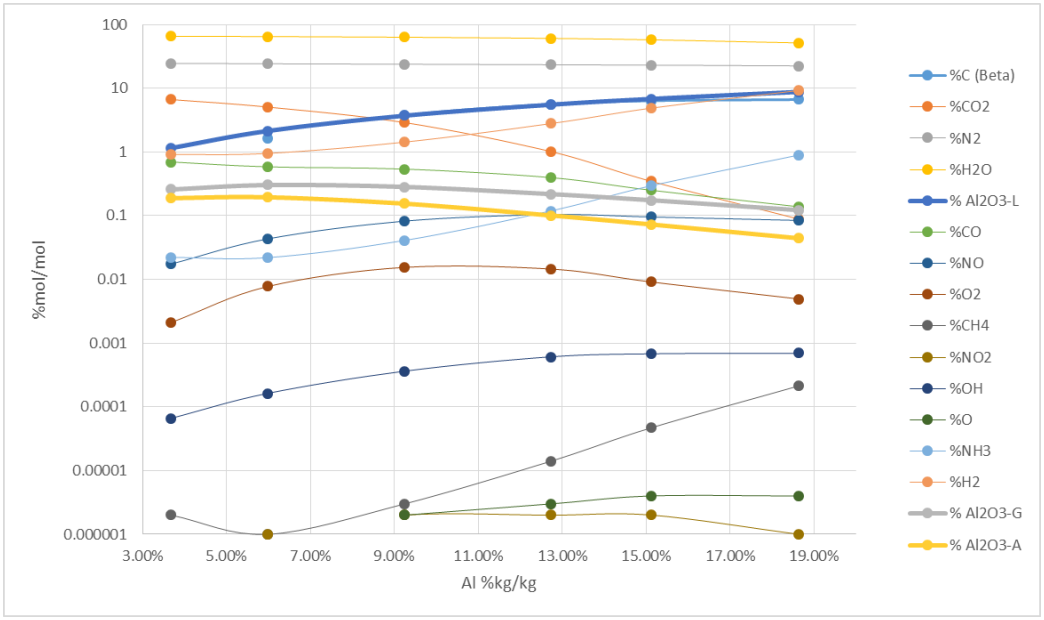

Figure 32 - Product Concentration G&M Method of Ammonium Nitrate and Aluminum Particle Detonation

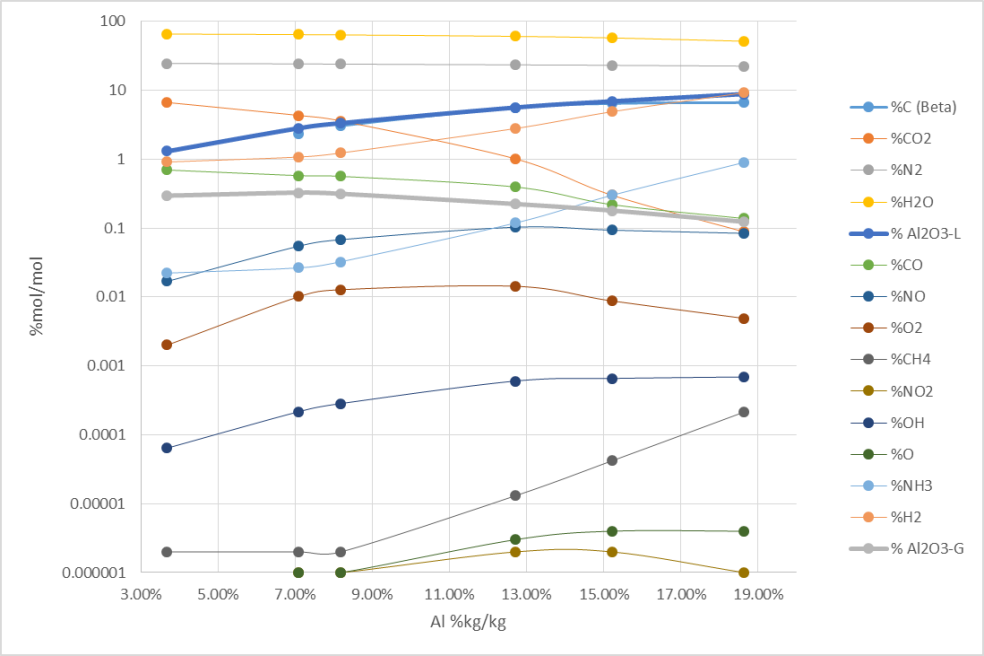

Figure 33 - Product Concentration MG+Debye Method of Ammonium Nitrate and Aluminum Particle Detonation

Analyzing the graphics above it's possible to realize that products formation concentration results are very similar. However, in the second method there is no Corundum formation. This result takes place because the temperature of Detonation (Figure 34) is higher than the melting temperature of Corundum (or α-Alumina), transforming all the Alumina in either gaseous or liquid phase, see Figure 2 (with transition at 2054 ºC (CRC Handbook of Chemistry and Physics, (Linde 1984)) for atmospheric pressure),

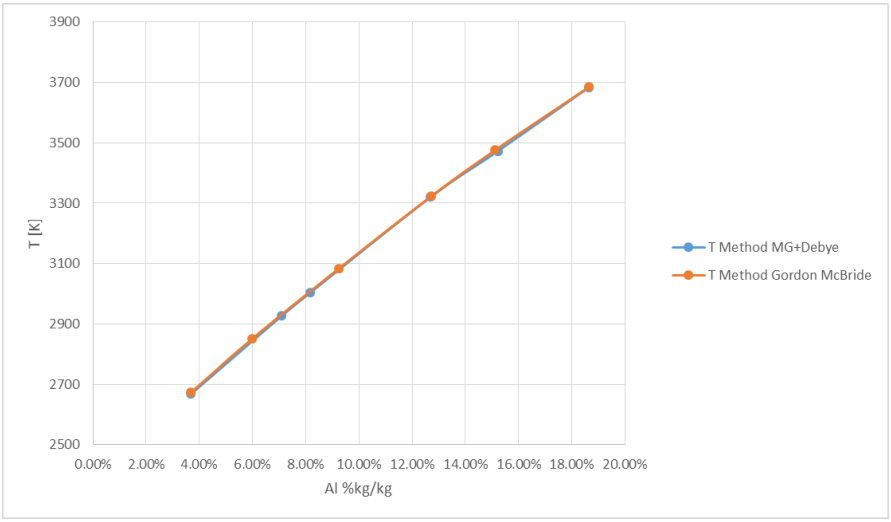

Figure 34- Temperature of Ammonium Nitrate and Aluminum Particle Detonation

With the figure above is possible to perceive that the non-formation of Corundum, in the second method, takes to a very similar detonation temperature in both models. Nevertheless, when the adiabatic expansion of the products (with consequently decrease in temperature) takes place, corundum is formed, although with the implications presented in the beginning of this work. Then, for the formation of corundum in the detonation reaction it's necessary a lower temperature detonation.

Supporting the result denoted above, Caflin et al., 2012, showed clearly the impossibility of a metal particle to react immediately after the first detonation shock. This occurs as the main explosive and metal particles only react with the detonation products, in a post detonation reaction. The same conclusion was verified by Mendes et al., 2011, where experimental values of detonation velocity and pressure were studied in identical emulsion explosives with aluminum. Detonation velocity decreases with increasing concentrations of aluminum. Detonation pressure profile shows a non-monotonic behavior. These conclusions are in excellent accordance to theoretical prediction and prove the behavior of aluminum as an inert addiction in the detonation front or reacting far away from the shock front.

Consequently, these assumptions allows to predict calculations with ammonium nitrate and metal nitrate precursors (used in real production system), in order to get the participation of metal reactant in the first zone of detonation reaction. Preliminary calculations from Campos et al., 2012, show the strong decreasing behavior of detonation temperature (necessary to particle formation during detonation) when metal particles are substituted by metal-nitrate precursors. For a better analysis of this alternative, THOR is used and the detonation results of ammonium nitrate and metal nitrate precursors are presented, being the new explosives compositions, with the two methods described before (the results are presented in Figure 35 and Figure 36, respectively).

A mixture of ammonium nitrate and aluminum nitrate, hydrated, is introduced in THOR, in the emulsion compositions [starting by the basic composition of 34.70 mass % of AN, 54.21 % of AL(NO3)3 *9H2O, 2.40 mass % of Fuel Oil, 4.69 % of Water, 0.11 % of Air and 3.90 % of Aluminum] and the products of detonation [C(beta), H2O, N2, Al2O3(L), CO2, NO2, NO, O2, H2, OH, Al2O3 (corundum or Al2O3-A), Al2O3(g), H, N, O, C(gas), C(alpha), NH3, CO components], increasing the mass concentration of Al from 3.90 until ~9.95 % and maintaining the mass concentration of other reactants.

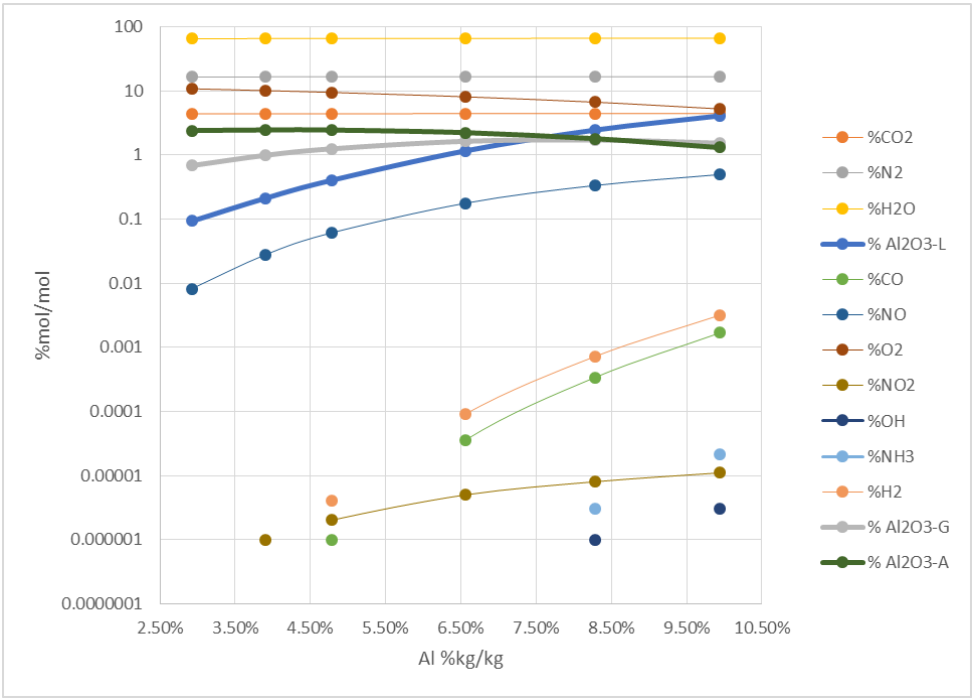

Figure 35 - Product Concentration G&M Method of Ammonium Nitrate and Aluminum Nitrate Precursors Detonation

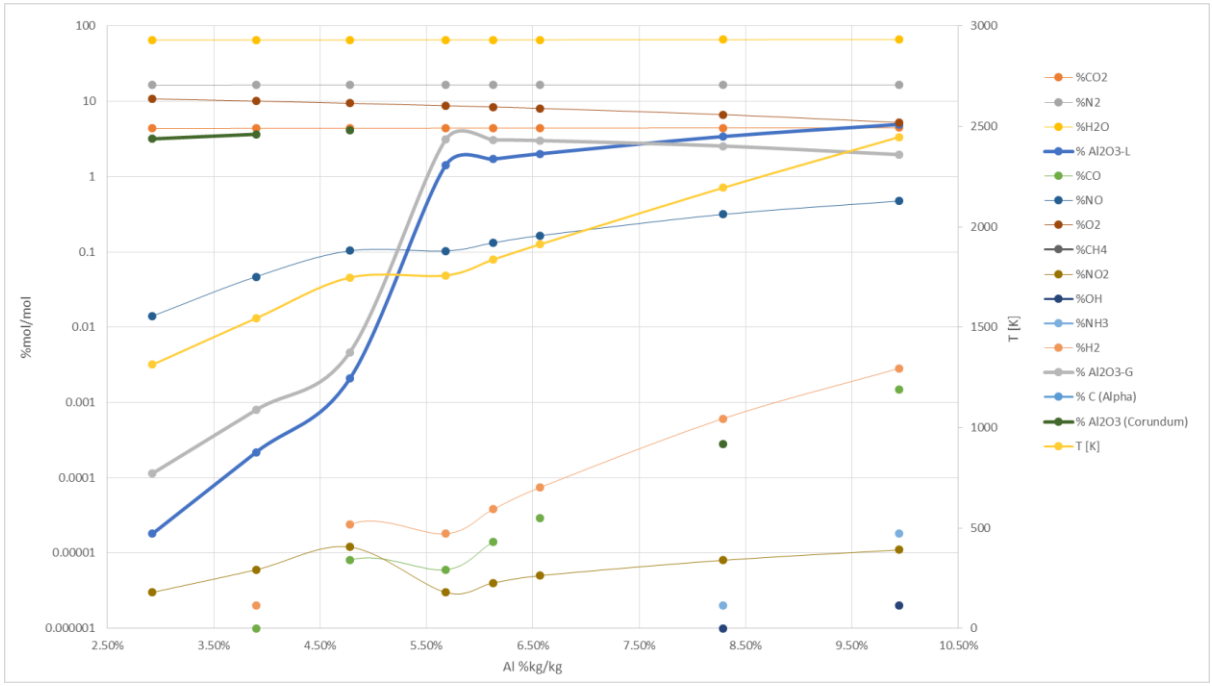

Figure 36 -Product Concentration MG+Debye Method of Ammonium Nitrate and Aluminum Nitrate Precursor Detonation

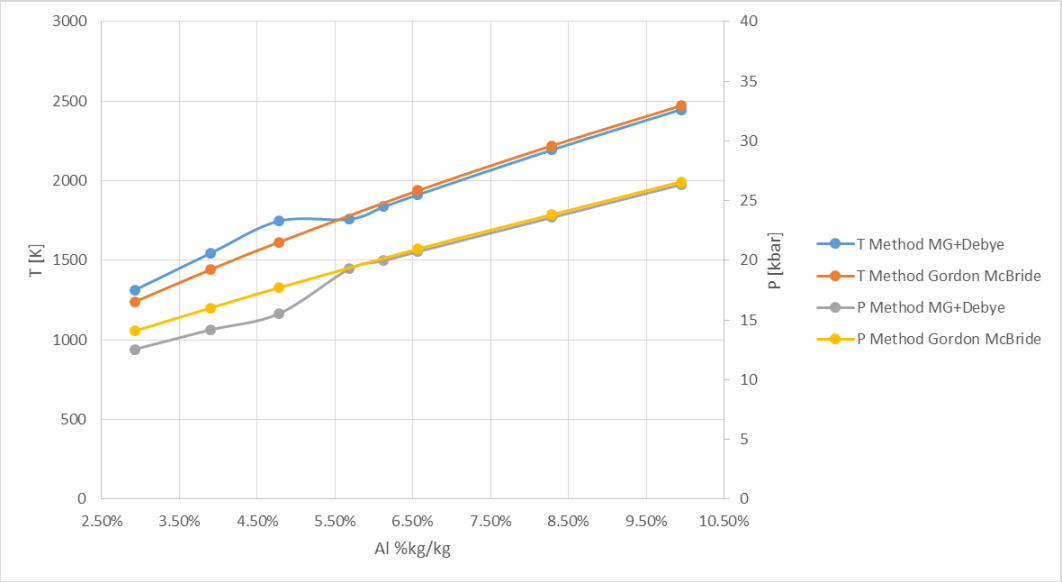

Figure 37 - Temperature and Pressure of Ammonium Nitrate and Aluminum Nitrate Precursors Detonation

In the figures above it's shown that the concentration of Corundum formed in detonation before it reaches the melting temperature is similar in both simulations. However, in the model studied in this work, the corundum stops appearing when Al %kg/kg equals 5.68% (when it reaches a temperature close to melting temperature). This is a great result that represents accurately the phase transition phenomena: when the solid species are formed, the temperature increases due to the energy release of the phase change, and the pressure decreases due to the decrease of volume (solid phase) (see Figure 37).

However, when there is no solid phase condensation in the simulation using the method presented in this work, the temperature is equal to the temperature in the Gordon McBride Modeling (that represents solid phase as high density gas).

This proves the major advantage of this method, as the experimental setup depends greatly on the detonation temperature and the capacity of the simulations to better represent real phenomena, having a strong relation with metal-oxide particle formation and its subsequent syntherization of the initial formed crystallites.

Besides the excellent results obtained by this model, it's important to keep in mind a critical analysis of the results. In the simulations made, sometimes, the modeling converge to a different outcome, taken by the difficulty of the program to balance between the energy released by a phase transformation and the expansion of gaseous products that quickly decreases the temperature. This errors could be denoted, as an example, by the high temperature given or by the instantaneous formation of a condensed phase.

As predicted by Campos et al., 2014, and can be seen in Figure 38, the detonation temperature decreases, for the same aluminum reactant concentration, using aluminum nitrate precursors.

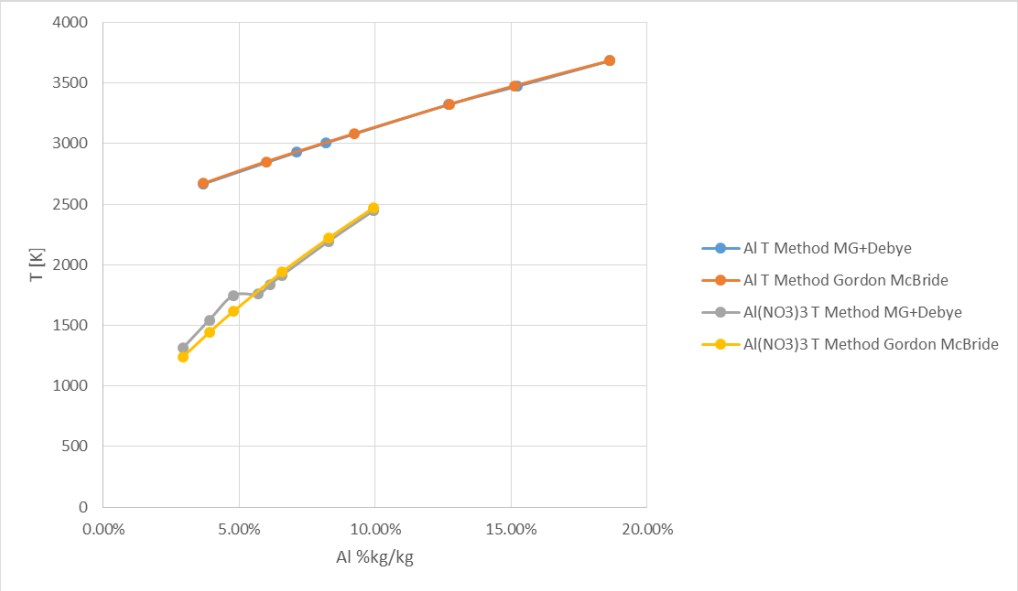

Figure 38 - Relation between Temperatures Detonation with or without Aluminum Nitrate Precursors

This temperature decrease allows the formation in detonation of Al_2O_3 solid condensed specie in a Mie-Grüneisen model, for the aluminum nitrate reaction, as in experimental reactions (Campos et al. 2014).

7.2.2. Titania

The reaction of titanium and emulsion explosive can be predicted using THOR code, through the first method where the polynomials were derived in, Campos et al., 2014; Campos et al., 2008; Matias et al., 2010, and through the second and presented method with the previous represented parameters for Rutile (Table 9), as the interval of values of detonation pressure for this process are inferior to formation of the high pressure phases (see Figure 8).

In a similar way, keeping the basic starting composition [of 84.11 mass % of AN, 4.36 % of Fuel Oil, 7.54 % of Water, 0.21 % of Air and 3.78 % of Titanium] and the products of detonation [CO2, H2O, N2, H2, TiO2(L), NO2, NO, CO, O2, OH, H, N, O, C(alpha), C(gas), C(beta), NH3, TiO2(G) and TiO2(Rutile or TiO2-S) components] the mass concentration of Ti was increased from 3.78 until 24.44 %, keeping the mass concentration

of other reactants unchanged. The following graphics show the evolution of products concentration with the mass concentration of Titanium in the reactants, for both described methods. Figure 41 shows the influence in temperature and pressure with the mass concentration of titanium in reactants for this two methods.

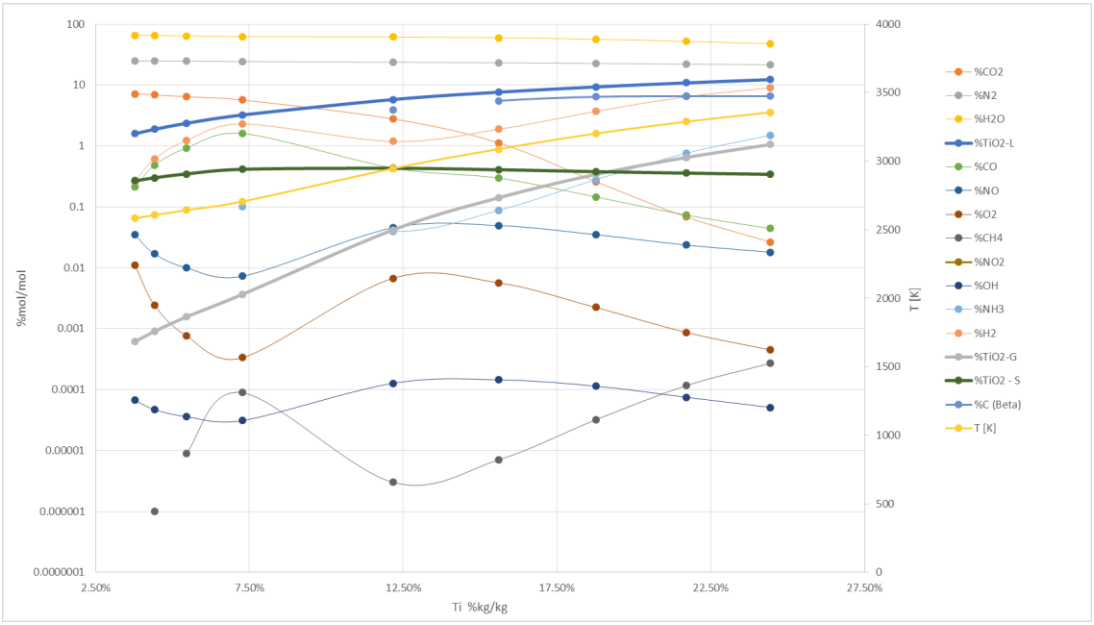

Figure 39 - Product Concentration G&M Method of Ammonium Nitrate and Titanium Particles Detonation

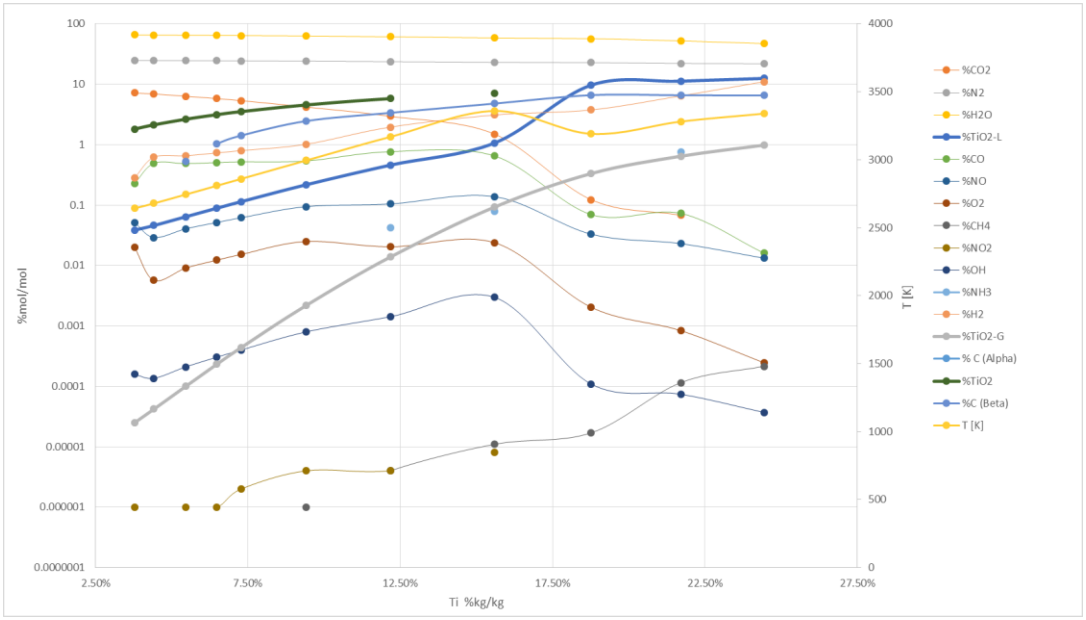

Figure 40 - Product Concentration MG+Debye Method of Ammonium Nitrate and Titanium Particles Detonation

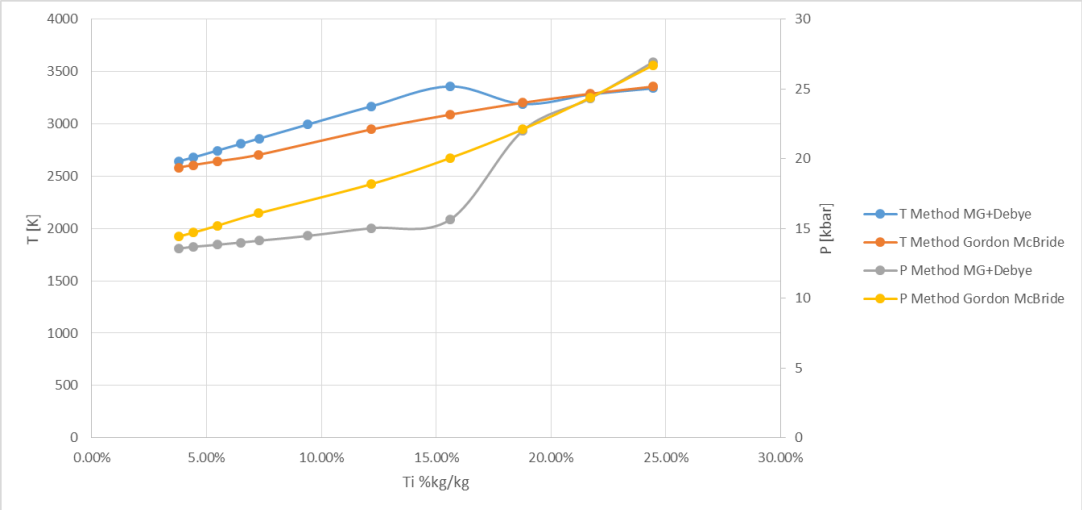

Figure 41 - Temperature and Pressure of Ammonium Nitrate and Titanium Particles Detonation

With this simulations it's possible to see that the model presented in this work represents with great accuracy the phenomena of the phase transition, with the inherent increase in temperature and decrease in pressure, when there is solid phase specie formation; and the decrease of temperature and increase in pressure when the temperature reached is superior to the melting temperature of Rutile, which transforms the solid phase into liquid phase.

This proves the major advantage of this method, as the experimental setup depends greatly on this temperature and the capacity of the simulations to better represent real phenomena.

The Rutile stops appearing at a Titanium concentration of 15.6%kg/kg, for a temperature of 3359K, which represents the simulation melting temperature of the solid phase, at the detonation pressure. Further studies most attain and validate this value, through an equation of melting curve (P-T), as for atmospheric pressure a low melting temperature is presented (1750 ºC , CRC Handbook of Chemistry and Physics, 1984)

Titania formation can be predicted and formed with ammonium nitrate and metal particles reaction, however it appears predominantly in post-detonation, as described before. As in Alumina formation, this material can be formed with the reaction of metal nitrate precursors, however the anhydrous titanium nitrate is a volatile solid at ambient temperature (READE), being the open market of Solid Titanium Nitrate very difficult. This makes Titanium to be the easy reactant.

7.2.3. Zirconia

The reaction of zirconium and emulsion explosive can be predicted using THOR code, by the first method where the polynomials were derived in, Campos et al., 2014; Campos et al., 2008; Matias et al., 2010, and by the second and presented method with the previous represented parameters for Cubic Fluorite Type (Table 9), as the detonation temperature is representative of this phase and the pressure is inferior to formation of the high pressure phases (see Figure 6). However, in post detonation the temperature will drop and this phase will be transformed into Monoclinic phase, unless it's stabilized with Yttrium, or other elements, giving a cubic or tetragonal shape at low temperatures (Ingel & Lewis III 1986; Mashimo et al. 1995).

In a similar way, keeping the basic starting composition [of 80.58 mass % of AN, 4.17 % of Fuel Oil, 8.16 % of Water, 0.20 % of Air and 6.89 % of Zirconium] and the products of detonation [CO2, N2, H2, H2O, ZrO2(L), NO2, NO, CO, O2, OH, H, N, O, C(alpha), C(gas), C(beta), NH3, ZrO2(G) and ZrO2(Cubic Fluorite Type or ZrO2-S1 (G&M Method)) components] the mass concentration of Zr was increased from 6.89 until 32.30%, keeping the concentration of other reactants.

The following graphics show the evolution of products concentration with the mass concentration of Zirconium in the reactants, for both methods described above. Figure 44 shows the influence in temperature and pressure with the mass concentration of Zirconium in reactants for this two methods.

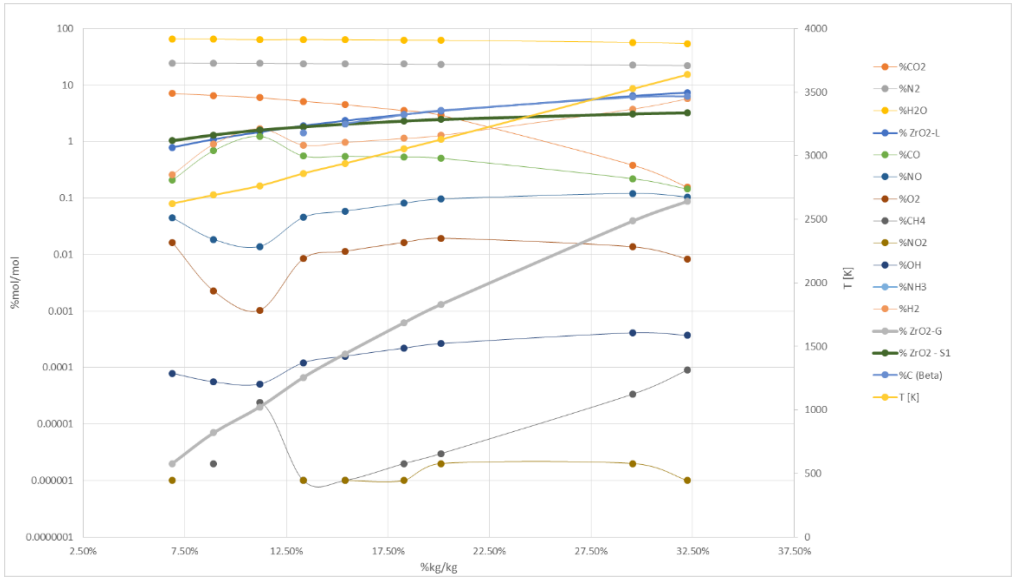

Figure 42 - Product Concentration G&M Method of Ammonium Nitrate and Zirconium Particles Detonation

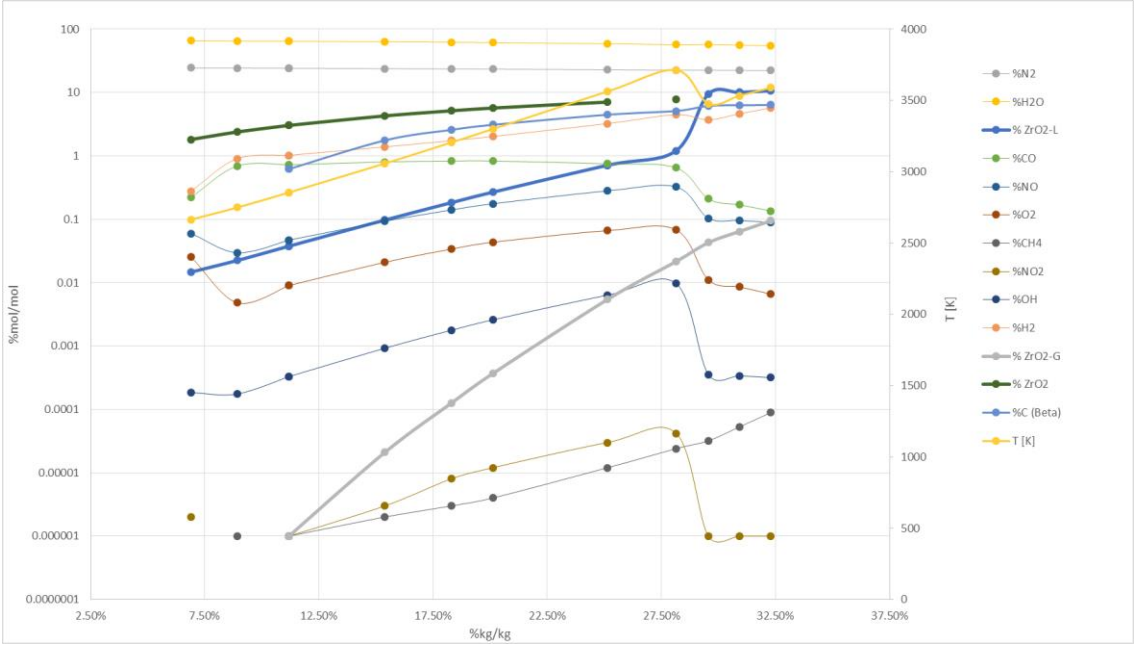

Figure 43 - Product Concentration MG+Debye Method of Ammonium Nitrate and Zirconium Particles Detonation

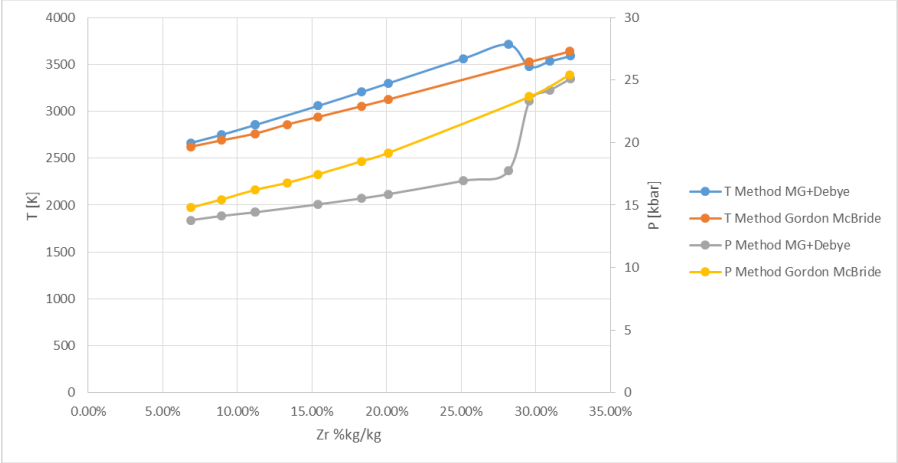

Figure 44 - Temperature and Pressure of Ammonium Nitrate and Zirconium Particles Detonation

With this simulations is possible to see that the model presented in this work represents with great accuracy the phenomena of the phase transition, proving the main advantage of the method. It's also shown the good correlation between the two methods of the concentrations of other products, validating its use.

The Zirconia stops appearing at a Zirconium concentration of 28.15%kg/kg, for a temperature of 3712K, which represents the simulation melting temperature of the solid, at the given pressure.

As for Alumina, ammonium nitrate and metal particles reactants were changed by a mixture of ammonium nitrate and zirconium nitrate, hydrated, in the emulsion

compositions [starting by the basic starting composition of 43.62 mass % of AN, 42.37 % of ZRO(NO3)2.H2O, 3.01 mass % of Fuel Oil, 5.89 % of Water, 0.15 % of Air and 4.97 % of Zirconium] and the products of detonation [CO2, N2, H2, H2O, ZrO2(L), NO2, NO, CO, O2, OH, H, N, O, C(alpha), C(gas), C(beta), NH3, ZrO2(G) and ZrO2(Cubic Fluorite Type or ZrO2-S1 (G&M Method)) components], and the mass concentration of Zr was increased from 4.97 until 27.69 %, keeping the mass concentration of other reactants (results in Figure 45, Figure 46 and Figure 47).

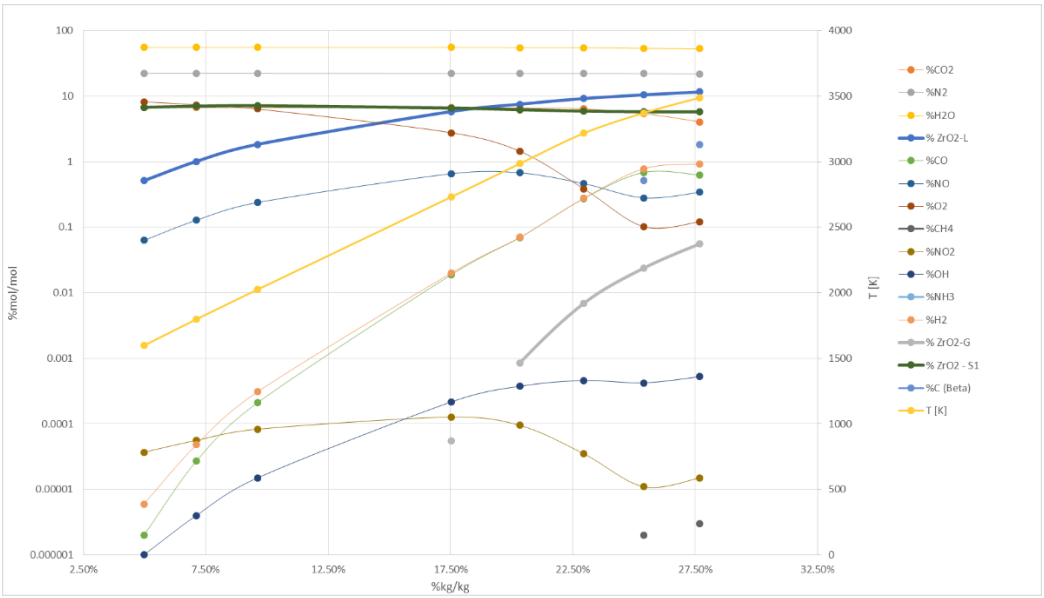

Figure 45 - Product Concentration G&M Method of Ammonium Nitrate and Zirconium Nitrate Precursors Detonation

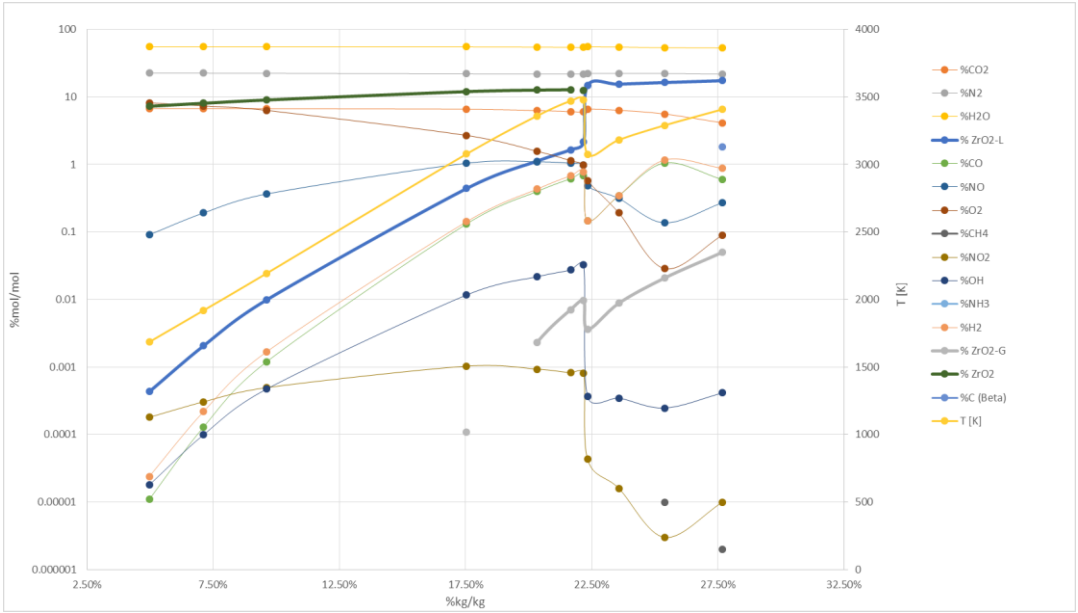

Figure 46 - Product Concentration MG+Debye Method of Ammonium Nitrate and Zirconium Nitrate Precursors Detonation

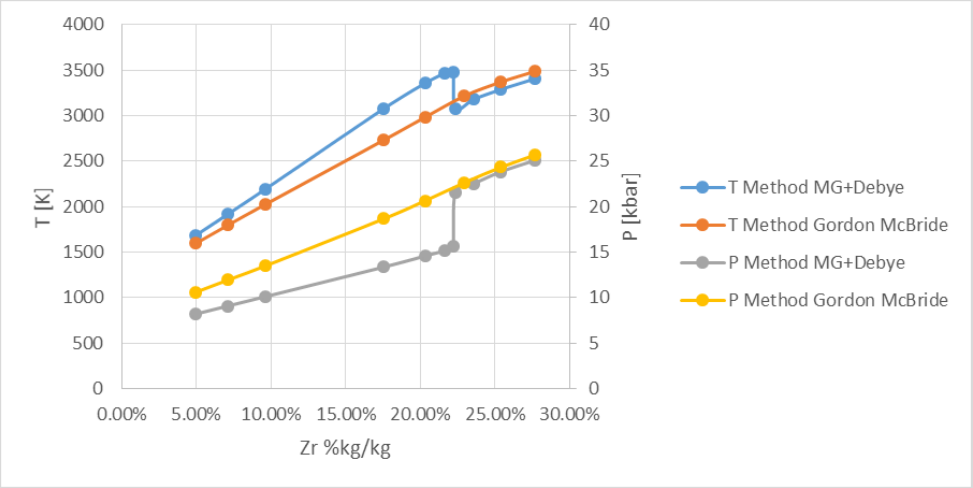

Figure 47 - Temperature and Pressure of Ammonium Nitrate and Zirconium Nitrate Precursors Detonation

As before the same phenomena is demonstrated in the figures above. Zirconia formation stops at a Zirconium concentration of 22.18%kg/kg, for a temperature of 3475K, which represents the simulation melting temperature of the solid, at the given pressure.

As shown, the detonation temperature decreases (for the same zirconium reactant concentration) using zirconium nitrate precursors, which leads to a higher production of Zirconia in detonation reaction (before reaches melting temperature), 12.48% with Nitrate precursors and 7.73% with just metal particles, see Figure 43 and Figure 46.

7.2.4. Magnesia

As for the other materials, similar modeling was made for magnesia. The reaction of magnesium and emulsion explosive can be predicted using THOR code, by the first method where the polynomials were derived in, Campos et al., 2014; Campos et al., 2008; Matias et al., 2010, and by the second and presented method with the previous represented parameters for B1 Phase (Table 9), as the detonation pressure is inferior to the formation of the high pressure phase (see Figure 11).

Keeping the basic starting composition [of 78.55 mass % of AN, 4.32 % of Fuel Oil, 8.26 % of Water, 0.41 % of Air and 8.46 % of Magnesium] and the products of detonation [C(alfa), H_2O, N_2, NH_3, MgO(G), NO_2, MgO (B1 or MgO-S (G&M Method)), MgO(L), NO, CO, H_2, OH, H, N, O, O_2, C(gas), C(beta), CO_2 components] it is possible to increase the concentration of Mg from 8.46 until 34.21 %, keeping the mass concentration of other reactants the same (results in Figure 48, Figure 49, Figure 50).

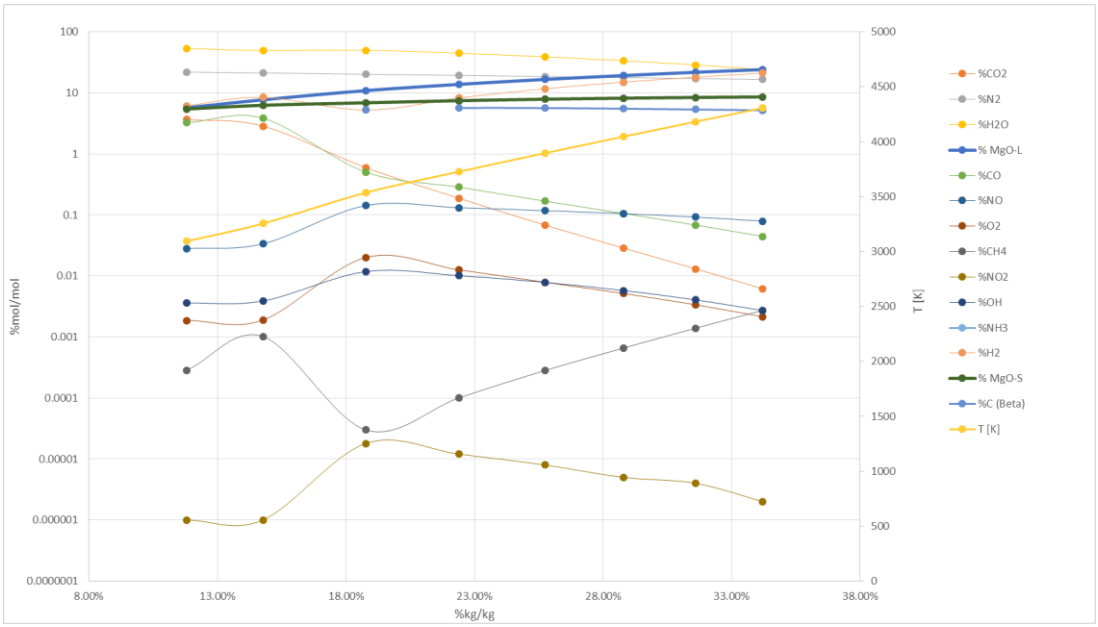

Figure 48 - Product Concentration G&M Method of Ammonium Nitrate and Magnesium Particles Detonation

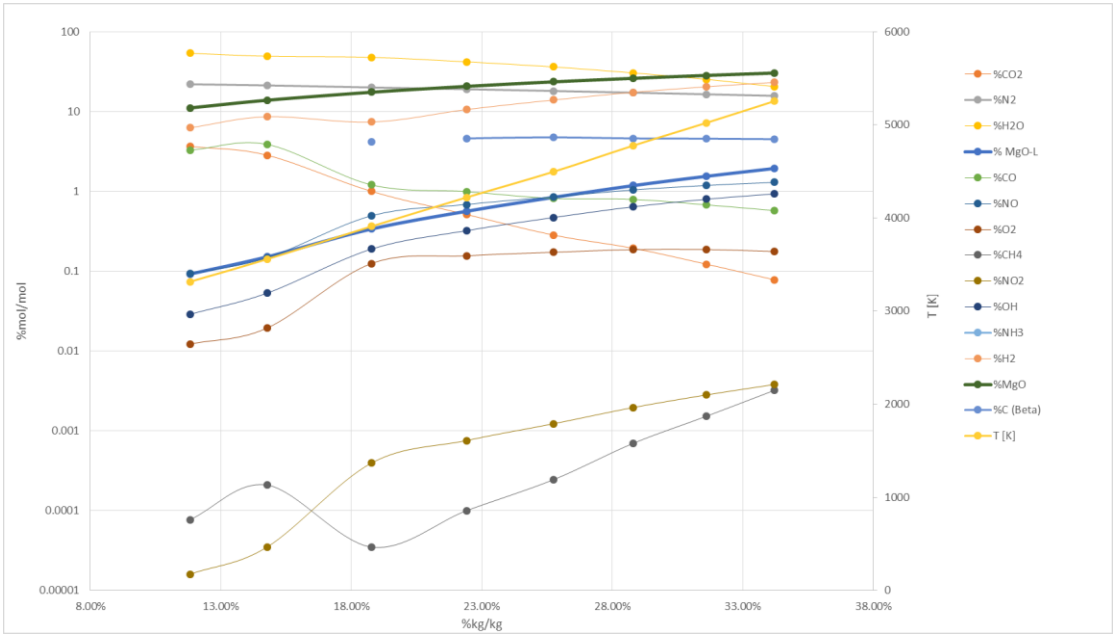

Figure 49 - Product Concentration MG+Debye Method of Ammonium Nitrate and Magnesium Particles Detonation

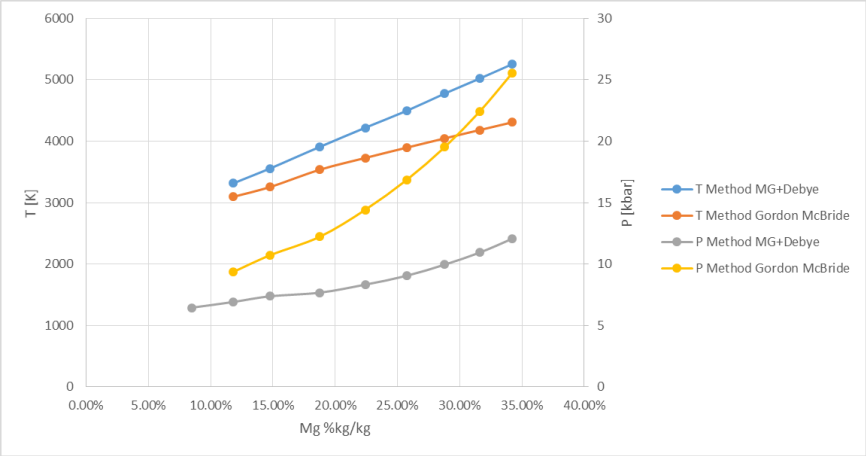

Figure 50 - Temperature and Pressure of Ammonium Nitrate and Magnesium Particles Detonation

The same phenomena is demonstrated in the figures above as for the other materials. Magnesia continues its formation with increasing percentage of Mg in reactants even for high temperatures (Figure 50). This results have to be analyzed through more studies to stablish the equation of melting curve (P-T) and see the validity the results. In Figure 11 high melting temperatures are showed, however for atmospheric pressure the melting temperature is around 2832 ºC ((Linde 1984)CRC Handbook of Chemistry and Physics).

Magnesia formation can be predicted and formed with ammonium nitrate and metal particles reaction, however it appears predominantly in post-detonation, as described before. As in Alumina formation, this material can be formed with the reaction of metal nitrate precursors, however the open market of solid Magnesium Nitrate is very difficult. This makes Magnesium to be the easy reactant.

8. CONCLUSIONS

In this work were derived thermal equations of state and energetic equations of state to represent the behavior of condensed solid products, for each material phase, showing more accurate representation of the phase change phenomena and results, compared to the previously used, which represented this products as high density gases. The materials studied were: Carbon (for comparison and validation of extrapolation), Alumina, Zirconia, Titania and Magnesia, being the two sets of equations defined for each phase, implemented in THOR program through the main parameters (vd Table 9). With this analysis the necessity of well described solid products is proven, with the aim of better modulate the final results, considering phase change phenomena. However, some of these materials need more research to better define its high temperature or high pressure phases and the respective behaviors.

A Cowan and Fickett EoS is used, in this work , representing with great accuracy the EoS extrapolated from other works, given its empirical formulation. However, in P-V-T relations there are still great uncertainties in the obtained data and most importantly in temperature relation. For a more extended analysis on the less studied materials, a theoretical high temperature approach can be made (as presented in chapter 3.2.2), with cold compression curve given in this work and temperature dependence given by the formulation presented in that chapter, where the parameters can be extrapolated from other papers. Another and more accurate way to obtain this EoS is through more studies in Theoretical Ab Initio Calculations or experimental procedures in conjunction with X-Ray Diffraction Measurements at high temperatures.

The model applied in order to represent Energetic Equations of State was a Mie-Grüneisen Approach with Thermal Contribution given by Debye Model. This model showed great improvements for the representation of solid condensed phases. For the implementation of this model, Grüneisen parameter was extensively studied. However, with a better and improved P-V-T relation, a more accurate parameter can be found. Some other represented parameters have to be also well studied in order to improve this equations, as the Debye Temperature (namely its sensibility in simulation), and Enthalpy and Entropy Formation, which would allow the implementation in the simulation of all phases studied.

As mentioned above, the simulations with the implemented equations for solids, were made in THOR program, with the parameters inscribed in its database. For a first simulation, carbon phases formation were analyzed, as it is a well studied material with extensive data for comparison. For this reason, its comparison of formation in reactive mixtures, as in Nitromethane, TNT and Ammonium Nitrate Emulsion detonations, is an important step to confirm simulations validity. Excellent results were obtained, which validates the equations derived and the extrapolation method of the parameters. This conclusion lead to the implementation of this method in the metal oxides study.

The most important variables to consider in simulation of metal oxide production are the concentration of reactants, detonation pressures and temperatures. The detonation CJ temperature and its evolution (by the post detonation expansion and cooling process) are the most relevant parameters in formation of final particles. The final temperature of the process can be associated to metal oxide melting temperature, conditioning final syntherized particles from initial cluster of nanocrystals. For this reason, a better prediction and representation of detonation temperature was the main objective of this thesis, implementing a different and more accurate model for solid specie representation.

It is assumed that its formation starts under shock behavior of detonation, according to classical theory of detonation. However, with ammonium nitrate emulsion and metal particle reagents, metal oxide formation occurs mainly in a post detonation zone. In order to reduce this delay, instead of reacting ammonium nitrate with metal, emulsion reactants can be formed from metal nitrated precursors. The use of precursors, as it was done in the prediction of Alumina and Zirconia, generates low detonation temperatures.

The results obtained from the simulations showed an excellent agreement with values of previous works, showing their high dependence on detonation temperature. For an even better analysis, the equation of melting curve (P-T) of each material can be compared with the detonation temperature that the solid product formation stops appearing, giving it’s melting temperature for a given pressure.

In conclusion, this is a very complex phenomena, evolving high pressure, very short delay times, fast complex reactions and expansion and cooling effects. The lack of information stay enormous and most of the times, equilibria calculations are abusively assumed. Nevertheless, the present work contributes to clarify these problems and the presented results show a very promising way of producing nano scale ceramic powders. It

proves the validity of prediction method which allows a more accurate process of choosing the initial reactants in the production phase.

BIBLIOGRAPHY

Abou El-Nour, K.M.M., Eftaiha, A., Al-Warthan, A. and Ammar, R. a a, 2010. Synthesis and applications of silver nanoparticles. *Arabian Journal of Chemistry*, 3(3), pp.135–140. Available at: http://dx.doi.org/10.1016/j.arabjc.2010.04.008.

Ahrens, T., Anderson, D. and Ringwood, A., 1969. Equations of State and Crystal Structures of High Pressure Phases of Shocked Silicates and Oxides. *Reviews of Geophysics*, 7(4), p.667.

Ahrens, T.J., 1966. High-Pressure Electrical Behavior and Equation of State of Magnesium Oxide from Shock Wave Measurements. *Journal of Applied Physics*, 37(7), pp.2532–2541. Available at: http://ieeexplore.ieee.org/xpls/abs_all.jsp?arnumber=5135017.

Ahrens, T.J., Gust, W.H. and Royce, E.B., 1968. Material strength effect in the shock compression of alumina. *Journal of Applied Physics*, 39(10), pp.4610–4616.

Ahrens, T.J. and Kondo, K., 1983. Shock Compression of Diamond Crystal. *Geophysical Research Letters*, 10(4), pp.281–284.

Al-Khatatbeh, Y., Lee, K.K.M. and Kiefer, B., 2009. High-pressure behavior of TiO2 as determined by experiment and theory. *Physical Review B - Condensed Matter and Materials Physics*, 79, pp.1–9.

Al-Khatatbeh, Y., Lee, K.K.M. and Kiefer, B., 2010. Phase relations and hardness trends of ZrO2 phases at high pressure. *Physical Review B*, 81, pp.1–10.

Anderson, O., 1995. *Equations of state of solids for geophysics and ceramic science*, Oxford Monographs on Geology and Geophysics.

Anderson, O.L. and Isaak, D., 1992. High-Temperature Elastic Constant Data on Minerals Relevant to Geophysics. *Reviews of Geophysics*, 30(91), pp.57–90.

Anderson, O.L. and Zou, K., 1990. Thermodynamic Functions and Properties of MgO at High Compression and High Temperature. *Journal of Physical and Chemical Reference Data*, 19, p.69. Available at: http://link.aip.org/link/JPCRBU/v19/i1/p69/s1&Agg=doi.

Arlt, T., Bermejo, M., Blanco, M., Gerward, L., Jiang, J., Staun Olsen, J. and Recio, J., 2000. High-pressure polymorphs of anatase TiO2. *Physical Review B*, 61(21), pp.14414–14419.

Arthur, J.S., 1950. The specific heats of MgO, TiO2, and ZrO2 at high temperatures. *Journal of Applied Physics*, 21(8), pp.732–733.

Belonoshko, A.B., Arapan, S., Martonak, R. and Rosengren, A., 2010. MgO phase diagram from first principles in a wide pressure-temperature range. *Physical Review B - Condensed Matter and Materials Physics*, 81(5), pp.1–9.

Birch, F., 1952. Elasticity and Constituition of the Earth's Interior. *Journal of Geophysical Research*, 57(2).

Blanco, J.A.S., 1986. *Desarrollo de un Metodo para el Calculo de las Caracteristicas Teoricas de los Explosivos*. Universidad Politecnicaa de Madrid.

Boettger, J.C., 1997. High-precision, all-electron, full-potential calculation of the equation of state and elastic constants of corundum. *Physical Review B*, 55(2), pp.750–756.

Bouvier, P., Djurado, E., Ritter, C., Dianoux, a J. and Lucazeau, G., 2001. Low temperature phase transformation of nanocrystalline tetragonal ZrO2 by neutrons and Raman Scattering studies. *International Journal of Inorganic Materials*, 3(7), pp.647–654. Available at: <Go to ISI>://WOS:000172827300009.

Bouvier, P., Dmitriev, V. and Lucazeau, G., 2003. The high-pressure phase sequence in nanocrystalline zirconia. *European Physical Journal B*, 35(3), pp.301–309.

Bouvier, P., Godlewski, J. and Lucazeau, G., 2002. A Raman study of the nanocrystallite size effect on the pressure-temperature phase diagram of zirconia grown by zirconium-based alloys oxidation. *Journal of Nuclear Materials*, 300(2-3), pp.118–126.

Bradley, D.K., Eggert, J.H., Smith, R.F., Prisbrey, S.T., Hicks, D.G., Braun, D.G., Biener, J., Hamza, a. V., Rudd, R.E. and Collins, G.W., 2009. Diamond at 800 GPa. *Physical Review Letters*, 102, pp.1–4.

Braithwaite, M. and Allan, N.L., 2006. Thermodynamic Representations for Solid Products in Ideal Detonation Predictions. *13th Symposium (International) on Detonation*. Available at: http://www.intdetsymp.org/detsymp2002/PaperSubmit/FinalManuscript/pdf/Braithwaite-157.pdf.

Bridgman, P.W., 1949. Linear Compressions to 30,000 Kg/Cm, including Relatively Incompressible Substances. *Proceedings of the American Academy of Arts and Science*, 77(6), pp.189–234.

Brinkley, S.R. and Wilson, E.B., 1943. *OSRD-1707*,

Bundy, F.P., Bassett, W. a., Weathers, M.S., Hemley, R.J., Mao, H.K. and Goncharov, a. F., 1996. The pressure-temperature phase and transformation diagram for carbon; updated through 1994. *Carbon*, 34(2), pp.141–153.

Butland, A.T.D. and Maddison, R.J., 1973. The specific heat of graphite: An evaluation of measurements. *Journal of Nuclear Materials*, 49, pp.45–56.

Caflin, K.C., Anderson, P.E., Cook, P., Hummers, W., Baker, E. and Stiel, L., 2012. The Detonation Properties of Combined Effects Explosives. In *in Proc. of the 43rd International Annual Conference of ICT, Karlsruhe, Fraunhofer-Institut für Chemische Technologie*. Karlsruhe, Germany.

Cai, J., Raptis, Y.S. and Anastassakis, E., 1993. Stabilized cubic zirconia: A Raman study under uniaxial stress. *Applied Physics Letters*, 62(22), pp.2781–2783.

Caldirola, P., 1946. On the Equation of State for Gases at Extremely High Pressure. *The Journal of Chemical Physics*, 14(12), p.738. Available at: http://scitation.aip.org/content/aip/journal/jcp/14/12/10.1063/1.1724096.

Campos, J., Durães, L., Andrade-Campos, A. and Portugal, A., 2007. Decomposition path of pyrolisis and combustion of thermite/nitrate/metal compositions. In *Proc. of the 38th International Annual Conference of ICT, Karlsruhe, Fraunhofer-Institut für Chemische Technologie*. Karlsruhe, Germany.

Campos, J., Matias, T., Durães, L., Andrade-Campos, A. and Portugal, A., 2012. Prediction Al, Ti and Zr Derived Oxides Formation by Detonation. In *Proc. of the 43rd International Annual Conference of ICT*. Karlsruhe, Germany: Fraunhofer-Institut für Chemische Technologie.

Campos, J., Mendes, R., Calado, J., Antunes, E., Durães, L., Portugal, A. and Andrade-Campos, A., 2008. Pedricted Kinetic Mechanisms Of Ceramic Formation From Detonation of Metal/Nitrates Compositions. In *Proc. of the 39th International Annual Conference of ICT, Karlsruhe, Fraunhofer-Institut für Chemische Technologie*. Karlsruhe, Germany.

Campos, J., Mendes, R., Santos, P., Duarte, B. and Oliveira, N., 2014. Metal oxide nanoparticle production from detonation – modelling and experimental developments. In *ICT*.

Caracas, R. and Cohen, R.E., 2007. Effect of Chemistry on the Physical Properties of Perovskite and Post-Perovskite. *Geophysical Monograph Series*, 174, pp.115–128.

Caracas, R. and Cohen, R.E., 2005. Prediction of a new phase transition in Al2O3 at high pressures. *Geophysical Research Letters*, 32(6), pp.1–4.

Caravaca, M. a, Miño, J.C., Pérez, V.J., Casali, R. a and Ponce, C. a, 2009. Ab initio study of the elastic properties of single and polycrystal TiO(2), ZrO(2) and HfO(2)

in the cotunnite structure. *Journal of physics. Condensed matter : an Institute of Physics journal*, 21, p.015501.

Cengiz, F. and Ulas, a., 2009. Numerical prediction of steady-state detonation properties of condensed-phase explosives. *Journal of Hazardous Materials*, 172, pp.1646–1651.

Chase, M.W., 1998. NIST-JANAF Thermochemical Tables. *Physical and Chemical Reference Data*, 9.

Chung, D.H., 1968. Pressure and Temperature Dependences of the Isotropic Elastic Moduli of Polycrystalline Alumina. *Journal of Applied Physics*, 39(11), p.5316. Available at: http://ieeexplore.ieee.org/xpl/articleDetails.jsp?arnumber=5092702.

Cohen, R.E., Mehl, M.J. and Boyer, L.L., 1988. Phase transitions and elasticity in zirconia. *Physica B+C*, 150(1-2), pp.1–9.

Coleburn, N.L., 1964. Compressibility of Pyrolytic Graphite. *The Journal of Chemical Physics*, 40, p.71. Available at: http://link.aip.org/link/JCPSA6/v40/i1/p71/s1&Agg=doi.

Colonna, F., Fasolino, A. and Meijer, E.J., 2011. High-pressure high-temperature equation of state of graphite from Monte Carlo simulations. *Carbon*, 49(2), pp.364–368. Available at: http://dx.doi.org/10.1016/j.carbon.2010.09.029.

Cook, M. a., 1947. An Equation of State for Gases at Extremely High Pressures and Temperatures from the Hydrodynamic Theory of Detonation. *The Journal of Chemical Physics*, 15(7), p.518. Available at: http://scitation.aip.org/content/aip/journal/jcp/15/7/10.1063/1.1746576.

Coppari, F., Smith, R.F., Eggert, J.H., Wang, J., Rygg, J.R., Lazicki, A., Hawreliak, J. a., Collins, G.W. and Duffy, T.S., 2013. Experimental evidence for a phase transition of magnesium oxide at exoplanet pressures . Supplementary Information. *Nature Geoscience*, 6, p.926.

Cowan, R.D. and Fickett, W., 1956. Calculation of the Detonation Properties of Solid Explosives with the Kistiakowsky-Wilson Equation of State. *The Journal of Chemical Physics*, 24, p.932. Available at: http://scitation.aip.org/content/aip/journal/jcp/24/5/10.1063/1.1742718.

Cowperthwaite, M., 1965. Significance of Some Equations of State Obtained from Shock-Wave Data. , pp.1025–1030.

Dash, L., Vast, N., Baranek, P., Cheynet, M.-C. and Reining, L., 2004. Electronic structure and electron energy-loss spectroscopy of ZrO2 zirconia. *Physical Review B*, 70, pp.1–17.

Davis, W. and Fauquignon, C., 1995. Classical Theory of Detonation. *Journal de Physique IV, Colloque C4*, 5.

Desgreniers, S. and Lagarec, K., 1999. High-density ZrO2 and HfO2: Crystalline structures and equations of state. *Physical Review B*, 59(13), pp.8467–8472.

Dewaele, A., Datchi, F., Loubeyre, P. and Mezouar, M., 2008. High pressure-high temperature equations of state of neon and diamond. *Physical Review B - Condensed Matter and Materials Physics*, 77, pp.1–9.

Dewaele, A., Fiquet, G., Andrault, D. and Hausermann, D., 2000. P-V-T equation of state of periclase from synchrotron radiation measurements. *Journal of Geophysical Research*, 105(B2), p.2869.

Dewaele, A. and Torrent, M., 2013. Equation of State of α -Al2O3. *Phys. Rev. B*, 88.

Dewhurst, J. and Lowther, J., 2001. Highly coordinated metal dioxides in the cotunnite structure. *Physical Review B*, 64, pp.1–7.

Dewhurst, J. and Lowther, J., 1998. Relative stability, structure, and elastic properties of several phases of pure zirconia. *Physical Review B*, 57(2), pp.741–747.

Dobratz, B.M., 1972. *Properties of Chemical Explosives and Explosive Simulants*,

Doran, D.G., 1963. Hugoniot Equation of State of Pyrolytic Graphite to 300 kbars. *Journal of Applied Physics*, 34, p.844.

Dubrovinskaia, N. a, Dubrovinsky, L.S., Ahuja, R., Prokopenko, V.B., Dmitriev, V., Weber, H.P., Osorio-Guillen, J.M. and Johansson, B., 2001. Experimental and theoretical identification of a new high-pressure TiO2 polymorph. *Physical review letters*, 87(1), p.275501.

Dubrovinsky, L.S., Dubrovinskaia, N. a, Swamy, V., Muscat, J., Harrison, N., Ahuja, R., Holm, B. and Johansson, B., 2001. The hardest known oxide. *Nature*, 410, pp.653–654.

Dubrovinsky, L.S., Saxena, S.K. and Lazor, P., 1998. High-pressure and high-temperature in situ X-ray diffraction study of iron and corundum to 68 GPa using an internally heated diamond anvil cell. *Physics and Chemistry of Minerals*, 25(6), pp.434–441.

Dugdale, J. and MacDonald, D., 1953. The Thermal Expansion of Solids. *Physical Review*, 89(4), pp.832–834.

Durães, L., Campos, J. and Portugal, A., 1996. Thermal Decomposition of Energetic Materials Using THOR Code. In *Proc. of the Twenty Second International Pyrotechnics Seminar*. Fort Collins, Colorado, pp. 497–508.

Eggert, J.H., Hicks, D.G., Celliers, P.M., Bradley, D.K., McWilliams, R.S., Jeanloz, R., Miller, J.E., Boehly, T.R. and Collins, G.W., 2010. Melting temperature of diamond at ultrahigh pressure. *Nature Physics*, 6(1), pp.40–43. Available at: http://dx.doi.org/10.1038/nphys1438.

Erskine, D.J. and Nellis, W.J., 1992. Shock-induced martensitic transformation of highly oriented graphite to diamond. *Journal of Applied Physics*, 71, pp.4882–4886.

Fadda, G., Colombo, L. and Zanzotto, G., 2009. First-principles study of the structural and elastic properties of zirconia. *Physical Review B - Condensed Matter and Materials Physics*, 79, pp.40–43.

Fadda, G., Zanzotto, G. and Colombo, L., 2010. First-principles study of the effect of pressure on the five zirconia polymorphs. I. Structural, vibrational, and thermoelastic properties. *Physical Review B - Condensed Matter and Materials Physics*, 82, pp.1–13.

Fahy, S. and Louie, S.G., 1987. High-pressure structural and electronic properties of carbon. *Physical Review B*, 36(6), pp.3373–3385.

Fei, Y., 1999. Effects of temperature and composition on the bulk modulus of (Mg,Fe)O. *American Mineralogist*, 84, pp.272–276.

Fei, Y., Li, J., Hirose, K., Minarik, W., Van Orman, J., Sanloup, C., van Westrenen, W., Komabayashi, T. and Funakoshi, K., 2004. A critical evaluation of pressure scales at high temperatures by in situ X-ray diffraction measurements. *Physics of the Earth and Planetary Interiors*, 143-144, pp.515–526.

Fried, L.E. and Howard, W.M., 2000. Explicit Gibbs free energy equation of state applied to the carbon phase diagram. *Physical Review B*, 61(13), pp.8734–8743.

Fu, C.L. and Ho, K.M., 1983. First-principles calculation of the equilibrium ground-state properties of transition metals: Applications to Nb and Mo. *Physical Review B*, 28(10), pp.5480–5486.

Fujihisa, H., Sidorov, V. a., Takemura, K., Kanda, H. and Stishov, S.M., 1996. Pressure dependence of the lattice constant of diamond: Isotopic effects. *Pis'ma Zh. Eksp. Teor. Fiz.*, 63, pp.73–77.

Gerward, L. and Staun Olsen, J., 1997. Post-Rutile High-Pressure Phases in TiO2. *Journal of Applied Crystallography*, 30, pp.259–264. Available at: http://scripts.iucr.org/cgi-bin/paper?S0021889896011454.

Gillet, P., Fiquet, G., Daniel, I., Reynard, B. and Hanfland, M., 1999. Equations of state of 12C and 13C diamond. *Physical Review B*, 60(21), pp.14660–14664.

Gordon, S. and McBride, B.J., 1994. Computer Program for Calculation of Complex Chemical Equilibrium Compositions and Applications I. Analysis. , p.58.

Goto, T., Anderson, O.L., Ohno, I. and Yamamoto, S., 1989. Elastic constants of corundum up to 1825 K. *Journal of Geophysical Research*, 94(B6), p.7588.

Gueddim, a, Bouarissa, N. and Villesuzanne, a, 2009. First-principles determination of structural properties of MgO. *Physica Scripta*, 80(5), p.055702.

Gust, W.H., 1980. Phase transition and shock-compression parameters to 120 GPa for three types of graphite and for amorphous carbon. *Physical Review B*, 22(10), pp.4744–4756.

Gust, W.H. and Royce, E.B., 1971. Dynamic yield strengths of B4C, BeO, and Al2O 3 ceramics. *Journal of Applied Physics*, 42(1), pp.276–295.

Haick, H., 2015. *Nanotechnology and Nanosensors Introduction to Nanotechnology*, Technion - Israel Institute of Technology.

Haines, J. and Léger, J.M., 1993. X-ray diffraction study of TiO2 up to 49 GPa. *Physica B: Condensed Matter*, 192, pp.233–237.

Haines, J., Léger, J.M. and Atouf, A., 1995. Crystal Structure and Equation of State of Cotunnite-Type Zirconia. *Journal of the American Ceramic Society*, 78(2), pp.445–448. Available at: http://doi.wiley.com/10.1111/j.1151-2916.1995.tb08822.x.

Hama, J. and Suito, K., 2002. The evidence for the occurrence of two successive transitions in Al2O3 from the analysis of Hugoniot data. *High Temperatures - High Pressures*, 34(3), pp.323–334.

Hanaor, D. a H. and Sorrell, C.C., 2011. Review of the anatase to rutile phase transformation. *Journal of Materials Science*, 46(4), pp.855–874.

Hanfland, M., Beister, H. and Syassen, K., 1989. Graphite under pressure: Equation of state and first-order Raman modes. *Physical Review B*, 39(17), pp.12598–12603.

Harris, P., 1972. *Some Physics of the Gruneisen Parameter*, Available at: http://www.dtic.mil/dtic/tr/fulltext/u2/751130.pdf.

Hervouët, A., Desbiens, N., Bourasseau, E. and Maillet, J.B., 2008. Microscopic approaches to liquid nitromethane detonation properties. *Journal of Physical Chemistry B*, 112(16), pp.5070–5078.

Heuzé, O., 2001. A Complete Equaiton of State for Detonation Products in Hydrocodes. *Shock Compression of Condensed Matter*, p.450.

Heuzé, O., Goutelle, J.C. and Baudin, G., 2001. A New Temperature-Dependent Equation of State for Inert, Reactive and Composite Materials. *Shock Compression of Condensed Matter*, pp.169–172. Available at: http://link.aip.org/link/?APC/620/169/1&Agg=doi.

Hicks, D.G., Boehly, T.R., Celliers, P.M., Bradley, D.K., Eggert, J.H., McWilliams, R.S., Jeanloz, R. and Collins, G.W., 2008. High-precision measurements of the diamond Hugoniot in and above the melt region. *Physical Review B - Condensed Matter and Materials Physics*, 78, pp.1–8.

Ingel, R.P. and Lewis III, D., 1986. Lattice Parameters and Density for Y203-Stabilized ZrO2. *Journal of the American Ceramic Society*, 69(4), pp.325–32t.

Isaak, D.G., 1990. Calculated Elastic and Thermal Properties of MgO at High Pressures and Temperatures. *journal of geophysical Research*, 95(B5), pp.7055–7067.

Isaak, D.G., Carnes, J.D., Anderson, O.L., Cynn, H. and Hake, E., 1998. Elasticity of TiO2 rutile to 1800 K. *Physics and Chemistry of Minerals*, 26(1), pp.31–43.

Iuga, M., Steinle-Neumann, G. and Meinhardt, J., 2007. Ab-initio simulation of elastic constants for some ceramic materials. *European Physical Journal B*, 58(2), pp.127–133.

Jacobsen, S.D., Holl, C.M., Adams, K. a., Fischer, R. a., Martin, E.S., Bina, C.R., Lin, J.F., Prakapenka, V.B., Kubo, A. and Dera, P., 2008. Compression of single-crystal magnesium oxide to 118 GPa and a ruby pressure gauge for helium pressure media. *American Mineralogist*, 93, pp.1823–1828.

Jaffe, J.E., Bachorz, R. a. and Gutowski, M., 2005. Low-temperature polymorphs of ZrO2 and HfO2: A density-functional theory study. *Physical Review B - Condensed Matter and Materials Physics*, 72(14), pp.1–9.

Jaffe, J.E., Snyder, J.A., Lin, Z. and Hess, A.C., 2000. LDA and GGA calculations for high-pressure phase transitions in ZnO and MgO. *Physical Review B*, 62(3), pp.1660–1665.

Jansen, H.J.F., 1991. Electronic structure of cubic and tetragonal zirconia. *Physical Review B*, 43(9), pp.7267–7278.

Jayaraman, A., Wang, S.Y., Sharma, S.K. and Ming, L.C., 1993. Pressure-induced phase transformations in HfO2 to 50 GPa studied by Raman spectroscopy. *Physical Review B*, 48(13), pp.9205–9211.

Jin, K., Li, X., Wu, Q., Geng, H., Cai, L., Zhou, X. and Jing, F., 2010. The pressure-volume-temperature equation of state of MgO derived from shock Hugoniot data and its application as a pressure scale. *Journal of Applied Physics*, 107, pp.0–6.

Jin, L., Ni, L., Yu, Q., Rauf, A. and Zhou, C., 2012. Theoretical calculations of thermodynamic properties of tetragonal ZrO2. *Computational Materials Science*, 65, pp.170–174. Available at: http://dx.doi.org/10.1016/j.commatsci.2012.07.008.

Jones, H. and Miller, a. R., 1948. The Detonation of Solid Explosives: The Equilibrium Conditions in the Detonation Wave-Front and the Adiabatic Expansion of the Products of Detonation. *Proceedings of the Royal Society A: Mathematical, Physical and Engineering Sciences*, 194(1039), pp.480–507.

Kihara, T. and Hikita, T., 1953. Equation of state for hot dense gases and molecular theory of detonation. *Symposium (International) on Combustion*, 4(1), pp.458–464.

Kisi, E. and Yuxiang, M., 1999. Debye temperature, anharmonic thermal motion and oxygen non-stoichiometry in yttria stabilized cubic zirconia. *Journal of Physics: Condensed Matter*, 10(17), pp.3823–3832.

Kisi, E.H. and Howard, C.J., 1998. Crystal Structures of Zirconia Phases and their Inter-Relation. *Key Engineering Materials*, 153-154, pp.1–36.

Kleiser, G.J., Chhabildas, L.C. and Reinhart, W.D., 2011. Comparison of dynamic compression behavior of single crystal sapphire to polycrystalline alumina. *International Journal of Impact Engineering*, 38, pp.473–479.

Koči, L., Kim, D.Y., de Almeida, J.S., Mattesini, M., Isaev, E. and Ahuja, R., 2008. Mechanical stability of TiO2 polymorphs under pressure: ab initio calculations. *Journal of Physics: Condensed Matter*, 20, p.345218.

Krumhansl, J. and Brooks, H., 1953. The Lattice Vibration Specific Heat of Graphite. *The Journal of Chemical Physics*, 21(10), p.1663. Available at: http://link.aip.org/link/JCPSA6/v21/i10/p1663/s1&Agg=doi.

Kunc, K., Loa, I. and Syassen, K., 2003. Equation of state and phonon frequency calculations of diamond at high pressures. *Physical Review B*, 68, pp.1–9.

Lagarec, K. and Desgreniers, S., 1995. Raman study of Single Crystal Anatase TiO2 upto 70 GPa. *Solid State Communications*, 94(7), pp.519–524.

Lawless, W.N. and Gupta, T.K., 1983. Thermal properties of tetragonal ZrO2 at low temperatures. *Physical Review B*, 28(10), pp.5507–5510.

Leger, J.M., Tomaszewski, P.E., Atouf, a. and Pereira, a. S., 1993. Pressure-induced structural phase transitions in zirconia under high pressure. *Physical Review B*, 47(21), pp.14075–14083.

Li, C.W., McKerns, M.M. and Fultz, B., 2011. A Raman spectrometry study of phonon anharmonicity of zirconia at elevated temperatures. *Journal of the American Ceramic Society*, 94(1), pp.224–229.

Liang, Y., Zhang, B. and Zhao, J., 2008. Mechanical properties and structural identifications of cubic TiO2. *Physical Review B*, 77, pp.30–34.

Linde, D., 1984. *CRC Handbook of Chemistry and Physics* 65th Editi.,

Liu, L., 1980. New high pressure phases of ZrO2 and HfO2. *J. Phys. Chem. Solids*, 41, pp.331–334.

Liu, Q.J., Liu, Z.T. and Feng, L.P., 2011. Elasticity, electronic structure, chemical bonding and optical properties of monoclinic ZrO2 from first-principles. *Physica B: Condensed Matter*, 406(3), pp.345–350. Available at: http://dx.doi.org/10.1016/j.physb.2010.10.057.

Lowitzer, S., Winkler, B. and Tucker, M., 2006. Thermoelastic behavior of graphite from in situ high-pressure high-temperature neutron diffraction. *Physical Review B - Condensed Matter and Materials Physics*, 73, pp.1–8.

Lowther, J.E., Dewhurst, J.K., Leger, J.M. and Haines, J., 1999. Relative stability of ZrO2 and HfO2 structural phases. *Physical Review B*, 60(21), pp.14485–14488. Available at: http://link.aps.org/doi/10.1103/PhysRevB.60.14485\nhttp://prb.aps.org/abstract/PRB/v60/i21/p14485_1\nhttp://prb.aps.org/pdf/PRB/v60/i21/p14485_1.

Luo, W., Yang, S.F., Wang, Z.C., Wang, Y., Ahuja, R., Johansson, B., Liu, J. and Zou, G.T., 2005. Structural phase transitions in brookite-type TiO2 under high pressure. *Solid State Communications*, 133, pp.49–53.

Lynch, R.W. and Drickamer, H., 1966a. Effect of High Pressure on the Lattice Parameters of Diamond, Graphite, and Hexagonal Boron Nitride. *The Journal of Chemical Physics*, 44, p.181. Available at: http://link.aip.org/link/?JCP/44/181/1&Agg=doi.

Lynch, R.W. and Drickamer, H., 1966b. Effect of High Pressure on the Lattice Parameters of Diamond, Graphite, and Hexagonal Boron Nitride. *The Journal of Chemical Physics*, 44(1), p.181. Available at: http://link.aip.org/link/?JCP/44/181/1&Agg=doi.

Mader, C., 1963. *Detonation properties of condensed explosives computed using the BKW Equation of State*,

Mader, C., 1998. *Numerical Modelling of Explosives and Propellants* 2nd Editio., CRC Press, Boca Ration, FL, USA.

Mallard, W.G. and Linstrom, P.J., 2011. NIST Livro de Química na Web. Available at: http://webbook.nist.gov/chemistry/ [Accessed June 7, 2015].

Manghnani, M.H., 1969. Elastic constants of single-crystal rutile under pressures to 7.5 kilobars. *Journal of Geophysical Research*, 74(17).

Mao, H.K. and Bell, P.M., 1979. Equations of State of MgO and e Fe Under Static Pressure Condition. *Journal of Geophysical Research*, 84(B9), pp.4533–4536.

Marquardt, H., Speziale, S., Marquardt, K., Reichmann, H.J., Konôpková, Z., Morgenroth, W. and Liermann, H.P., 2011. The effect of crystallite size and stress condition on the equation of state of nanocrystalline MgO. *Journal of Applied Physics*, 110.

Marsh, S., 1980. *LASL shock Hugoniot data*, Available at: http://books.google.com/books?hl=en&lr=&id=-PCJtmM91JcC&oi=fnd&pg=PA1&dq=LASL+Shock+Hugoniot+Data&ots=T2EZfiMc-C&sig=mCYVlQJ9c9061ikGxzHBArEZDjc.

Mashimo, T., Elert, M., Furnish, M.D., Chau, R., Holmes, N. and Nguyen, J., 2007. Shock Compression Properties of Hard Materials. *Shock Compression of Condensed Matter*, pp.175–180. Available at: http://scitation.aip.org/content/aip/proceeding/aipcp/10.1063/1.2833002.

Mashimo, T., Hanaoka, Y. and Nagayama, K., 1988. Elastoplastic properties under schock compression of Al2O3 single crystal and polycrystal. *Journal of Applied Physics*, 63.

Mashimo, T., Nakamura, A., Kodama, M., Kusaba, K., Fukuoka, K. and Syono, Y., 1995. Cubic Zirconia Single Crystal and Polycrystal. *Journal of Applied Physics*, 77(10).

Mashimo, T., Tsumoto, K., Nakamura, K., Fukuoka, K., Noguchi, Y. and Syono, Y., 2000. High Pressure Phase Transformation of Corundum (α-Al2O3) Observed under Shock Compression. *Geophysical Research Letters*, 27(14), pp.2021–2024.

Matias, T., Durães, L., Andrade-Campos, A., Mendes, R., Campos, J., Portugal, A., Antunes, E., Calado, J., Lagoa, A. and Silva, S.M.P. da, 2010. Prediction and Experimental Al, Mg, Ti and Zr derived Oxides and Spinels Formation by Detonation. In *ICT 2010*.

Matsui, M., Parker, S.C. and Leslie, M., 2000. The MD simulation of the equation of state of MgO: Application as a pressure calibration standard at high temperature and high pressure. *American Mineralogist*, 85(2), pp.312–316.

Mattesini, M., De Almeida, J.S., Dubrovinsky, L., Dubrovinskaia, N., Johansson, B. and Ahuja, R., 2004. High-pressure and high-temperature synthesis of the cubic

TiO2 polymorph. *Physical Review B - Condensed Matter and Materials Physics*, 70, pp.1–4.

MCQueen, R., Jamieson, J. and Marsh, S., 1967. Shock-Wave Compressin and X-Ray Studies of Titanium Dioxide. *Science*, 15, p.360.

McSkimin, H. and Andreatch, P., 1972. Elastic Moduli of Diamond as a Function of Pressure and Temperature. *Journal of Applied Physics*, 43, pp.2944–2948. Available at: http://scitation.aip.org/content/aip/journal/jap/43/7/10.1063/1.1661636.

Mei, Z.-G., Wang, Y., Shang, S. and Liu, Z.-K., 2014. First-principles study of the mechanical properties and phase stability of TiO2. *Computational Materials Science*, 83, pp.114–119. Available at: http://www.sciencedirect.com/science/article/pii/S0927025613006927.

Mendes, R., Ribeiro, J., Plaksin, I. and Campos, J., 2011. Non ideal detonation of emulsion explosives mixed with metal particles. *Shock Compression of Condensed Matter*, 1426, pp.267–270.

Mendes, R., Ribeiro, J., Plaksin, I., Campos, J. and Tavares, B., 2014. Differences between the detonation behavior of emulsion explosives sensitized with glass or with polymeric micro-balloons. *Journal of Physics: Conference Series*, 500. Available at: http://stacks.iop.org/1742-6596/500/i=5/a=052030?key=crossref.3f74aa5715c48bf4a423f999b5d10377.

Milman, V., Perlov, A., Refson, K., Clark, S.J., Gavartin, J. and Winkler, B., 2009. Structural, electronic and vibrational properties of tetragonal zirconia under pressure: a density functional theory study. *Journal of physics. Condensed matter : an Institute of Physics journal*, 21(48), p.485404.

Miloua, R., Kebbab, Z., Benramdane, N., Khadraoui, M. and Chiker, F., 2011. Ab initio prediction of elastic and thermal properties of cubic TiO2. *Computational Materials Science*, 50(7), pp.2142–2147. Available at: http://dx.doi.org/10.1016/j.commatsci.2011.02.020.

Ming, L. and Manghnani, M., 1979. Isothermal Compression of TiO2 (Rutile) Under Hydrostatic Pressure to 106 kbar. *journal of geophysical Research*, 84, pp.1–3.

Mitra, S., Brafman, O., Daniels, W. and Crawford, R., 1969. Pressure Induced Phonon Frequency Shifts Measured by Raman Scattering. *Physical Review*, 186(3), pp.942–944.

Mo, S. Di and Ching, W.Y., 1995. Electronic and optical properties of three phases of titanium dioxide: Rutile, anatase, and brookite. *Physical Review B*, 51(19), pp.13023–13032.

Molodets, A.M., Shakhray, D. V., Golyshev, a. a., Babare, L. V. and Avdonin, V. V., 2006. Equation of state of solids from high-pressure isotherm. *High Pressure Research*, 26(3), pp.223–231.

Mukherjee, D., Joshi, K.D. and Gupta, S.C., 2013. High pressure equation of state and ideal compressive and tensile strength of MgO single crystal: Ab-initio calculations. *Journal of Applied Physics*, 113.

Munson, D.E. and Lawrence, R.J., 1979. Dynamic Deformation of Polycrystalline Alumina. *Journal of Applied Physics*, 50(10), pp.6272–6282.

Murnaghan, F.D., 1937. Finite Deformations of an Elastic Solid. *American Journal of Mathematics*, 59(2), pp.235–260.

Muscat, J., Swamy, V. and Harrison, N., 2002. First-principles calculations of the phase stability of TiO2. *Physical Review B*, 65, pp.1–15.

NASA Glenn Reasearch Center, 2010. Chemical Equilibrium With Applications. *http://www.grc.nasa.gov/WWW/CEAWeb/ceaHome.htm*.

Neves, N., Lagoa, A., Calado, J., Botelho do Rego, a. M., Fortunato, E., Martins, R. and Ferreira, I., 2014. Al-doped ZnO nanostructured powders by emulsion detonation synthesis - Improving materials for high quality sputtering targets manufacturing. *Journal of the European Ceramic Society*, 34(10), pp.2325–2338. Available at: http://dx.doi.org/10.1016/j.jeurceramsoc.2014.02.019.

Nihira, T. and Iwata, T., 2003. Temperature dependence of lattice vibrations and analysis of the specific heat of graphite. *Physical Review B*, 68, pp.1–16.

Nishio-Hamane, D., Shimizu, A., Nakahira, R., Niwa, K., Sano-Furukawa, A., Okada, T., Yagi, T. and Kikegawa, T., 2010. The stability and equation of state for the cotunnite phase of TiO2 up to 70 GPa. *Physics and Chemistry of Minerals*, 37, pp.129–136.

Occelli, F., Loubeyre, P. and LeToullec, R., 2003. Properties of diamond under hydrostatic pressures up to 140 GPa. *Nature materials*, 2, pp.151–154.

Oganov, A.R. and Ono, S., 2005. The high-pressure phase of alumina and implications for Earth's D" layer. *Proceedings of the National Academy of Sciences of the United States of America*, 102(31), pp.10828–10831.

Ohtaka, O., Andrault, D., Bouvier, P., Schultz, E. and Mezouar, M., 2005. Phase relations and equation of state of ZrO2 to 100 GPa. *Journal of Applied Crystallography*, 38(5), pp.727–733.

Ohtaka, O., Fukui, H., Funakoshi, K., Utsumi, W., Irifune, T. and Kikegawa, T., 2002. Phase Relations and EOS of ZrO 2 and HfO 2 Under High-temperature and High-pressure. *High Pressure Research*, 22, pp.221–226.

Olsen, J.S., Gerward, L. and Jiang, J.Z., 1999. On the rutile/alpha-PbO2-type phase boundary of TiO 2. *Journal of Physics and Chemistry of Solids*, 60, pp.229–233.

Ono, S., Oganov, A.R., Koyama, T. and Shimizu, H., 2006. Stability and compressibility of the high-pressure phases of Al2O3 up to 200 GPa: Implications for the electrical conductivity of the base of the lower mantle. *Earth and Planetary Science Letters*, 246, pp.326–335.

Ornellas, D.L., 1968. The Heat and Products of Detonation of Cyclotetramethylenetetranitramine , 2,4,6-Trinitroluene, Nitromethane, and Bis[2,2-dinitro-2-fluoroethyl]formal. *journal of physical Chemistry*, 72(7), pp.2390–2394.

Overney, R., 2010. *Nanothermodynamics and Nanoparticle Synthesis*,

Parsons, B.J., 1977. Spectroscopic Mode Gruneisen Parameters for Diamond. *Proceedings of the Royal Society A: Mathematical, Physical and Engineering Sciences*, 352, pp.397–417.

Paterson, S., 1948. The hydrodynamic theory of detonation; on absolute calculations for condensed explosives. *Research*, 1(5), pp.221–233.

Poirier, J.-P., 2000. *Introduction to the Physics of the Earth's Interior*, Available at: http://ebooks.cambridge.org/ref/id/CBO9781139164467.

Quareni, F. and Mulargia, F., 1989. The Grüneisen parameter and adiabatic gradient in the Earth's interior. *Physics of the Earth and Planetary Interiors*, 55, pp.221–233.

READE, READE Advanced Materials. Available at: http://www.reade.com/ [Accessed July 4, 2015].

Reeber, R.R. and Wang, K., 1996. Thermal expansion, molar volume and specific heat of diamond from 0 to 3000k. *Journal of Electronic Materials*, 25(1), pp.63–67.

Reinhart, W.D. and Chhabildas, L.C., 2003. Strenght Properties of Coors AD995 Alumina in the Shocked State. *International Journal of Impact Engineering*, 29, pp.601–619.

Ren, H., Zhu, B., Zhu, J., Hao, Y., Yu, B. and Li, Y., 2011. The structural phase transition and elastic properties of zirconia under high pressure from first-principles calculations. *Solid State Sciences*, 13(5), pp.938–943. Available at: http://dx.doi.org/10.1016/j.solidstatesciences.2011.02.013.

Sato, Y. and Akimoto, S., 1979. Hydrostatic compression of four corundum-type compounds: α-Al2O3, V2O3, Cr2O3, and α-Fe2O3. *Journal of Applied Physics*, 50(8), p.5285. Available at: http://link.aip.org/link/JAPIAU/v50/i8/p5285/s1&Agg=doi.

Schauer, A., 1965. Thermal Expansion, Grueneisen Parameter, and Temperature Dependence of Lattice Vibration Frequencies of Aluminum Oxide. *Canadian Journal of Physics*, 43, pp.523–531.

Schleife, A., Fuchs, F., Furthmüller, J. and Bechstedt, F., 2006. First-principles study of ground- and excited-state properties of MgO, ZnO, and CdO polymorphs. *Physical Review B - Condensed Matter and Materials Physics*, 73(24), pp.1–14.

Schreiber, E. and Anderson, O.L., 1966. Pressure Derivatives of the Sound Velocities of Polycrystalline Alumina. *Journal of The American Ceramic Society*, 49(4), pp.184–190.

Silva, J.M.C. da and Antunes, E.M. dos S., 2013. Nanometric-Sized Ceramic Materials, Process for Their Synthesis and Uses Thereof.

Silva, S.M.P. da and Silva, J.M.C. da, 2013. Continuous Process for Nanomaterial Synthesis from Simultaneous Emulsification and Detonation of an Emulsion.

Speziale, S., Zha, C.S., Duffy, S., Hemley, J. and Mao, H.-K., 2001. Quasi-hydrostatic compression of magnesium oxide to 52 GPa: Implications for the pressure-volume-temperature equation of state. *J. Geophys. Res.*, 106(B1), pp.515–528.

Stapper, G., Bernasconi, M., Nicoloso, N. and Parrinello, M., 1999. Ab initio study of structural and electronic properties of yttria-stabilized cubic zirconia. *Physical Review B*, 59(2), pp.797–810.

Stir, M., Nicula, R. and Burkel, E., 2006. Pressure-temperature phase diagrams of pure and Ag-doped nanocrystalline TiO2 photocatalysts. *Journal of the European Ceramic Society*, 26(9), pp.1547–1553.

Sućeska, M., 2004. Calculation of Detonation Parameters by EXPLO5 Computer Program. *Materials Science Forum*, 465-466, pp.325–330.

Sumino, Y., Anderson, O.L. and Suzuki, I., 1983. Temperature coefficients of elastic constants of single crystal MgO between 80 and 1,300 K. *Physics and Chemistry of Minerals*, 9(1), pp.38–47.

Swamy, V., Dubrovinskaia, N. a and Dubrovinsky, L.S., 2002. Compressibility of baddeleyite-type TiO 2 from static compression to 40 GPa. *Alloys and Compounds*, 340, pp.46–48.

Swamy, V. and Muddle, B.C., 2007. Ultrastiff cubic TiO2 identified via first-principles calculations. *Physical Review Letters*, 98, pp.1–4.

Terki, R., Bertrand, G., Aourag, H. and Coddet, C., 2006. Structural and electronic properties of zirconia phases: A FP-LAPW investigations. *Materials Science in Semiconductor Processing*, 9(6), pp.1006–1013.

Van Thiel, M. and Ree, F.H., 1987. Properties of carbon clusters in TNT detonation products: Graphite-diamond transition. *Journal of Applied Physics*, 62(5), pp.1761–1767.

Van Thiel, M. and Ree, F.H., 1989. Theoretical description of the graphite, diamond, and liquid phases of carbon. *International Journal of Thermophysics*, 10(1), pp.227–236.

Van Thiel, M. and Ree, F.H., 1992. Thermodynamic properties and phase diagram of the graphite-diamond-liquid carbon system. *High Pressure Research*, 10, pp.607–627.

Thompson, K., Wentzcovitch, R.M. and Bukowinski, M.S.T., 1996. Polymorfs of Alumina Predicted by First Principles: Putting Pressure on the Ruby Pressure Scale. *Science*, 274, pp.1880–1882.

Toraya, H., Ohtaka, O. and Kume, S., 1987. Unit Cell Parameters and Densities of Non-Doped and 2 mol% Y2O3 doped Orthorhombic (high pressure form) ZrO2. *Mineralogical Journal*, 13(8), pp.500–504.

Tsuchiya, J., Tsuchiya, T. and Wentzcovitch, R.M., 2005. Transition from the Rh2O3(II)-to-CaIrO3 structure and the high-pressure-temperature phase diagram of alumina. *Physical Review B - Condensed Matter and Materials Physics*, 72.

Turkel, M.-L. and Charlet, F., 1995. Carbon in Detonation Products. A "Three-Phase" Modelisation. *Journal de Physique IV*, 5, pp.407–416.

Vahora, A.Y., Chaudhari, P., Bhatt, N.K., Thakore, B.Y., Jani, A.R., Vahora, A.Y., Chaudhari, P., Bhatt, N.K., Thakore, B.Y. and Jani, A.R., 2013. Phase Transition and Shock Hugoniot of MgO using Tight-Binding Model. *AIP Conference Proceedings 1536 (2013)*, 421, pp.2013–2015.

Victor, A.C., 1962. Heat Capacity of Diamond at High Temperatures. *The Journal of Chemical Physics*, 36(7).

Vinet, P., Ferrante, J., Rose, J.H. and Smith, J.R., 1987. Compressibility of Solids. *Journal of Geophysical Research*, 92(B9), pp.9319–9325.

Wang, W., Liang, Z., Han, X., Chen, J., Xue, C. and Zhao, H., 2015. Mechanical and thermodynamic properties of ZrO 2 under high-pressure phase transition : A first-

principles study. *JOURNAL OF ALLOYS AND COMPOUNDS*, 622, pp.504–512. Available at: http://dx.doi.org/10.1016/j.jallcom.2014.08.114.

White, G.K. and Anderson, O.L., 1966. Gruneisen parameter of magnesium oxide. *Journal of Applied Physics*, 37(1), pp.430–432.

Whitney, E., 1962. Effect of Pressure on Monoclinic-TetragonaI Transition of Zirconia; Thermodynamics. *Journal of the American Ceramic Society*, 45(12), pp.612–613.

Wu, a. Y. and Sladek, R.J., 1982. Elastic Debye temperatures in tetragonal crystals: Their determination and use. *Physical Review B*, 25(8), pp.5230–5233.

Wu, X., Holbig, E. and Steinle-Neumann, G., 2010. Structural stability of TiO2 at high pressure in density-functional theory based calculations. *Journal of physics. Condensed matter : an Institute of Physics journal*, 22, p.295501.

Zha, C.S., Mao, H. and Hemley, R.J., 2000. Elasticity of MgO and a primary pressure scale to 55 GPa. *Proceedings of the National Academy of Sciences of the United States of America*, 97(25), pp.13494–13499.

Zhang, J., 2000. Effect of pressure on the thermal expansion of MgO up to 8.2 GPa. *Phys. Chem. Minerals*, 27, pp.145–148.

Zhao, X.S., Shang, S.L., Liu, Z.K. and Shen, J.Y., 2011. Elastic properties of cubic, tetragonal and monoclinic ZrO2 from first-principles calculations. *Journal of Nuclear Materials*, 415(1), pp.13–17. Available at: http://dx.doi.org/10.1016/j.jnucmat.2011.05.016.

ANNEX A – P-V-T RELATIONS

Alumina

Rh_2O_3(II)-type

For this case only theoretical data are found (Oganov & Ono 2005; Caracas & Cohen 2005; Thompson et al. 1996). As the data presented is only for T=0K, the Solid EoS will not depend in temperature. Therefore:

$$P = (168.435 - 592.258\eta + 424.0157\eta^2) \quad \textbf{(69)}$$

With ρ_0=2.755476 g/cm^3 (for T_0=0K and P=0 GPa). This value was derived from Tsuchiya et al., 2005, where V=30.163 cm^3/mol at P=80 GPa.

Perovskite

For this structure only theoretical data are obtained (Oganov & Ono 2005; Caracas & Cohen 2005) As the data presented is only for T=0K, the Solid EoS will not depend on temperature. The solid EoS is:

$$P = (194.76 - 605.625\eta + 411.0202\eta^2) \quad \textbf{(70)}$$

With ρ_0=4.259522 g/cm^3 (for T_0=0K and P=0 GPa). This value was derived from Caracas & Cohen, 2007, where ρ =5.697 g/cm^3 at P=120 GPa.

$CaIrO_3$-type (post-perovskite structure)

In this structure three paper's data were analyzed (Ono et al. 2006; Oganov & Ono 2005; Caracas & Cohen 2005). In this case the equation of state was based in Caracas & Cohen, 2005, because it is a good representation of experimental data (Ono et al. 2006), as shown in Figure 51.

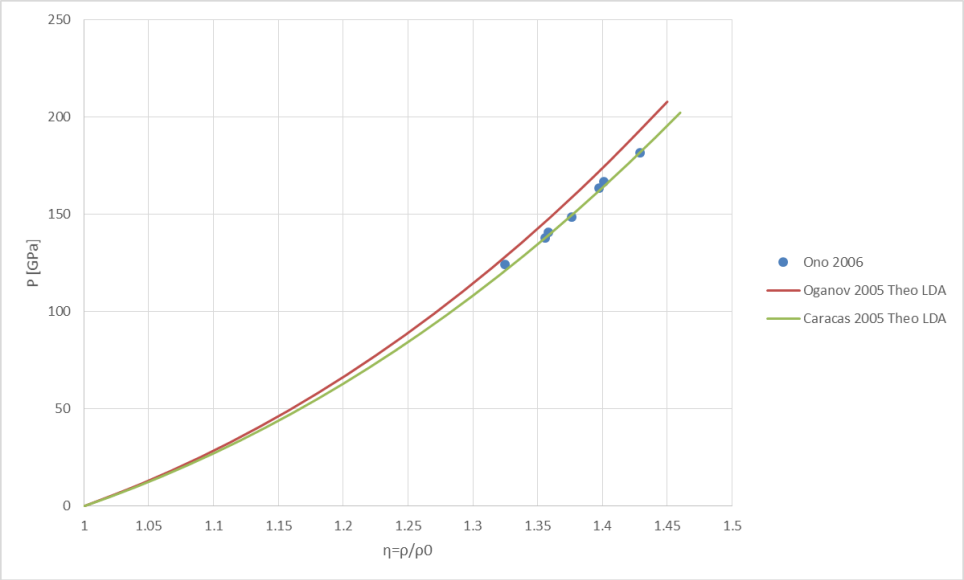

Figure 51 - Post-Perovskite EoS

The solid EoS is:

$$P = (270.2204 - 753.612\eta + 483.9595\eta^2) \quad (71)$$

With ρ_0=4.219438 g/cm^3 (for T_0=300K and P=0 GPa). This value was derived from Tsuchiya et al., 2005, where V=17.552 cm^3/mol at P=150 GPa.

Zirconia

Monoclinic structure

For this phase the studied data, both theoretical (Ren et al. 2011; Dewhurst & Lowther 1998; Iuga et al. 2007; Al-Khatatbeh et al. 2010; Jaffe et al. 2005; Terki et al. 2006; Zhao et al. 2011; Lowther et al. 1999; Stapper et al. 1999; Dash et al. 2004) and experimental (Al-Khatatbeh et al. 2010; Leger et al. 1993; Desgreniers & Lagarec 1999), presented a large range of results, making the extrapolation of the EoS very difficult (Figure 52).

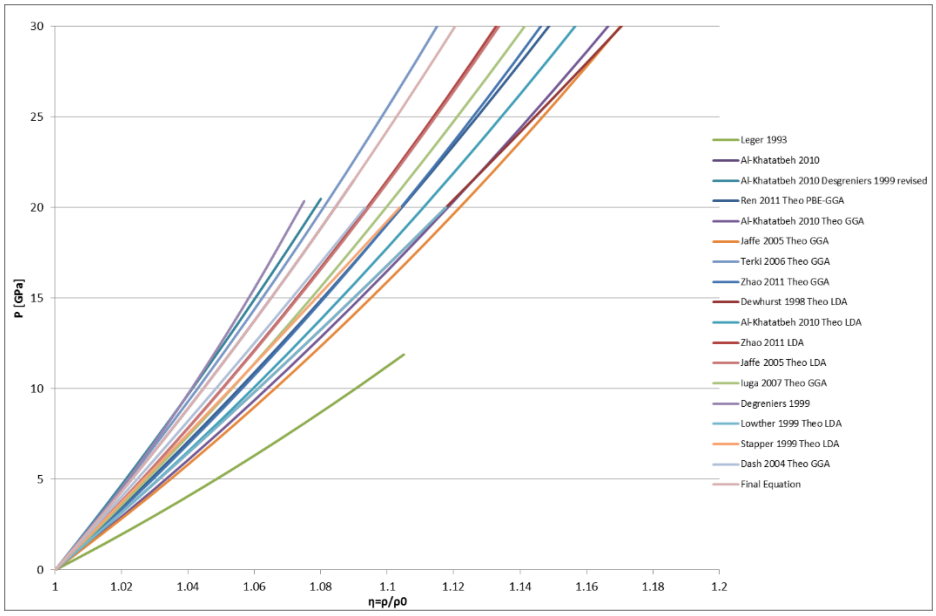

Figure 52 - Monoclinic EoS

Therefore, only experimental values were evaluated,allowing a more accurate analysis. As the experimental data studied have only isotherm curves at T=298K, the Solid EoS will not depend on temperature. In this case, the equation of state was based in Al-Khatatbeh et al., 2010, because is the most compatible with Desgreniers & Lagarec, 1999, also experimental data. The solid EoS is:

$$P = (119.1132 - 447.561\eta + 328.4539\eta^2) \quad \textbf{(72)}$$

With ρ_0=5.644479 g/cm^3 (for T_0=298K and P=0 GPa).

This value was derived from Whitney ,1962, where a V(T,P) relation is presented and for T=298K and P=0, V=21.82946 cm^3/mol.

Tetragonal structure

For this material phase there are theoretical (Dewhurst & Lowther 1998; Jaffe et al. 2005; Terki et al. 2006; Zhao et al. 2011; Stapper et al. 1999; Dash et al. 2004; Jin et al. 2012; Milman et al. 2009) and mostly experimental data , for T=298K and T=1273K (Ohtaka et al. 2002; Bouvier et al. 2003), which makes possible a solid equation of state dependent of T. Representing the Data above in Figure 53.

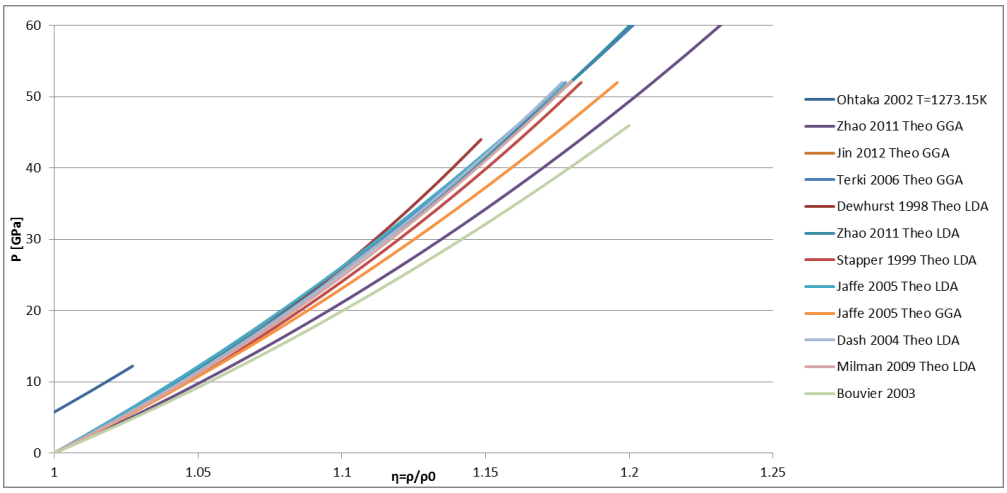

Figure 53 - Tetragonal EoS

The solid EoS developed is obtained for T=298K with the data represented in Figure 53, with special focus on Bouvier et al., 2001, and for T=1273K with Ohtaka et al., 2002. These data are represented by Murnaghan-Birch EoS, where η=ρ/ρ0, with ρ0 for P=0 and T=1273K. Consequently, it was necessary to make a change of variable in order to make the Cowan Fickett EoS, transforming each η into η298K= ρ/ρ0/298K. This was accomplished with the relation V(T,P) from Whitney, 1962. As before, for other temperatures, ρ0 is equal to ρ0 at T0. The solid EoS is:

$$P = (146.297 - 446.017\eta + 297.9606\eta^2) + (-0.013249 - 0.0219293\eta + 0.0410829\eta^2)\mathrm{T} \quad (73)$$

With ρ_0=6.0498 g/cm^3 (for T_0=298K and P=0 GPa). This value was derived from Whitney, 1962, where a V(T,P) relation is presented and for T=298K and P=0, V=20.368 cm^3/mol.

Orthol structure

For this phase both theoretical (Ren et al. 2011; Dewhurst & Lowther 1998; Al-Khatatbeh et al. 2010; Jaffe et al. 2005; Terki et al. 2006; Lowther et al. 1999; Stapper et al. 1999) as experimental data (Al-Khatatbeh et al. 2010; Haines & Léger 1993; Desgreniers & Lagarec 1999) are found. The solid EoS for the average of the curves is:

$$P = (335.8018 - 888.142\eta + 552.71\eta^2) \quad (74)$$

With ρ_0=6.07 g/cm^3 (for T_0=298K and P=0 GPa) (Toraya et al. 1987). Which is in very good agreement with Leger et al., 1993, experimental data.

OrthoII Structure

For this phase a lot of data are available, both theoretical (Ren et al. 2011; Dewhurst & Lowther 1998; Al-Khatatbeh et al. 2010; Jaffe et al. 2005; Terki et al. 2006; Lowther et al. 1999; Cohen et al. 1988) and experimental(Al-Khatatbeh et al. 2010; Ohtaka et al. 2005; Desgreniers & Lagarec 1999; Ohtaka et al. 2002; Haines et al. 1995), however there is a high scattered data. For a better analysis, Desgreniers & Lagarec 1999, and all the theoretical data were removed, which allows to describe more accurately the equation of state for T=298K, as shown in Figure 54.

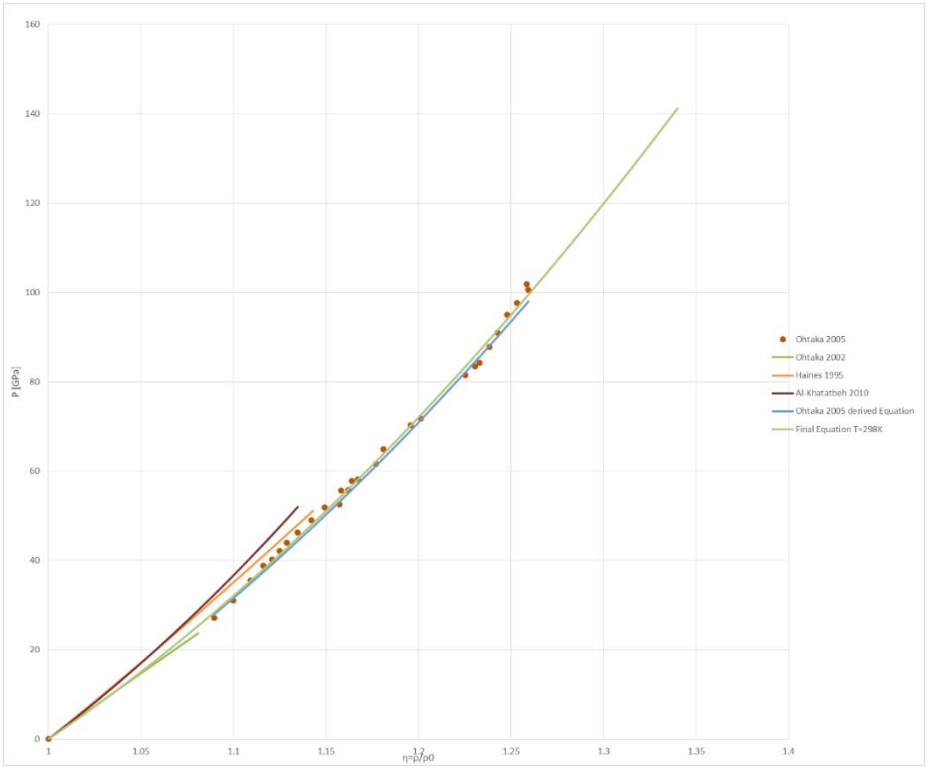

Figure 54 - Ortho II EoS Experimental Data

For P-V-T relation is also necessary P-V data at other Temperatures, which can be obtained from Ohtaka et al. 2002, experimental data for T=1273K. For this temperature a Murnaghan-Birch EoS is presented, where $\eta=\rho/\rho_0$, with ρ_0 for P=0 and T=1273K, for this reason, it was necessary to make a change of variable in order to make the Cowan Fickett EoS, transforming each η into $\eta_{298K}= \rho/\rho_{0/298K}$. For this modification was used the Thermal Expansion Coefficient from Ohtaka et al. 2005(Ohtaka et al. 2005). The solid EoS is:

$$P = (95.26468 - 476.364\eta + 380.3499\eta^2) + (0.058484 - 0.10215\eta + 0.046179\eta^2)T \quad (75)$$

with ρ_0=6.796624 g/cm^3 (for T_0=298K and P=0 GPa). This value was derived from Liu, 1980, where V=18.13 cm^3/mol, for T=298K and P=0.

Titania

Anatase

For anatase there are theoretical (Arlt et al. 2000; Al-Khatatbeh et al. 2009; Iuga et al. 2007) and experimental (Arlt et al. 2000; Dubrovinsky et al. 2001; Haines & Léger 1993; Lagarec & Desgreniers 1995) studies.

. With the equations given by these studies, a high scattered data is denoted, for that reason it was given more importance to experimental data. For experimental, Arlt et al. 2000, and Dubrovinsky et al. 2001, have a very good correlation, however Haines & Léger 1993 is very different from that results. As data is only for T=298K the Solid EoS is:

$$P = (151.345 - 468.035\eta + 317.229\eta^2) \quad \textbf{(76)}$$

With ρ_0=3.8941 g/cm^3 (for T_0=298K and P=0 GPa) (Arlt et al. 2000).

This EoS was made by extrapolation of Dubrovinsky et al., 2001, and Arlt et al., 2000, experimental data.

Brookite

Brookite is the rarest natural Titania crystal and very little information is available about its EoS, however there are a few theoretical (Mei et al. 2014) and an experimental (Luo et al. 2005) studies. Has this two curves are not in agreement, this phase have to be more studied in order to well describe an equation of state.

Columbite

For Columbite were analyzed theoretical (Swamy & Muddle 2007; Al-Khatatbeh et al. 2009; Wu et al. 2010) and experimental (Arlt et al. 2000; Nishio-Hamane et al. 2010; Al-Khatatbeh et al. 2009; Haines & Léger 1993) data. Taking experimental results, for T=298K, due to high scatter outcomes, the Solid EoS is:

$$P = (339.7824 - 889.22\eta + 550.0806\eta^2) \quad \textbf{(77)}$$

With ρ_0=4.336 g/cm^3 (for T_0=298K and P=0 GPa) (Arlt et al. 2000)

This EoS was made by extrapolation of Arlt et al., 2000, Nishio-Hamane et al., 2010, and Al-Khatatbeh et al., 2009, experimental data.

Baddeleyite

For this structure it's possible to observe an excellent correlation between experimental data (Arlt et al. 2000; Nishio-Hamane et al. 2010; Dubrovinsky et al. 2001; Al-Khatatbeh et al. 2009; Swamy et al. 2002; Olsen et al. 1999), however, theoretical results (Al-Khatatbeh et al. 2009; Wu et al. 2010) don't have a good correlation with the previous ones. For this reason, the solid EoS is derived using the experimental data only:

$$P = (183.0529 - 661.488\eta + 478.4741\eta^2) \quad \textbf{(78)}$$

With ρ_0=4.728 g/cm^3 (for T_0=298K and P=0 GPa) (Arlt et al. 2000)

Ortho I

For this phase theoretical (Swamy & Muddle 2007; Al-Khatatbeh et al. 2009; Wu et al. 2010) and experimental (Dubrovinskaia et al. 2001; Nishio-Hamane et al. 2010; Al-Khatatbeh et al. 2009) were studied. Analyzing all the data above, a large range of results are obtained, however Dubrovinskaia et al. 2001 and Al-Khatatbeh et al. 2009, experimental data, are in good agreement, which lead to a solid EoS:

$$P = (213.7463 - 734.867\eta + 521.2846\eta^2) \quad \textbf{(79)}$$

With ρ_0=4.8639 g/cm^3 (for T_0=298K and P=0 GPa). This value was derived from Dubrovinskaia et al., 2001, where V=16.42 cm^3/mol, for T=298K and P=0.

Ortho II

For Ortho II structure, theoretical (Al-Khatatbeh et al. 2009; Wu et al. 2010; Dewhurst & Lowther 2001; Caravaca et al. 2009; Koči et al. 2008) and experimental (Nishio-Hamane et al. 2010; Dubrovinsky et al. 2001; Al-Khatatbeh et al. 2009) data were analyzed. For the equations studied exists a large dispersed data, however Nishio-Hamane et al. 2010 and Al-Khatatbeh et al. 2009, experimental data, are in good correlation, this lead to a solid EoS:

$$P = (206.8439 - 720.129\eta + 513.4156\eta^2) \quad \textbf{(80)}$$

With ρ0=5.275166 g/cm3 (for T0=298K and P=0 GPa). This value was derived from Nishio-Hamane et al., 2010, where V=15.14 cm3/mol, for T=298K and P=0.

Cubic Fluorite- Type

For Cubic Fluorite structure were found, theoretical (Swamy & Muddle 2007; Liang et al. 2008; Koči et al. 2008) and experimental (Mattesini et al. 2004) equations of state. Mattesini et al., 2004, reported the synthesis of cubic TiO2 at a pressure of 48 GPa and temperatures of 1900-2100K by heating anatase in a DAC and have interpreted their results in terms of the fluorite structure. Nevertheless, Swamy & Muddle, 2007, have calculated the bulk and shear modulus of the fluorite and pyrite phases using the linear combination of atomic orbital (LCAO) method and claimed that the experimental observation was closer to the pyrite phase.

The solid EoS was extrapolated from all the data, except Mattesini et al., 2004:

$$P = (294.1222 - 869.842\eta + 575.7195\eta^2 \quad (81)$$

With V0=112.11 $Å^3$ (T0=0K) (Liang et al. 2008)

Magnesia

B2

For this structure, only theoretical studies are available (Vahora et al. 2013; Gueddim et al. 2009; Schleife et al. 2006; Jaffe et al. 2000). For the Solid EoS an average of all the curves is used. The solid EoS is:

$$P = (164.262 - 462.456\eta + 298.1938\eta^2) \quad (82)$$

With ρ_0=3.71 g/cm^3 (Coppari et al. 2013)

ANNEX B – GRÜNEISEN

Alumina

Rh_2O_3(II)-Type; Perovskite; Post-Perovskite

For these phases, as we only have a P-V equation, only Slater, Dugdale and MacDonald and Vachenko and Zubarev equations can be used. For η=1.2 these parameters are:

Table 15 - Grüneisen Parameter - Rh_2O_3(II)-Type; Perovskite; Post-Perovskite

Rh_2O_3(II)- type	Perovskite	Post-Provskite
$\boldsymbol{\gamma_S = 1.529}$	$\gamma_S = 1.628$	$\gamma_S = 1.757$
$\boldsymbol{\gamma_{DM} = 1.330}$	$\gamma_{DM} = 1.435$	$\gamma_{DM} = 1.573$
$\boldsymbol{\gamma_{VZ} = 1.086}$	$\gamma_{VZ} = 1.201$	$\gamma_{VZ} = 1.350$
γ=1.01 for P=80GPa at T=300K (Tsuchiya et al. 2005)		γ=1.26 for P=150GPa at T=300K. (Tsuchiya et al. 2005)

With this table it's possible to see the good agreement between Gru VZ and Gruneisen Parameters calculated in other papers.

Zirconia

Monoclinic

For this phase, as we only have a P-V equation, only Slater, Dugdale and MacDonald and Vachenko and Zubarev equations can be used. For η=1.2 these equations are:

$$\gamma_S = 1.490$$
$$\gamma_{DM} = 1.287 \quad (83)$$
$$\gamma_{VZ} = 1.040$$

For monoclinic phase it's made an average of Li et al. 2011 experimental results, that gives **γ=1.57.**

Tetragonal

In Figure 55are represented the Slater, Dugdale and MacDonald and Vachenko and Zubarev equations, for η=1.2.

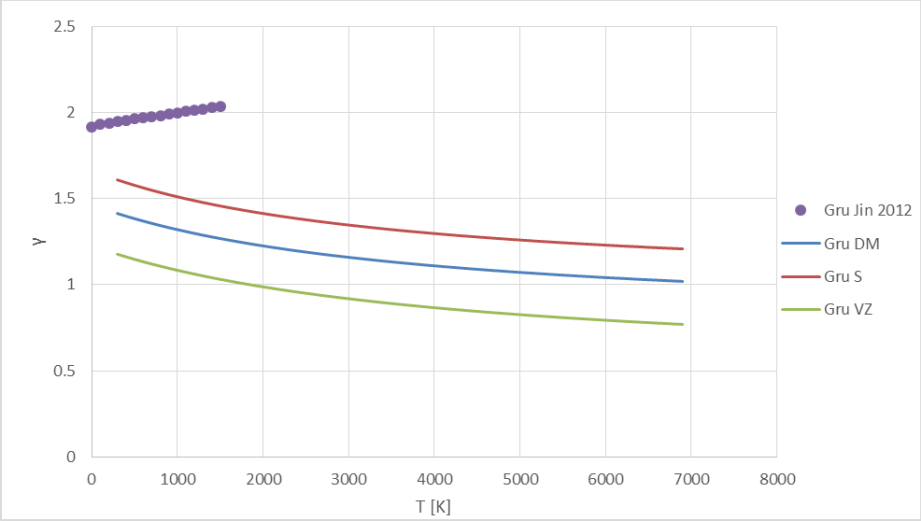

Figure 55 - Grüneisen Parameter - Tetragonal Zirconia

Phonons play an important role at higher temperatures. For much higher values than the Debye temperature, the Grüneisen parameter γ of zirconia is a constant. Between 1160ºC to 1925 ºC, γ=2.3 (Jansen 1991). An average of Grüneisen mode parameters (Fadda et al. 2010) is made, giving a value of γ=1.78. With theoretical calculations, for T=0K, γ=1.92 (Jin et al. 2012), the variation of Grüneisen with temperature is represented in Figure 55. This demonstrates the difference between results with Gru VZ, DM or S to the papers studied.

Ortho II

In Figure 56 are represented the Slater, Dugdale and MacDonald and Vachenko and Zubarev equations, for η=1.2.

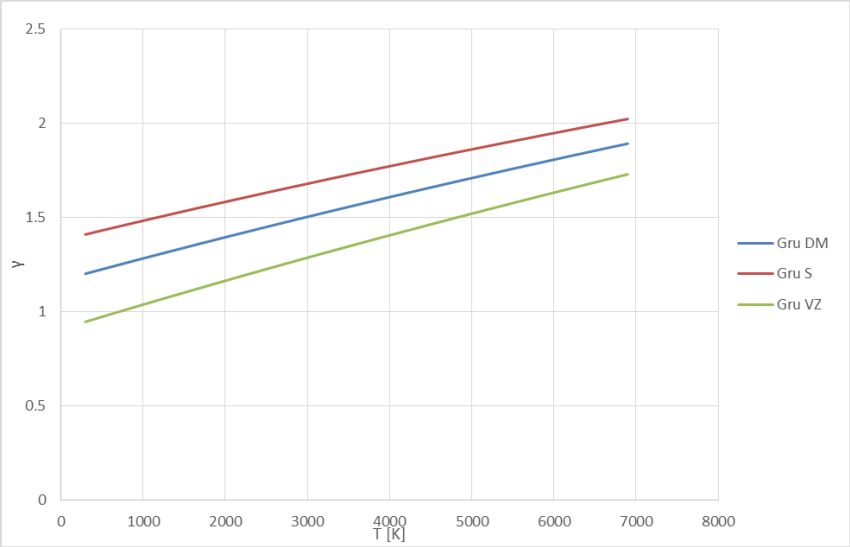

Figure 56 - Grüneisen Parameter - Ortho II Zirconia

Titania

Anatase; Columbite; Baddeleyite; Ortho I; Ortho II; Cubic Fluorite

For these phases, as we only have a P-V equation, only Slater, Dugdale and MacDonald and Vachenko and Zubarev equations can be used. For η=1.2 these equation are:

Table 16 - Grüneisen Parameter - Anatase; Columbite; Baddeleyite; Ortho I; Ortho II; Cubic Fluorite

Anatase	Columbite	Baddeleyite	Ortho I	Ortho II	Cubic Fluorite
$\boldsymbol{\gamma_S = 1.631}$	$\gamma_S = 1.865$	$\gamma_S = 1.513$	$\gamma_S = 1.545$	$\gamma_S = 1.536$	$\gamma_S = 1.683$
$\boldsymbol{\gamma_{DM} = 1.439}$	$\gamma_{DM} = 1.687$	$\gamma_{DM} = 1.311$	$\gamma_{DM} = 1.346$	$\gamma_{DM} = 1.337$	$\gamma_{DM} = 1.493$
$\boldsymbol{\gamma_{VZ} = 1.206}$	$\gamma_{VZ} = 1.472$	$\gamma_{VZ} = 1.066$	$\gamma_{VZ} = 1.104$	$\gamma_{VZ} = 1.094$	$\gamma_{VZ} = 1.262$

For cubic Fluorite was estimated a Grüneisen parameter of 2.04 (Miloua et al. 2011). This value is different from the obtained by the equation above.

Magnesia

B2

For this phase, as we only have a P-V equation, only Slater, Dugdale and MacDonald and Vachenko and Zubarev equations can be used. For η=1.2 these equations are:

$$\gamma_{DM} = 1.560$$
$$\gamma_S = 1.747 \quad \textbf{(83)}$$
$$\gamma_{VZ} = 1.335$$

ANNEX C – SIMULATION RESULTS

Table 17 - Nitromethane Isochoric Adiabatic Combustion Results

	Gru C Alpha	Gru C Beta	P [kbar]	T [K]	ρ[g/cm3]	$\Gamma = \frac{\partial H}{\partial E}\Big)_S$	%c(g)	%C(apha)	%C(beta)
Only C(gas)	-	-	56.383	2704.343	1.138952	2.77	0	0	0
Calpha and Cbeta (Campos et al. 2014)	-	-	48.017	3151.396	1.138952	2.56	0	0	25.07383
Calpha and Cbeta This Work	0.97	0.526	49.319	3178.834	1.138952	2.58	0	0	24.92474
calpha 0.23	0.23	0.526	49.319	3178.834	1.138952	2.58	0	0	24.92474
Calpha 2	2	0.526	49.319	3178.834	1.138952	2.58	0	0	24.92474
cbeta 0.23	0.97	0.23	48.461	3182.804	1.138952	2.58	0	0	24.9325
cbeta 1	0.97	1	53.278	3023.072	1.138952	2.66	0	0	24.95817
cbeta 1.5	0.97	1.5	49.973	3147.471	1.138952	2.59	0	0	24.99811
cbeta 2	0.97	2	50.386	3107.825	1.138952	2.59	0	0	25.10123
cbeta 2.5	0.97	2.5	50.904	3045.467	1.138952	2.59	0	0	25.26245
cbeta 2.8	0.97	2.8	50.848	3016.58	1.138952	2.58	0	0	25.38989
cbeta 3	0.97	3	46.773	2705.468	1.138952	2.65	0	0	25.05723

Table 18- Nitromethane Isobaric Adiabatic Combustion Results

	Gru C Alpha	Gru C Beta	P [kbar]	T [K]	ρ[g/cm3]	$\Gamma = \frac{\partial H}{\partial E}\Big)_S$	%c(g)	%C(apha)	%C(beta)
C(gas)	-	-	1	2312.855	0.000105	1.21	0	0	0
Calpha e Cbeta (Campos et al. 2014)	-	-	1	2312.861	0.000105	1.21	0	0.00004	0
Calpha e Cbeta This Work	0.97	0.526	1	2312.907	0.000105	1.21	0	0.00137	0
Calpha 0.23	0.23	0.526	1	2312.908	0.000105	1.21	0	0.001405	0
Calpha 2	2	0.526	1	2312.908	0.000105	1.21	0	0.001441	0
cbeta 0.23	0.97	0.23	1	2312.911	0.000105	1.21	0	0.001457	0

cbeta 1	0.97	1	1	2312.92	0.000105	1.21	0	0.000064	0
cbeta 1.5	0.97	1.5	1	2312.911	0.000105	1.21	0	0	0
cbeta 2	0.97	2	1	2312.841	0.000105	1.21	0	0.000009	0
cbeta 2.5	0.97	2.5	1	2312.921	0.000105	1.21	0	0	0
cbeta 2.8	0.97	2.8	1	2371.072	0.000106	1.2	0	0	2.75328
cbeta 3	0.97	3	1	2406.387	0.000106	1.23	0	0	4.403396

Table 19 - Nitromethane Detonation Results

	Gru Alpha	**Gru Beta**	**VOD [m/s]**	**PCJ [kbar]**	**T [K]**	**ρ[g/cm3]**	$\Gamma = \frac{\partial H}{\partial E}\Big)_S$	**c(g) %**	**C(apha) %**	**C(beta) %**
c(gas)	-	-	6325.89	115.12	3121.107	1.52439	2.96	0	0	0
Calpha e Cbeta (Campos et al. 2014)	-	-	5819.94	105.9	3354.437	1.468429	2.79	0	0	25.48746
Calpha e Cbeta This Work	0.97	0.526	5918.43	108.5	3417.988	1.470588	2.82	0	0	25.29093
Calpha 0.23	0.23	0.526	5918.43	108.5	3417.988	1.470588	2.82	0	0	25.29093
calpha 2	2	0.526	5918.43	108.5	3417.988	1.470588	2.82	0	0	25.29093
cbeta 0.23	0.97	0.23	5853.39	106.62	3403.694	1.468429	2.81	0	0	25.29236
cbeta 1	0.97	1	6094.74	113.54	3414.354	1.477105	2.85	0	0	25.30288
cbeta 1.5	0.97	1.5	6266.36	120.19	3321.879	1.459854	2.88	0	0	25.31553
cbeta 2	0.97	2	6075.52	99.926	3345.426	1.455604	2.84	0	0	25.40611
cbeta 2.5	0.97	2.5	6114.53	117.23	3269.143	1.445087	2.84	0	0	25.60361
cbeta 2.75	0.97	2.75	6144.45	118.84	3219.995	1.440922	2.84	0	0	25.73734
cbeta 2.8	0.97	2.8	5751.97	102.89	3469.215	1.464129	2.82	0	24.58987	0
cbeta 2.96	0.97	2.96	5751.97	102.89	3469.215	1.464129	2.82	0	24.58987	0
cbeta 3	0.97	3	6697.35	126.33	3185.541	1.512859	3.05	0	0	0